University of the Basque Country

Computational studies on photophysical properties of molecular aggregates

Olatz Uranga Barandiaran

Thesis Directors: Dr. David CASANOVA and Prof. Frédéric CASTET

2022

TE ESCUCHÉ

Te escuché, a cada progreso le sumabas un nuevo límite, un nuevo "no vas a poder" y otro nuevo miedo a traspasar sin palabras.

Te escuché, confundiendo entre tanta sensación si esa voz surgía de las profundidades de mí misma.

Y, mientras te escuchaba, aprendí a respirar con calma lo que decías; a notar cómo al exhalar te despegabas de mí como el aceite lo hace del agua, diferenciando cuál es la naturaleza de cada sustancia.

Escuché llenándome de aire, que ya no eras más que pensamiento flotando en la superficie.

Te escucho ahora. Ya sé quién eres, pero lo más importante es que tú, mente asustada, emepiezas a saber quién soy YO.

Olatz Uranga Barandiaran

Dedication

Joni,

Txiki-txikitatik izan zara nire erreferente eta zure pausoak jarraitzeagatik iritsi naiz izatera gaur naizena. Zuri eskatu dizut gainontzekoei eskatzera ausartu ez naizen guztia. Ezin zenuen hobeto bete anaia nagusiaren papera, eman dizkidazu mila aholku eta gidatu nauzu beti nire karrera profesionalean; baina orain dena beste modu batera ikusten dut eta esango nuke gehiegi babestu naizela zugan eta nire bidea egin nahi dut, agian, eta, seguraski, erratuko naiz, baina altxatzen ere ikasiko dut. Asko maite zaitut, Jon!

Acknowledgements

Damutu al naiz tesia egitea erabaki izanaz? Lan gogorra izan dela argi daukat eta nire bakardadea nabarmendu egin da: zenbat eta blokeatuago egon, orduan eta bakarrago sentitzeraino. Eta dena nik nahi izan dudalako, noski. Ez nago ziur zergatik izan den, baina betidanik funtzionatu dut horrela. Laguntza eskatzea inoiz ez zait gustatu eta halako lan zaila nik bakarrik egiteko gai nintzela pentsatu dut; eta horrek are gehiago irentsi nau, aislatu eta tristetu. Lerro hauekin taldeko jende guztia eskertu nahiko nuke, niregana gerturatu zaretelako laguntza eman nahian eta nik ukatu egin dizuet; beraz, barkatu.

Quizás he pensado que hacer el trabajo sola me haría más fuerte y valiosa. Pero es que esto sólo me ha desgastado, entristecido y aislado aún más. Por eso, este es el capítulo para agradecer a todo el grupo que me ha querido acompañar en estos años. Irene, a ti en especial, gracias de todo corazón por compartir conmigo esta experiencia: las conversaciones en los congresos, los nervios, el aburrimiento, las risas, las eternas dudas con el papeleo y, finalmente, la escritura de la tesis. David, me has enseñado mucho y siempre serás un referente para mí; has sido un director maravilloso; siempre con paciencia y dejándome el espacio y tiempo que te pedía: ¡gracias! Abel, por enseñarme todo lo más básico de programación, y a todo el grupo de David: Veró, Claire, Maru, Maria...

Xabi eta Txoni, zuei esker hasi nuen nire ibilbidea Kimika Teorikoan, zuek sentiarazi zenidaten hainbesteko kuriositatea alor honekiko. Zuen laguntza asko eskertzen dut, zuen umorea eta irribarrea, baina batez ere, momentu zailenetan (eta asko izan dira!) beti egon zaretelako han: Holandan, masterrean, doktoradutzako paperak egiten etab. Xabi, behin gutun bat idatzi zenidan eta askotan eman dizkit indarrak, amore eman beharrean, tesia bukatzeko. Eli eta Txema, plazerra izan da praktiketan zuengandik ikastea. Txema, zuk, gainera, informatikako buruhauste askotatik atera nauzu! Ion, ez ditut ahaztuko masterreko garaiak. Zure fisikako oinarria izan ez balitz, han jarraituko nuke oraindik... Mireia, contigo también he compartido momentos geniales, lo siento por haberme apartado. ¡En definitiva, creo que todo el grupo es impresionante!

Meme si cette thèse est un travail personnel, je souhaite ici rendre hommage et exprimer ma profunde gratitude à tous les personnes à Bordeaux qui, de loin, ont contribue à sa réalisation et à son aboutissement. Je sais que je n'ai guère partagé de moments avec vous, puisque je

n'aimais pas quitter Saint-Sébastien, et, regardez que Bordeaux est proche! Plusieurs fois, je regrette de ne pas l'avoir fait. Honnêtement, je pensais que faire le travail seul me rendrait plus fort et plus précieux. Mais cela n'a fait que m'user, m'attrister et m'isoler encore plus. C'est donc le chapitre pour remercier tout le groupe qui a voulu m'accompagner dans ces années.

Mes remerciements s'adressent tout d'abord à mon Directeur de thèse, Frèdèric. Tout au long de ce travail, vous avez su m'apporter un soutien constant, une disponibilité, une écoute, des conseils précieux et avisés et tout le temps je t'ai demandé, à la hauter de votre compétences et de votre réelles qualités humaines. Je tiens, tout particulièrement, à témoigner une vive reconnaisance à tout le groupe total qui a accepté de participer à cette expérience. Je voudrais insister sur la chaleur de l'accueil, la disponibilité et la gentilesse de l'ensemble des membres qui j'ai pu cotoyer tout au long de ce travail.

Iñaki, zu bai txintxoa! Mila esker bihotz bihotzez zure eguneroko goxotasunagatik, maitasun, eta bereziki, nire agobio eta negar saioak irensteagatik. Garai gogorra izan da, baina irribarre bat aterarazi didazu beti!

Y, por último, pero muy importante: ¡¡gracias, Mayte!! Me has empoderado y has sido el empujón que necesitaba para finalizar esta etapa. He tenido ganas de tirar la toalla mil veces, pero me has recordado que la vida es así, llena de sonidos que distorsionan nuestro mundo idealizado y que me hago más fuerte justo gracias a esos momentos donde todo pesa el triple.

Cómo cuesta asumir que hay que volver a empezar, no una, ni dos, sino millones de veces. No es fácil porque antes de empezar hay que transitar y acoger un mejunje de emociones variopintas. Verte ahí en ese laberinto emocional es duro y, sin embargo, es la clave más verdadera para seguir viviendo.

Y cuando, finalmente, he terminado de escribir, me he sentido afortunada porque quien puede volver a empezar es quien sigue vivo, aprendiendo.

Sigo siendo una emoción con patas, pero estoy aprendido a llevarme bien con mi mundo interno, porque sé que sin él no estaría aquí. Y estar aquí es el principio de todo. En esa casilla de salida, respiras y ahí, justo ahí, se celebra la vida sin daño. Y te das cuenta de que cada momento así, es digno de festejo. Lo celebras. Y sí, el mundo sigue patas arriba, pero hay un segundo donde tú estás celebrando a escondidas que sientes el suelo bajo tus pies. Y eso, marca la diferencia. Vaya que sí la marca.

Contents

Abstract

The present project is devoted to analyze the electronic structure of the ground and excited electronic states and the associated optical properties of organic dyes and supramolecular assemblies of potential interest for optical applications. Following these points, the project has been classified in three interrelated research lines. First, we report a join experimental and computational investigation at the DFT level on monomers and covalently-linked dimers of borondifluoride complexes of curcuminoid derivatives, a prototype example of conjugated organic dyes. The nature of the electronic states was analyzed by employing an effective approach based on the development of the electronic wave functions in terms of diabatic basis states. A similar approach was used in a second study for rationalizing the absorption and fluorescence emission properties of conjugated dyes composed of dimethylamino flavylium heterocycles linked by a polymethine chain, which were recently reported to act as efficient shortwave infrared emitters. Finally, a third study focused on the development of a new theoretical approach allowing the precise characterization of electronic excited states resulting from the interaction between chromophoric units in model molecular aggregates. Theoretical descriptions of such systems are usually achieved by means of excitonic models, using effective Hamiltonians built on a basis of diabatic states that enable physical interpretations in terms of local excitations, charge transfer, or multiexcitonic configurations. The alternative approach that has been developed is based on a diabatization scheme, which allows the decomposition of the adiabatic excited state energies of molecular aggregates into contributions issued from intermolecular couplings, without requiring any a priori definition of diabatic states. This methodology constitutes a promising tool to extract accurate *ab initio* diabatic state energies and interstate couplings for eventual derivation of model excitonic Hamiltonians.

Laburpena

Jarraian aurkezten den tesia kolorante organiko eta agregatu molekularren egoera fundamental eta kitzikatuen estruktura elektronikoa eta horiei dagozkien propietate optikoak aztertzean datza. Gainera, beren izaera fisikoa eta agregatu egonkorrak sortzeko beharrezkoak diren indar eta interakzioak identifikatzea ere izan dugu helburu. Azkenik, lan honen bidez espezie molekular berriei dagozkien propietate optiko eta prozesu fotofisiko bakarren arrazoiketa eta aurreikuspena bultzatu da.

Absortzio eta emisio fluoreszente propietateak dituzten kolorante organikoen diseinuak berebiziko garrantzia hartu du, hainbat aplikazio eskaintzen baitituzte alor zientifiko eta teknologikoan. Biologia zientzian, esaterako, ehunen argazkigintzan eta fotokaltean [1, 2, 3] oso erabilgarriak dira; ikuspegi eta argi detekzioan [4, 5, 6] ere abantailak dituzte; fotosintesi eta konplexu antenak [7, 8] sortzeko; teknologia munduan, fotokatalisirako [9, 10], gailu fotoboltaikoak egiteko [11, 12], argazkigintzan [13, 14], fotoaparatuak egiteko [15, 16], espektroskopia konbentzionalean, zein denboraz ebatzirikoan [17, 18]; etab. Izugarrizko erabilgarritasun hau eskaintzen dituzten abantailen ondorioa da: merkeak dira, jasangarriak, finak, arinak, tolesgarriak, gardenak eta aldatzen errazak diren propietate elektroniko eta optikoak dituzte. Normalean, aipatutako aplikazio guzti horietan behar diren prozesu fotofisikoak ez ditu monomero isolatuak erakusten, baizik eta molekulen asoziazio baten ondorio dira. Horiei agregatu molekular deritze; kobalenteki lotu gabe, entropikoki eta van der Waals indarren eraginez sortzen diren molekula taldeak dira. Interakzio horiek, enpaketatze moduaren menpe daude eta horien araberakoa da agregaturiko fasean erakutsiko duten erantzun fotofisikoa, baita agregatu hauek izango duten energia eta karga garraioa ere. Tesi honetan garrantzi handia eman zaio π-

sistemen kromoforoen arteko interakzioei, izan ere, berriki interes handia piztu dute ikasketa konputazional munduan, oraindik erronka handia suposatzen duten galdera asko erantzun gabe daudelako. Konturatu gaitezen, ordenagailuen hardwareetan eman den aurrerapena dela medio eta azkenaldian kimika kuantikoan sortu diren algoritmo berrien ondorioz bakarrik izan dela posible tesi honetan biltzen diren adibideei kimika kuantikoari dagokion goi mailako trataera ematea.

π-hurrenkera duten agregatuetan kromoforoen artean dagoen interakzioak baldintzatzen du beren karga zein energia garraioa [19, 20, 21, 22, 23, 24]. Ikusi dugunez, agerikoa da elektronika orkanikoaren munduan eta fotonikan zein garrantzitsu den molekulen agregazioa eta, beraz, komeni da ikertzea zer lotura dagoen solido organikoetan orbitalen gainjartzea eta haien propietate optiko eta elektronikoen artean. Hala ere, betebehar zaila da halakoa; izan ere, kristal egoeran exzitoien arteko interakzioa parametro estruktural anitzen araberakoa da. Gainera, kristaletan eta film mehetan dagoen hiru-dimentsioko molekulen agregazioa aurreikustea oso zaila da [25]. Gauzak horrela, garbi dago neurrira egindako material berrien diseinua ez dela batere lan xamurra.

Hasteko, kitzikaturiko egoera elekronikoen kontzeptu basikoak aurkezten saiatu gara. Horrez gain, molekula isolatuta egotetik beste askorekin taldekatu eta agregatuta dagoenera pasatzen denean bere egoera elektronikoan ematen diren aldaketak erakustarazi nahi izan dira. Horretarako, modelo exzitoniko bat garatu dugu, egoera kitzikatuen karakterizazio zehatza egiten ahalbidetu diguna. Lan honetan "exziton" terminoak honakoa adierazten du: bere baitan kromoforo asko biltzen dituen egoera kitzikatu bat da, delokalizatuta dagoena kromoforo horietako batean edo gehiagotan, baina, aldi berean, subunitate jakinetan espazialki lokalizatuta dauden egoera kiztikatu desberdinen konbinazio lineal moduan errepresentatu daitekeena. Exzitoien teoria molekularra aspalditik erabili izan da biologikoki eta fotosintesian garrantzi berezia duten sistemen portaera espektroskopikoa ulertzeko; berriki, ordea, antena konplexuen agregazio propietateak karakterizatzeko ere erabilgarria suertatzen ari da.

Beraz, agregatuen fotofisika ulertzeko egoera elektroniko desberdinen kalkulua egiteaz gainera, funtsezkoa da oinarrizko eta kitzikatutako egoeren karakterizazio zehatza burutzea, bereziki es-

pezie molekular horiei behatu ez zaizkien prozesuetarako. Lan honetan, egitura elektronikoan oinarritutako adierazle errazak definitu ditugu, maila baxuko egoera kitzikatuen propietateak neurtzeko, baita oinarrizko egoeraren trantsizio elektronikoak ere. Zehatzago esanda, kalkulatu digun egoerak momentu dipolar lokalen eta totalaren, osziladoreen indarren eta elektroidentsitatearen lokalizazio espazialaren bidez aztertu dira. Puntu hauek jarraituz, agregatu molekularretan unitate kromoforikoen arteko elkarrekintzaren ondoriozko egoera kitzikatu elektronikoak karakterizatzeko aukera ematen duen prozedura garatu dugu. Azkenik, kontuan izan, nahiz eta eskala kuantikoko kimika fisikoaren arloko proiektu teoriko eta konputazionala den, lanak esperimentuarekin lotura sendoak ezartzea ere izan duela helburu, konposatu berrien propietateak simulatuz eta arrazionalizatuz eta sistema molekular berriak diseinatuz eta proposatuz, zeinak esperimentalki probatu beharreko propietate interesgarriak dituzten.

Proiektu honetan zehar erabili den metodologia algoritmo konputazional eta sistema kimiko desberdinen egitura elektroniko eta atomikoa ondo deskribatzen duten tresna desberdinei dagokie. Guztiek dute gaitasuna ikasitako sistema molekular eta prozesuen egitura eta energia mailak zehaztasun handiz deskribatzeko. Aurrean dugun erronkaren arabera, ordea, beren konplexutasuna dela medio, beharrezkoa da modelo kuantiko batzuk sortzea, egitura eta propietate fotofiskoak modu egokian arakatu ahal izateko. Zehazki, nahitaezkoa izan da (i) hurbilketen hierarkia bat ezartzea parametro garrantzitsuen konputaziorako eta zehaztasun estandarrak ezartzea; (ii) zentzuzko hurbilketa teorikoak sortzea koste konputazionala murrizteko eta ikerketa sistema handiagoetara zabaltzeko; (iii) literaturan sortzen ari diren kimika kuantikoko ereduen berri izan iragarpenen zehaztasuna areagotzeko.

Azken urteetan, metodo konputazional ugari erabili izan dira egoera kitzikatuen propietateak kalkulatzeko. Tesi honetan garrantzi gehien dutenen oinarriak argitu ditugu. Guztien artean, Time-Dependent Density Functional Theory (TDDFT) deritzona da bereziki nabarmendu dena sistema organikoen egoera kitzikatuak kalkulatzeko. Horrenbeste, lan honetan ageri diren emaitza gehienek TDDFT kalkuluetan dute funtsa. Izan ere, metodologia honek zehaztasunaren eta koste konputazionalaren artean konpromiso ona adierazten du eta ertarinak zein handiak diren molekulen egoera kitzikatuak kalkulatzea posible egiten du.

Proiektuak hiru ardatz nagusi ditu.

Lehenik eta behin, kurkuminen eratorri diren borodifluoruro konposatuen ikerketa experimental eta konputazionala aurkezten dugu. Konposatu hauek elektroi igorle zein hartzaile izaera duten unitateak konbinatzen dituzte, igorle-hartzaile-igorle arkitektura kuadroplarrean, non hartzailea erdian dagoen dioxaborano eraztuna den eta igroleak, berriz, bazterretan dauden eraztun aromatikoak diren. Gainera, kolorante organiko konjokatuak dira eta propietate optiko interesgarriak eskaintzen dituzte egoera solidoan. X-izpien difrakzio ikasketek borodifluoruro kurkuminak agregatu egiten direla adierazten dute, beraien artean interakzio indartsuak sortuz. Horregatik, monomero gisa, zein kobalenteki lotutako dimero gisa aztertu ditugu, beraien artean dauden desberdintasunak zeintuk diren jakin nahian. Monomero eta dimero hauen UV-vis absortzio propietateak ikertu ditugu. Beren egoera elektronikoak karakterizatze aldera, oinarri diabatikoa aukeratu dugu, ongi definituriko egoera diabtikoak erabilita Hamiltoniano efektibo bat eraikitzeko. Ikerketa honen ondorioa honakoa izan da: monomeroen kasuan, absortzioa bazterretako igorle unitateetaik erdiko hartzaile unitatera gertatzen den karga transferentziak karakterizatzen du. Dimeroei dagokienean, absortzio propietateak bi monomeroen arteko karga transferentzien araberakoak direla frogatu dugu. Lan hau Pr. F. Fages-en taldearekin (CINAM, Marseilako Unibertsitatea) batera eraman da aurrera.

Bigarren ikerketa modura, flavinen familia aurkezten dugu. Beste behin, igorle-hartzaile-igorle arkitekitura kuadrupolarra duten konposatu konjokatuak aztertu ditugu. Gainera, uhin luzera txikiko argi infragorriaren igorle (SWIR deritzon 1000-2000 nm tarte optikoa) on gisa ezagunak diren molekulak dira. Irradiazio horietan lan egiteak abantaila ugari ditu aplikazio biologikoetan, ugaztunen ehunak inbaditu gabe barneratzea lortzen baita. Hauekin ere antzeko jarduera burutu dugu: DFT kalkuluak burutu ditugu eta diabatizazioaren bidez beren absorpzio eta emisio fluoreszentea ikasi nahi izan ditugu. Flavinen familia honetan lau molekula aztertzen hasi gara, denak ere polimetilo kate bidez loturiko dimetilamino flavilio heterozikloak. Aldaketa bakarra polimetil katearen luzera izan da (Flav1-Flav7), zenbat eta luzeago, orduan eta konjokazio elektroniko handiagoa izanik. Emaitzek agerian utzi digute katea luzatu ahala, konposatuen emisioa batokromatikoki aldatzen dela, gero eta igorle hobeak lortuz. Hari honi jarraituz, aldaketa gehiago egin ditugu molekula hauetan. Hartzaile izaera duen polimetil

kateari konjokaziorik gabeko ziklo bat eta elektroi hartzaile ona den kloro atomo bat gehitu dizkiogu, harik eta aldaketa batokromatiko handiagoa lortzen den arte emisioan. Azkenik, bazterretan dauden dimetilamino flavilio heterozikloen izaera igorlea areagotu nahi izan dugu. Horretarako, dimetilmino taldearen ordez difenilamino taldea sartu dugu eta emaitzek agerian uzten dutenez, sortutako molekula berria SWIR igorle onena da ikertu ditugun guztien artean. Honenbeste, aurkeztu dugun diabatizazio eskemak irudi arrazionalizatzaile argi eta intuitiboa eskaintzen du eta, horri esker, teorikoki diseinatutako fluoroforo berriak proposatu ahal izan ditugu, uhin laburreko eskualdean aurrekaririk gabeko igorpena dutenak eta, ondorioz, irudi biologikorako interes handia dutenak.

Azken ikerketa lanak metodo teoriko berri baten garapena aukezten du, kitzikatutako egoera elektronikoen ezaugarriratze zehatza emango diguna. Metdodo honek agregatu molekular modeloen unitate kromoforikoen interakzioa aztertzean du muina. Egoera kitzikatuen karakterizazio sakona egiteko Orbital Molekularrak erabiltzea lan nekeza da, orbitalak kromoforo askotan deslokalizatuta ageri direlako. Ondorioz, agregatu molekularren fotofisikaren deskribapen teoriko eta konputazionala normalean eredu exzitonikoak erabiliz lantzen da. Hala ere, planteamendu hauek egoera diabatiko jakinen definizioan oinarritzen dira, eta horrek aztergai dugun sistemaren aurre-ezagutza ona eskatzen du. Lan honen lorpen nagusietako bat estrategia alternatibo baten erabilera izan da, egoera kitzikatuen diabatizazio eskemen eta eredu exzitonikoetatik eratorritako energia-adierazpenen arteko lotura ahalbidetzen duena. Horrelako erlazioek agregatu molekularren trantsizio elektronikoen propietateak ezaugarritzea ahalbidetzen dute eta, are gehaigo, haien kitzikapen-energiak jatorri fisiko ezberdina duten akoplamendu ekarpenetan deskonposatzea. Prozedura honen bidez egoera adiabatikoen ezaugarriak ikusgarri gelditzen dira, oso ongi definitutako egoera diabatikoetan deskonposatzen baitira, konbinazio linealaren bidez. Egoera diabatiko hauek honakoak izan daitezke: kitzikapen monomerikoak; monomeroen arteko karga tarnsferentzia edo, azkenik, egoera multiexzitonikoak, non bi kromoforo edo gehiagoren aldi bereko kitzikapena gerta litekeen. Egoera adiabtikoen deskonposaketak informazio erabilgarria ematen du, baina, horrez gainera, egoera diabatikoen arteko interakzioak ere ezaugarri asko eskaintzen dizkigu. Gure hautua diabatizazio prozedura izan da. Horrela, agregatu molekularren kitzikatutako egoera adibatikoen energiak deskonposatu

ditugu akoplmemendu intermolekularrak oinarri dituzten kontribuzioetan; egoera diabatikoen inolako aurretiako definiziorik sortu gabe. Metodologia hau tresna bikaina da energia diabatiko eta egoera diabatikeon arteko akoplamendu energiak lortzeko ab initio, gerora Hamiltoniano exzitoniko modeloak sortu ahal izateko. Gauzak horrela, eskuizkribu honetan egoera kitzikatuak zehazki deskribatzeko baliagarriak diren ekuazio orokorrak aurkeztu ditugu eta egoera kitzikatuen energiak ekarpen mota desberdinetan deskonposatu ditugu dimero molekular baliokideentzat eta ez-baliokideentzat. Tresna guzti hauek, azkenik, etileno-etileno eta etileno-tetrafluoroetileno dimeroen konformazioak sistema eredu gisa hartuta, beren energia baxuko kitzikapenak aztertzeko aplikatu ditugu.

Laburbilduz, kimika konputazionalaren ikuspegi global batetik, lan honek frogatu du karakterizazio tresna sinpleak garatzearen garrantzia, kimikariaren intuiziotik hurbil, sistema organiko (supra)molekularretako egoera kitzikatuen izaera arrazionalizatzeko eta haien propietate optikoak hobeto ulertzeko eta kontrolatzeko. Lan honetan aurkezten den metodologia ekarpen ezberdinen pisua kuantifikatzeko gai da supersistemaren egitura elektronikoko *ab initio* kalkuluetatik, aldez aurretik definitutako egoera diabatikoen erabilera saihestuz, bai eta akoplamendu elektronikoen kalkuluetarako hurbilketa sendoak egin beharrik gabe ere. Oro har, metodologia honek kromoforo elkarreragileetan eragina duten exzitoien egonkortze-indarren eragile garrantzitsuenak identifikatzea ahalbidetzen du.

Chapter 1

Introduction

1.1 General context of the thesis

The design of organic dyes with targeted absorption or fluorescence emission properties is a red hot topic for applications in many scientific and technological advanced fields. In biological sciences, they are related to photoaging and photodamage [1, 2, 3], to vision and light detection [4, 5, 6], to photosynthesis and light harvesting [7, 8]. In technology, they are central for photocatalysis [9, 10], photovoltaics, [11, 12] imaging, [13, 14] photodevices, [15, 16] conventional and time-resolved spectroscopy [17, 18]. This is so because of the wide variety of advantages they offer: they are cheap, sustainable, thin, light in weight, foldable, transparent and have tunable electronic and optical properties. Usually, the photophysical processes exploited in the applications listed above do not originate from an isolated monomer, but arise from an association of dyes. We define molecular aggregates as noncovalently bound molecular assemblies formed via entropic and van der Waals driving forces. Such interactions, strongly dependent on the packing arrangement, play a crucial role in determining the photophysical response as well as the nature of energy and charge transport in the aggregated phase. In this work, special focus is laid on the interactions between chromophores in π-systems, which have recently attracted substantial interest for computational studies because many challenging questions are still to be answered. Note that as a consequence of progress in computer hardware and quantum chemical

algorithms, high-level quantum chemistry treatment of many of the examples discussed in this thesis has become accessible only in the last years. The present project is devoted to (i) analyze the electronic structure of the ground and excited states in molecular aggregates and the associated electronic properties; (ii) identify the physical nature and strength of the interactions involved in their formation and stability; and (iii) rationalize and predict the unique optical properties and photophysical processes that are not present in the pristine molecular species.

The methodologies to be employed throughout the course of this work correspond to a variety of computational algorithms and tools for the description of the atomic and electronic structure of chemical systems. The project heavily relies on their capability to accurately describe the structures and energy levels implicated in the studied molecular systems and processes. Their complexity will make it necessary to integrate several quantum chemistry models depending on the type of problem to be studied in order to properly explore their structural and photophysical properties. In this sense, this research work has taken advantage of a variety of state-of-the-art methods and computational tools in the study of the ground and excited states. In particular, it has been necessary to (i) establish a hierarchy of approximations to be applied for the computation of the key parameters and set up accuracy standards; (ii) introduce reasonable theoretical approximations to reduce computational costs and to extend the study to larger systems; (iii) be aware of emerging quantum chemistry models in the literature to increase the accuracy of the predictions.

In addition to the computation of electronic states, the detailed characterization of the ground and excited states is fundamental in order to understand the photophysics in aggregates, especially for those processes not observed for the corresponding molecular species. In this work, we have defined simple indicators based on the electronic structure to measure the properties of the low-lying excited states as well as the electronic transitions from the ground state. More precisely, the computed states were analyzed by means of local and total dipole moments, oscillator strengths and spatial localization of the electron density. Following these points, we have developed a procedure that allows the characterization of electronic excited states resulting from the interaction between chromophoric units in molecular aggregates. Finally, note that, although this is a theoretical and computational project within the area of physical chemistry

at the quantum scale, the work also aimed to establish strong connections with experiment, by simulating and rationalizing the properties of novel compounds and by designing and proposing new molecular systems with interesting properties to be tested experimentally.

1.2 Outline and structure of the thesis

In this thesis, different organic dyes with interest for optoelectronic applications have been studied from a computational point of view. In addition, the manuscript also presents the development of a theoretical procedure in order to characterize the electronic excited states resulting from interchromophoric interactions in molecular aggregates. The rest of this manuscript is divided in five chapters:

Basic concepts on electronic excited states are introduced in Chapter 2. In this Chapter, we also discuss how the electronic states of molecules change as they assemble to form an aggregate. We introduce an exciton model that enables the characterization of excited states. In our work, the term "exciton" refers to an excited state of a collection of chromophores that is delocalized across one or more of them, but which can nevertheless be represented as a linear combination of excited states that are spatially localized on particular subunits. Molecular exciton theory has been applied in the past to explain the spectroscopic behaviour of systems of interest in biology and photosynthesis [26] and, more recently, to characterize the aggregation properties of light harvesting complexes [27].

Over the last years, a large number of computational methods have been employed to calculate excited-state properties. The foundations of the most important ones are summarized in Chapter 3. Among the theoretical approaches available in the computational chemist toolbox, those rooted on the Time-Dependent Density Functional Theory (TDDFT) are probably the most widely exploited in the calculation of excited states of organic systems. Hence, most of the results presented in this work are based on TDDFT calculations. This methodology represents a balanced compromise between accuracy and computational cost, and allows to perform excited states calculations of medium and large sized molecules.

In the following chapters the results obtained during the thesis are presented. In Chapter 4 we report a computational investigation on monomers and dimers of borondifluoride complexes of curcuminoid derivatives, a prototype example of conjugated organic dyes. This study shows that the absorption in monomers is characterized by an intramolecular charge transfer process, arising from the combination of electron donor (D) and acceptor (A) units in a D-A-D quadrupolar-like architecture, in which A is the central dioxaborine ring and D is the terminal aromatic moiety acting as an electron donor substituent. Then, we considered covalent dimers of curcuminoid derivatives linked through a polymethylenic chain, which mimic aggregated structures in the solid-state, and demonstrated that the absorption properties in these systems are driven by a significant charge transfer between the two monomeric units. In order to provide an accurate description of the charge transfer interactions between the monomers, we used a localized diabatic model by constructing an effective Hamiltonian that describes the electronic structure in terms of a few diabatic basis states. This work was conducted in collaboration with the group of Pr. F. Fages (CINAM, University of Marseille) and was the object of an article published in 2018 [28].

A similar computational approach is used in Chapter 5 for rationalizing the absorption and fluorescence emission properties of conjugated dyes composed of dimethylamino flavylium heterocycles linked by a polymethine chain, which were recently reported to act as efficient shortwave infrared emitters [29]. In this part, TDDFT is used to characterize the electronic structure of the low-lying excited states as a function of the polymethine chain length. Decomposition of the computed excitations in terms of diabatic states was also performed to deconvolute the excited states wavefunction into charge-transfer intramolecular excitations. Based on these results, chemical substitution patterns consisting in enhancing the electron-withdrawing strength of the polymethine bridge and the electron-donating ability of the lateral flavylium fragments, were proposed to further redshift the photoluminescence of the fluorophores. This work was published in 2020 [30].

Finally, Chapter 6 presents the development of a new theoretical approach allowing the precise characterization of electronic excited states resulting from the interaction between chromophoric units in molecular aggregates. Theoretical descriptions of such systems are usually achieved by

means of excitonic models, using effective Hamiltonians built on a basis of diabatic states that enable physical interpretations in terms of local excitations, charge transfer, or multiexcitonic configurations. The alternative approach that has been developed is based on a diabatization scheme, which allows the decomposition of the adiabatic excited state energies of molecular aggregates into contributions issued from intermolecular couplings, without requiring any *a priori* definition of diabatic states. This methodology constitutes a useful tool to extract accurate *ab initio* diabatic state energies and interstate couplings for eventual derivation of model excitonic Hamiltonians, and was published in 2019 [31].

Chapter 2

Photophysics of molecular aggregates

2.1 Chemist's description of electronic excited states

In order to model and understand the interaction between light and matter, several approximations are usually adopted. The first one is to treat light as a classical electromagnetic field while matter is treated with quantum mechanics, within the framework of the semiclassical theory of light-matter interactions. Then, the most popular approximation in the physics community is imposed, which is the first order truncation of the perturbation operator, expressed as a multipolar expansion of the electric field. This is called the electric dipole approximation [32] and it is valid if the wavelength of the electromagnetic radiation inducing the transition is much larger than the size of the considered molecule interacting with the photons. This is a reasonable assumption when dealing with UV/Visible range of the electromagnetic spectrum. Because of the coupling between the oscillating electric field of the radiation and the electronic density of the molecule, an excitation may occur.

Frontier molecular orbitals (MOs) are among the tools used by chemists to characterize photo-induced electronic transitions from the ground state. Promotion of electrons from occupied to virtual orbitals leads to different excited states, which can be classified according to their symmetry. For instance, the spatial symmetry of an excited state dominated by a single configuration of an HOMO-LUMO transition is given by the direct product of the irreducible

representations to which these two orbitals belong. Moreover, the excited states have also different spin symmetries. In this thesis we have mainly dealt with singlet spin states. The ground state of the molecules under investigation has always been a closed shell singlet, and low-lying singlet excited states have been systematically calculated and characterized.

In addition, excited states can be optically active or dark. When the molecule has a well defined symmetry and belongs to a given point group, it is easy to know, within the transition dipole approximation, which transitions will be symmetry forbidden, based on the irreducible representation of each state and the coupling operator (the electric dipole moment). However, for molecules with no symmetry elements (except the trivial one), i.e., molecules belonging to the C_1 point group,the optical activity of the transition could be predicted by looking at the molecular orbitals and their overlap.

2.2 Photophysical processes

The diagram in Figure 2.1 gathers the principal photophysical processes investigated in this work. Both the ground (lowest energy electronic state) and excited states are shown as energy profiles represented as parabolas along a given normal mode distortion. The picture is very simplified, since each potential energy surface (PES) has $3N - 6$ dimensions, where N is the number of atoms of the molecule. According to the Born–Oppenheimer approximation, due to the fact that the nuclear masses are heavier than the electronic mass, the electronic transitions can be considered to be so fast as compared to the nuclear motion that the nuclei could be considered to be fixed during the transition. This is known as the Franck–Condon principle. The resulting state is called a Franck–Condon state. Such processes appear as straight vertical lines in the diagram and the computed interstate energy difference for a frozen molecular geometry is known as the vertical transition energy. This thesis only deals with photophysical processes described in this diagram. In photochemistry, when reactions occur in electronic excited states, the picture can be more complex.

Absorbance is the method by which an electron is excited from a lower energy level to a higher

energy level. The energy of the photon is transferred to the particular electron. That electron then transitions to a different eigenstate corresponding to the amount of energy transferred. For a closed shell ground state molecule, excited singlet states will be those mainly populated immediately after photoabsorption, according to whether they are dark or optical states. Once an electron is excited, there are a multitude of ways that the excess of energy is dissipated. One is vibrational relaxation, a non-radiative process. In this case the energy deposited by the photon into the electron is given away to other vibrational modes as kinetic energy: the energy is released through collisions with the environment triggered by molecular motion and resulting in the generation or transfer of heat energy. Such a relaxation is very fast and, thus, it is extremely likely to occur immediately following absorbance. Once molecule relaxes vibrationally to the minimum of the excited state, the vertical radiative process takes place: if the emission takes place from a singlet excited state, it is called fluorescence, while if it happens from a triplet state it is known as phosphorescence. Nonetheless, non-radiative processes may also happen before the minimum of the excited state PES is reached, since it may encounter crossings with other states. If vibrational energy levels strongly overlap electronic energy levels, a possibility exists that the excited electron can transition from a vibration level in one electronic state to another vibration level in a lower electronic state. This process is called internal conversion (IC) and mechanistically is identical to vibrational relaxation. IC occurs because of the overlap of vibrational and electronic energy states. As energies increase, the manifold of vibrational and electronic eigenstates becomes ever closer distributed. At energy levels greater than the first excited state, the manifold of vibrational energy levels strongly overlap with the electronic levels. This overlap gives a higher degree of probability that the electron can transition between vibrational levels that will lower the electronic state. IC occurs in the same time frame as vibrational relaxation, therefore, it is a very likely way for molecules to dissipate energy arising from light perturbation. Hence, it is easy to understand that, commonly, Kasha's rule [33] is obeyed; the rule states that emission takes place from the lowest excited state of a given multiplicity. Another possibility is the so called intersystem crossing (ISC), where the transition occurs between states of different spin multiplicity (say a singlet and a triplet). For this process to take place, the singlet and the triplet states must be coupled either via the spin-orbit coupling

(SOC) operator or through higher order terms (vibronic). In the case where they involve the decay to the ground state, the ISC and IC processes compete with the emission and, hence, the final scenario of the molecule will be governed by the relative rates of the different processes.

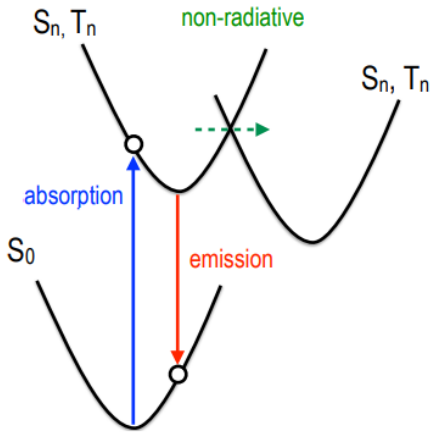

Figure 2.1: Schematic diagram of the ground and excited states with typical molecular photophysical processes studied in this thesis. Emission could be fluorescent or phosphorescent and the non-radiative transitions may be IC or ISC.

Each process outlined above can be represented in a Perrin-Jablonski diagram, commonly referred as Jablonski diagram, used to easily see the complex inner workings of how electrons change eigenstates in different conditions. Below is a typical Jablonski diagram illustrating the possible radiative and non-radiative transitions. It is important to note that the transition possibilities are dependent on their relative time scales. The faster the transition, the more likely it is to happen as determined by selection rules. Therefore, understanding the time scales each process can happen is imperative to understanding if the process may happen. The diagram also includes the typical time scale range for each process in parenthesis.

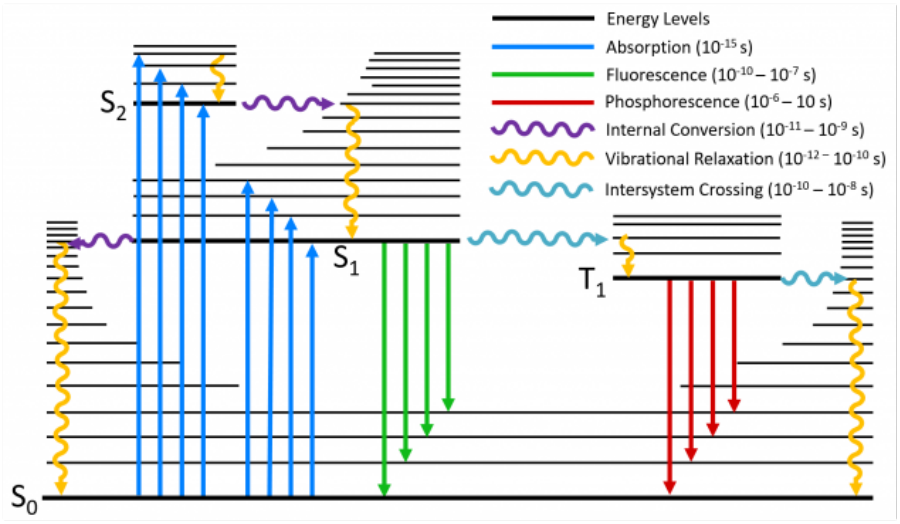

Figure 2.2: A typical Jablonski diagram showing the possible radiative and non-radiative transitions.

2.3 Photophysics of molecular aggregates through excitonic models

In addition to the calculation of excited wave functions and energies, the characterization of the electronic nature and properties of the states involved in the target processes is crucial in order to gather detailed physical insight. The computational characterization of electronic transitions becomes especially appealing in the study of molecular aggregates, molecular crystals or thin films of organic chromophores, where excited states hold recognizable properties of the electronic transitions of its molecular constituents, but also novel features may appear as a result of the interchromophoric interactions, which deeply affect the optical spectra.

The main blueprint for understanding how molecular aggregation impacts photophysical properties was drafted by Michael Kasha. He showed that an isolated molecule (a monomer) displays different optical properties than when it is aggregated or interacting with others [34, 35, 36]. In Figure 2.3 we present the electronic state diagram for an isolated monomer and interacting aggregates. Actually, we consider the simplest case of aggregation, *i.e.*, a dimer where two molecules are interacting with each other, and the electronic coupling is approximated as the

interaction between the transition dipole moments of each molecule. We may have two different cases of aggregation: H (shown in blue) and J (in red). In the case of H aggregation, the alignment of the transition dipoles is "side-by-side". This leads to a 1st excited state that is optically dark and a second one which is active and higher in energy than that of the monomer. Therefore, H aggregation results in a blue shift in the absorption spectra and a fluorescence quenching. On the other hand, in J aggregates, the transition dipole moments align head-to-tail leading to a spectral red shift (absorption energy is decreased) and an enhanced radiative decay.

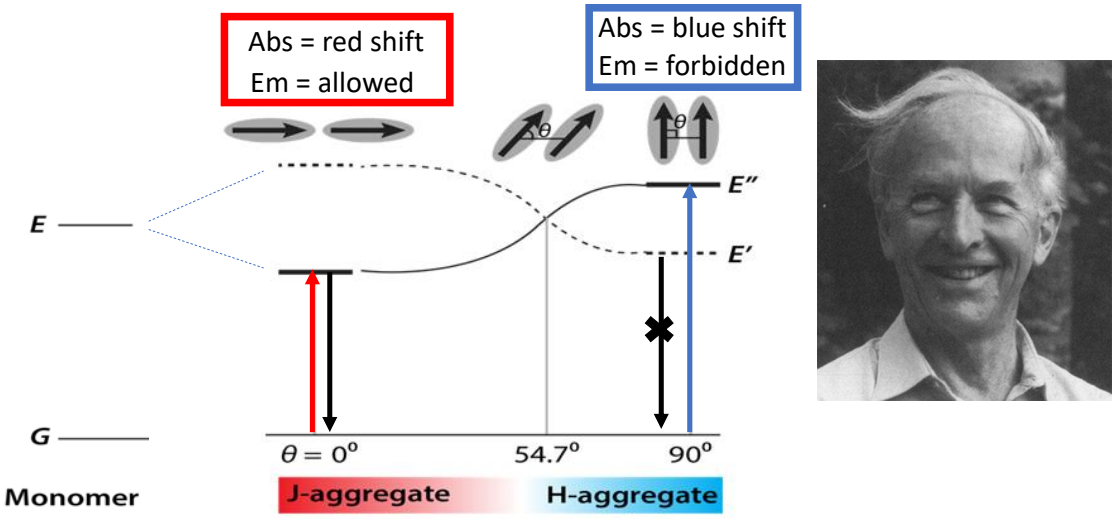

Figure 2.3: Left: ground (G) and excited (E) state energy diagrams of a monomer and conventional Kasha aggregates, in this case dimers. Each monomer is illustrated by its transition dipole moment. Right: image of Michael Kasha.

Although many examples of H and J aggregates have been observed, there are also many "unconventional" aggregates, which are not understood within the confines of Kasha's theory. In such aggregates the electron density of different molecules overlap [37, 38], and the dipole-dipole interaction approximation is no longer valid. Moreover, short separation might induce inter-monomer charge-transfer (CT) contributions to the excitation. Interchromophoric CT was early recognized as a source of impressive spectroscopic phenomena in absorption spectra of molecular materials, both in the visible and near-IR spectral regions [39]. A detailed under-

standing of the electronic states in photoactivated aggregates and the properties emerging from interchromophoric couplings allows the rationalization of the nature of low-lying transitions, e.g., the formation of the H- and J-aggregation phenomena, and can help to disentangle the mechanism of novel photophysical events resulting from the interaction of two or more optically active molecules, such as in singlet fission [40, 41, 42], triplet-triplet annihilation [43], or aggregation induced emission [44].

The analysis of the nature of the excited states in molecular aggregates by inspection of the MOs results to be rather difficult, since in many cases the MOs are delocalized over multiple chromophores. Therefore, theoretical descriptions for such systems are usually achieved by means of excitonic models, using effective Hamiltonians built on a basis of diabatic states. More precisely, excitonic models rely on the decomposition of the adiabatic wavefunctions as a linear combination of well-characterized diabatic configurations. Typically, electronic excitations in the presence of two or more chromophores can be deconvoluted in terms of monomeric excitations (LE) and possibly novel excitations emerging from dye-dye interactions, such as CT excitations, and multiexcitonic (ME) states corresponding to the concomitant excitation of two or more chromophores. In addition to the information derived from the decomposition of adiabatic states, the interaction between diabatic states contains very useful information.

The two-fold adiabatic or diabatic representation of electronic states arises from the fact that the nuclear kinetic energy operator ($\hat{T}_{nuc}$) and the electronic Hamiltonian ($\hat{H}_{el}$) do not commute, meaning that these two operators do not have a common basis set. The eigenstates of $\hat{H}_{el}$ are the adiabatic states typically calculated with electronic structure codes, while the eigenstates of $\hat{T}_{nuc}$ are the diabatic states, which are seldom used in computational quantum chemistry. Therefore, adiabatic states are coupled by $\hat{T}_{nuc}$ via nonadiabatic couplings while diabatic states are electronically coupled (the coupling terms being the off-diagonal elements of $\hat{H}_{el}$). Note that the nature of a diabatic state does not change with nuclear coordinates, since the off-diagonal terms of $\hat{T}_{nuc}$ in the diabatic representation are equal to zero, contrary to the situation in adiabatic states.

In 1982 Mead an Truhlar mathematically demonstrated that ideal diabats cannot be obtained

from a finite number of adiabatic states [45]. However, this does not mean that one cannot define diabatic states for different domains of applicability. Our interest in this thesis is in designing diabatic states which are relevant to describe electron transfer. We have used the Edmiston-Ruedenberg diabatization scheme [46], based on the maximization of the self-interaction of the diabatic states, in analogy to the MO localization technique [47]. Within this scheme, diabatic states ($\{\Xi_i\}$) are obtained as linear combinations of adiabatic states ($\{\Phi_i\}$) through a rotation matrix $\mathbf{U}$:

$$|\Xi_i\rangle = \sum_{j=1}^{N} |\Phi_j\rangle \, U_{ji}. \tag{2.1}$$

In practice, one has to choose a finite number of adiabatic states (N in Eq. 2.1) that represent the diabatic states of interest. In this sense, the off-diagonal terms of the diabatic electronic Hamiltonian will be the electronic couplings between the diabatic states. We will see in the next Chapters that the diabatization procedure allows the decomposition of the adiabatic excited state energies of molecular aggregates into contributions issued from intermolecular couplings, without requiring any *a priori* definition of diabatic states.

Chapter 3

Quantum chemistry methods

This chapter is devoted to describe the methods employed during this thesis work. The objective is to provide a general introduction of the theoretical methods and computational techniques employed, rather than an in depth and detailed report. The interested reader is referred to the given references.

3.1 Wave function based methods

Chemistry is the science dealing with construction, transformation and properties of molecules. Computational Chemistry is an interdisciplinary subfield where mathematical methods are combined with fundamental laws of the classical or quantum physics to study atoms, molecules and processes of chemical relevance by means of computational resources. Quantum Theory often describes the arrangement of protons, neutrons and electrons with a mathematical function called wave function, Ψ. All the information of a stationary quantum system, whether it is an atom, a molecule or a molecular assembly, is contained in such wave function. It is obtained solving the so-called time-independent Schrödinger Equation:

$$\hat{H}\Psi_{tot}(\mathbf{r}_i, \mathbf{R}_\alpha) = E_{tot}\Psi_{tot}(\mathbf{r}_i, \mathbf{R}_\alpha) \tag{3.1}$$

where $\hat{H}$ is the Hamiltonian operator and E_{tot} the energy of the system. $\mathbf{R}_\alpha$ and $\mathbf{r}_i$ are the set of nuclear and electronic coordinates, respectively. For a system with N_e electrons and N_N nuclei, the scalar non-relativistic Hamiltonian, in atomic units, would be expressed as follows,

$$\hat{H} = \hat{T}_e + \hat{T}_n + \hat{V}_{ee} + \hat{V}_{en} + \hat{V}_{nn} = -\sum_{i=1}^{N} \frac{\Delta_i^2}{2} - \sum_{A=1}^{M} \frac{\Delta_A^2}{2M_A} + \sum_{i>j}^{N} \frac{1}{r_{ij}} - \sum_{i=1}^{N}\sum_{A=1}^{M} \frac{Z_A}{r_{iA}} + \sum_{A>B}^{M} \frac{Z_A Z_B}{R_{AB}} \quad (3.2)$$

where $\hat{T}_e$ and $\hat{T}_n$ represent the kinetic energy operators of electrons and nuclei, while $\hat{V}_{ee}$, $\hat{V}_{en}$ and $\hat{V}_{nn}$ denote the electron-electron, electron-nucleus and nucleus-nucleus interactions, respectively. M_A is the mass of the nucleus A with respect to the mass of an electron, while Z_A and Z_B denote the atomic numbers of nuclei A and B. Finally, r_{ij}, r_{iA} and R_{AB} are the distance between the electrons i and j, electron i and nucleus A, and nuclei A and B, respectively.

3.1.1 Born-Oppenheimer approximation

Since nuclei are much heavier than electrons, on the time-scale of electron motion nuclei can be considered as stationary objects, fixed at certain positions in space. Accordingly, electrons are assumed to respond instantaneously to any change of the nuclear configuration. Based on this assumptions, the so-called Born-Oppenheimer approximation (BO hereafter), decouples the electronic and nuclear motions. For the electronic motion, the nuclear kinetic term $\hat{T}_n$ can be neglected and the nucleus-nucleus potential energy term $\hat{V}_{nn}$ can be regarded as a constant, since nuclei are considered to be fixed. Therefore, a simplified Schrödinger equation which does not treat nuclear motion is solved for electrons only.

$$\hat{H}_e \Psi_e = (\hat{T}_e + \hat{V}_{ee} + \hat{V}_{en} + \hat{V}_{nn})\Psi_e = E_e \Psi_e \quad (3.3)$$

The so-obtained electronic wave function Ψ_e explicitly depends on the electronic coordinates, but depends parametrically on the nuclear coordinates:

$$\hat{H}_e \Psi_e(\{\mathbf{r}_i\}, \{\mathbf{R}_\alpha\}) = E_e(\{\mathbf{R}_\alpha\})\Psi_e(\{\mathbf{r}_i\}, \{\mathbf{R}_\alpha\}) \quad (3.4)$$

Under the same assumptions made to formulate the electronic problem, it is possible to write down the equations for the nuclear motion. As the electrons move much faster than the nuclei, the latter are considered to move in the mean field generated by the former. In other words, the electronic energy E_e, added to the internuclear repulsion $\hat{V}_{nn}$, provides the potential energy surface V_N for the nuclei. Then, the nuclear part of the Schrödinger equation reads as:

$$(\hat{T}_n + E_e + \hat{V}_{nn})\Psi_n(\{\mathbf{R}_\alpha\}) = E_{tot}\Psi_n(\{\mathbf{R}_\alpha\}) \tag{3.5}$$

The potential energy surface of the system represent the central quantity to obtain information about the roto-vibrational levels, equilibrium geometries, and chemical reactivity.

3.1.2 The Hartree-Fock method

In 1927, Hartree introduced self consistent theory and later, Slater and Fock pointed out the requirement of an antisymmetrized determinant, giving rise to the Hartree-Fock (HF) method in 1930 [48, 49]. The HF method is central to attempts at providing an approximate solution to the electronic Schrödinger equation. It assumes that the electronic wave function can be represented by a single Slater determinant and finds out the set of spin orbitals which variationally minimize the energy of the system. The formulation of the method could be summarized as follows:

1. A N independent particle Schrödinger equation is broken down into separated N independent monoelectronic equations.

2. The approximated wave function Ψ_{HF} is obtained as a single determinant built up from the spin orbitals obtained in step 1.

3. A trial energy is computed for Ψ_{HF} constructed in step 2.

$$E_{HF} = \int \Psi^*_{HF}\hat{H}\Psi_{HF}d\tau \tag{3.6}$$

4. The variational principle, which states that the best wave function is the one providing the lowest possible energy, is applied to E_{HF}. By minimizing E_{HF} with respect to the

choice of the spin orbitals, one can derive a set of mono-electronic eigenvalue equations describing the motion of a given electron in the mean field generated by the rest of the $N-1$ electrons. These equations, known as HF equations, determine the optimal spin orbitals (ψ) and read as

$$\hat{f}(i)\psi(i) = \epsilon_i \psi(i) \tag{3.7}$$

where ϵ_i is the energy of the ith orbital and $\hat{f}(i)$ is the mono-electronic Fock operator of the form:

$$\hat{f}(i) = -\frac{1}{2}\nabla_i^2 - \sum_{A=1}^{M} \frac{Z_A}{r_{iA}} + \nu^{HF}(i) \tag{3.8}$$

where $\nu^{HF}(i)$ is the averaged potential experienced by the ith electron due to the other electrons.

5. Since $\nu^{HF}(i)$ depends on the spin orbitals of the other electrons, the HF equations are nonlinear and have to be solved iteratively, through the self-consistent-field (SCF) procedure, until $\nu^{HF}(i)$ no longer changes and the spin orbitals converge to the eigenfunctions of the Fock operator.

One might try to solve the HF equations numerically. In fact, numerical solutions are common in atomic calculations. In the case of molecules, however, no practical recipes are available for obtaining such solutions. Roothaan and Hall overcame this drawback showing that, by introducing a set of known spatial basis functions, the coupled differential equations could be transformed to a set of algebraic equations and solved by standard matrix techniques. Following the recipe proposed by Roothaan and Hall, let us write the unknown molecular orbitals $\psi(i)$ as a linear combination of K known basis functions ϕ_q

$$\psi(i) = \sum_{q=1}^{K} c_{iq}\phi_q; \quad i = 1, 2, ..., K \tag{3.9}$$

If the set ϕ_q was complete, equation 3.9 would be an exact expansion. For practical computational reasons, however, one is always restricted to a finite set of basis functions. Therefore, it is important to choose a set that will deliver, as much as possible, a reasonably accurate expansion for the exact molecular orbitals. Substituting equation 3.7 in equation 3.9, the Roothaan-Hall

equations are obtained:

$$\sum_{q=1}^{K} c_{iq}(F_{pq} - S_{pq}\epsilon_i) = 0; \quad i = 1, 2, ..., K \tag{3.10}$$

where the overlap matrix **S** with elements

$$S_{pq} = \int \phi_p^*(1)\phi_p(1)dr_1 \tag{3.11}$$

and the Fock matrix **F** with elements

$$F_{pq} = \int \phi_p^*(1)\hat{f}(1)\phi_p(1)dr_1 \tag{3.12}$$

have been introduced. In matrix notation, equation 3.10 reads as

$$\mathbf{FC} = \mathbf{SCE} \tag{3.13}$$

where **C** is a $K \times K$ square matrix of the expansion coefficients c_{ij} and **E** is a diagonal matrix of the orbital energies ϵ_i. The elements of the **F** matrix are:

$$F_{pq} = h_{pq} + \sum_r \sum_s P_{rs}\left(\langle pq|rs\rangle - \frac{1}{2}\langle ps|rq\rangle\right) \tag{3.14}$$

where h_{pq} stands for the mono-electronic integrals:

$$h_{pq} = \int \phi_p^*(1)\hat{h}(1)\phi_p(1)dr_1 \tag{3.15}$$

$\hat{h}(1)$ is the one-electron Hamiltonian operator for electron 1 and P_{rs} refers to the matrix elements of the so-called density matrix **P**:

$$P_{rs} = 2\sum_j c_{rj}^* c_{js} \tag{3.16}$$

and $\langle pq|rs\rangle$ represents the bi-electronic integrals of the form:

$$\langle pq|rs\rangle = \int \phi_p^*(1)\phi_q^*(1)\frac{1}{r_{12}}\phi_r(2)\phi_s(2)dr_1dr_2 \tag{3.17}$$

Note that the elements F_{pq} of the Fock matrix depend on the molecular orbital expansion coefficients c_{ij} by means of the density matrix $\mathbf{P}$. Thus, once again, the procedure has to be solved iteratively, using an initial guess for the density matrix and repeating the construction and the diagonalization of the Fock matrix until converegence is reached. Summarizing, the Roothaan-HF method comprises the following steps:

1. Evaluation of the mono- and bi-electronic integrals, h_{pq} and $\langle pq|rs\rangle$, for all the basis functions in the set $\{\phi_q\}$.
2. Assignment of an initial guess to the expansion coefficients c_{ij} and evaluation of the trial density matrix $\mathbf{P}$.
3. Construction of the Fock matrix $\mathbf{F}$.
4. Solution of the eigenvalue problem 3.13 to obtain the eigenvalues $\mathbf{C}$ and the eigenvectors $\mathbf{E}$.
5. Convergence check, by comparing the actual density matrix with that of the previous step.
   (a) If the procedure has not converged, return to step 2 with the new density matrix.
   (b) If the procedure has converged, use the resultant solutions to calculate expectation values and other quantities of interest.

3.1.3 Post-Hartree-Fock methods

The HF Method, though meeting with success in many cases, is a mean-field theory that neglects electron correlation, that is, explicit electron-electron interactions. The correlation energy is defined as follows [50]:

$$E_{corr} = E_0 - E_{HF} \tag{3.18}$$

where E_0 is the exact nonrelativistic energy of the system and E_{HF} stands for the HF energy. Since the HF method is variational, E_{HF} constitutes an upper bound to the exact energy and,

therefore, the correlation energy is negative. Typically, E_{HF} represents, in absolute terms, 99% of the E_0. The portion left, E_{corr}, small as it may be, undertakes sizable changes in chemical processes and much effort has been required to recover it. As a consequence, a plethora of quantum chemical approaches based on the HF determinant have emerged, also known as post-HF methods. Examples of such approaches are presented in the following lines.

Møller-Plesset Perturbation Theory

Within the Møller-Plesset Pertubation Theory [50] the model Hamiltonian $\hat{H}_0$, also called Fockian $\hat{F}$, represents a model of N non-interacting electrons and has the form:

$$\hat{F} = \sum_i (\hat{h}_i + \hat{J}_i + \hat{K}_i) = \sum_i (\hat{h}_i + \hat{g}_i) \tag{3.19}$$

where $\hat{g}_i$ is the bielectronic operator comprising the Coulomb ($\hat{J}_i$) and exchange ($\hat{K}_i$) operators.

$$\hat{J}_i\psi_j(1) = \int \psi_i^*(2)\frac{1}{r_{12}}\psi_i(2)dr_2\psi_j(1) \tag{3.20}$$

$$\hat{K}_i\psi_j(1) = \int \psi_i^*(2)\frac{1}{r_{12}}\psi_j(2)dr_2\psi_i(1) \tag{3.21}$$

The perturbation operator $\hat{V}$, also termed fluctutation potential, is given by the difference

$$\hat{V} = \hat{H} - \hat{F} \tag{3.22}$$

As one may notice from equation 3.19, the HF wave function $\Psi_0^{(0)}$ is eigenfunction of $\hat{F}$, and the corresponding eigenvalue $E_0^{(0)}$ is

$$E_0^{(0)} = \langle \Psi_0^{(0)} | \hat{F} | \Psi_0^{(0)} \rangle = \sum_a^N \epsilon_a \tag{3.23}$$

where a runs over the occupied orbitals. Similarly, any other Slater determinant, $\Psi_i^{(0)} = \{\Psi_a^r \Psi_{ab}^{rs}, ...\}$, built up from the HF wave function by substituing occupied molecular orbitals a, b with unoccupied r, s, is also eigenfunction of $\hat{F}$. The first order correction (MP1) delivers

the HF energy. Accordingly, the first contribution to the correlation energy comes from the second order term:

$$E_0^{(2)} = \langle \Psi_0^{(0)} | \hat{V} | \Psi_0^{(0)} \rangle = -\sum_{k \neq 0} \frac{|\langle \Psi_0^{(0)} | \hat{V} | \Psi_k^{(1)} \rangle|^2}{E_k^{(0)} - E_0^{(0)}} \tag{3.24}$$

Only doubly excited determinants contribute to equation 3.24. Singly-excited determinants do not interact with the HF wave function, as stated by Brillouin's theorem [50].

Configuration Interaction

The configuration interaction (CI) is a post-HF linear variational method. It expresses the wave function of a N-electron system $|\Phi_0\rangle$ as a linear combination of Slater determinants. The expansion reads as follows

$$|\Phi_0\rangle = c_0|\Psi_0\rangle + \sum_{ar} c_a^r |\Psi_a^r\rangle + \sum_{a<b,r<s} c_{ab}^{rs} |\Psi_{ab}^{rs}\rangle + \sum_{a<b<c,r<s<t} c_{abc}^{rst} |\Psi_{abc}^{rst}\rangle + ... \tag{3.25}$$

where $|\Psi_0\rangle$ stands for the ground state HF wave function and $|\Psi_a^r\rangle$, $|\Psi_{ab}^{rs}\rangle$ and $|\Psi_{abc}^{rst}\rangle$ refer to singly, doubly and triply excited configurations, with a, b and c denoting occupied orbitals and r, s, and t unoccupied ones in $|\Psi_0\rangle$. Coefficients c_0, c_a^r, c_{ab}^{rs}, c_{abc}^{rst}, etc., are variationally optimized. As the basis set becomes infinitely flexible, full CI (FCI) approaches the exact solution of the time-independent, non-relativistic Schrödinger equation. The FCI method has many of the desirable features of a theoretical model. It is well-defined, size-consistent, and variational. However, it is also computationally very expensive and impractical for all but the very smallest systems. Practical CI methods augment the HF wavefunction by adding only a limited set of substitutions, truncating the CI expansion at some level of substitution. For example, the CIS method adds only single excitations to the HF determinant, CID adds double excitations, CISD adds both singles and doubles, CISDT adds singles, doubles, and triples, and so on.

However, one of the main troubles of truncated CI models is that they do not satisfy the size-extensivity properties, in the sense that the energy does not grow linearly with the number of electrons in the system. Nevertheless, the truncation is often justified because the vast major-

ity of the excited configurations contribute minimally to the ground state wave function and correlation energy. According to the calculation of electronic excited states, the configuration interaction singles (CIS) method defined above is the simplest excited state method. However, excitation energies calculated with the CIS method are often overestimated by about 0.5-2.0 eV compared with experimental values or highly accurate calculations [51]. This is because CIS lacks dynamic correlation. A way to improve CIS is reached by including dynamical correlation through a perturbative correction. This is the case of the CIS(D) approach [52, 53], which introduces double excitation effects for the excited states. Within the CIS(D) approach, the excitation energies are improved relative to those calculated with CIS and it is applicable to relatively large molecules by the use of the resolution of identity (RI) approximation [54, 55], where the use of auxiliary basis expansions reduces considerably the computational cost. An additional improvement could be obtained by the SOS-CIS(D) approximation [56], which semi-empirically scales the opposite-spin components of the CIS(D) expression, leading to a greater accuracy and also to a reduction of computational cost. The RI and SOS approaches, however, are still rather expensive and limited to small and medium-size molecules.

Coupled Cluster

Within the Coupled Cluster (CC) method [57, 58] the exact wave function of the ground state of a N-electron system $|\Phi_0\rangle$, written in the second quantization language, reads as

$$|\Phi_0\rangle = e^{\hat{T}}|\Psi_0\rangle \tag{3.26}$$

where $|\Psi_0\rangle$ stands for the ground state HF wave function and $\hat{T}$ refers to the cluster operator. This latter comprises several terms

$$\hat{T} = \hat{T}_1 + \hat{T}_2 + \hat{T}_3 + ... \tag{3.27}$$

which, expressed in terms of the creation (a_r^+) and annihilation operators (a_a), have the form

$$\hat{T}_1 = \sum_{a,b} c_a^r a_r^+ a_a \tag{3.28}$$

$$\hat{T}_2 = \sum_{a,b} \sum_{r,s} c_{ab}^{rs} a_r^+ a_s^+ a_a a_b \tag{3.29}$$

where a and b denote occupied orbitals and r and s unoccupied ones. Recall that the creation operator (a_r^+) creates an electron in orbital r included in $|\Phi_0\rangle$, whereas the annihilation operator (a_a) annihilates an electron in orbital a, in such a way that

$$a_r^+ a_a |\Phi_0\rangle = |\Phi_a^r\rangle = |\Phi_1 \Phi_2 ... \Phi_{a-1} \Phi_r \Phi_{a+1} ... \Phi_N\rangle \tag{3.30}$$

$$a_r^+ a_s^+ a_a a_b |\Phi_0\rangle = |\Phi_{ab}^{rs}\rangle = |\Phi_1 \Phi_2 ... \Phi_{a-1} \Phi_r \Phi_{a+1} ... \Phi_{b-1} \Phi_s \Phi_{b+1} ... \Phi_N\rangle \tag{3.31}$$

The choice of the exponential ansatz effectively introduces high order excitations. For example, the quadruples and sextuples excitations can be written in term of the doubles. Besides, the exponential form of the CC ansatz guarantees the size extensivity of the solution as long as a suitable reference function is chosen. A criticism of the method is that it is not variational, so the total energy can be lower than the true total energy. However, this is not a problem since we are usually interested in relative energies rather than the absolute values. The abbreviations for coupled-cluster methods usually begin with the letters "CC" (for "coupled cluster") followed by S, D, T, Q for single, double triple or quadruple excitations, respectively. CCSD is often employed for benchmark purposes. CCSD(T) poses a further improvement, which includes the triples excitations in a perturbative fashion.

The post-HF methods presented up to now might be quite demanding computationally and they are amenable a limited set of small to medium size systems. Among the *ab initio* methods devised to recover the electronic correlation, the perturbative Möller-Plesset (MP) method, truncated to the second-order of perturbation (MP2), is probably the better suited for large systems. To understand the construction of the MP2 approach, the basic notions of the Rayleigh-Schrödinger Perturbation Theory should be given.

3.2 Density functional theory

The problem in wave function based methods is that the electronic wave function is a $3N$-dimensional object (or $4N$-dimensional if spin is considered) and its complexity rapidly increases with the size of the system. In this framework, density functional theory (DFT) [59] emerged as a promising method for electronic structure calculations. It replaced the N-electron wave function by the electron density, which is a function of three spatial variables, and, therefore, much simpler. In essence, the method takes the electron density as the variable of a functional, concretely, the energy of the system is described as the functional of the electron density, $E[\rho(\mathbf{r})]$.

In this work, DFT is applied within the Born-Oppenheimer approximation, which means that the nuclei are fixed and the electrons move in the potential created by those fixed nuclei, known as the external potential (see section 3.1.1).

Hohenberg-Kohn Theorems

In 1964 Hohenberg and Kohn came with a paper that constituted a real breakthrough [60]. Their theorems laid the theoretical foundations of the currently available DFT methodology.

Theorem 1: *The external potential $\hat{V}_{ext}(\mathbf{r})$ is a unique functional of the electron density $\rho(\mathbf{r})$. Since $\hat{H}$ is determined by $\hat{V}_{ext}(\mathbf{r})$, the full many particle ground state is a unique functional of $\rho(\mathbf{r})$.*

In other words, the ground state energy and other properties of a system are uniquely defined by the density $\rho(\mathbf{r})$, i.e., the energy is a functional of the electron density $E[\rho(\mathbf{r})]$. Remarkably, such a one-to-one mapping is only possible for the ground state density $\rho_0(\mathbf{r})$. The original Hohenberg-Kohn argument was limited to non-degenerate ground states. Such limitation was later lifted by Levy [61].

Let us write the ground state energy E_0 as a functional of the ground state density:

$$E_0 = E_0[\rho_0(\mathbf{r})] \tag{3.32}$$

Broken down into its several contributions, E_0 reads as

$$E_0[\rho_0] = T[\rho_0] + E_{ee}[\rho_0] + V_{ext}[\rho_0] = T[\rho_0] + E_{ee}[\rho_0] + E_{en}[\rho_0] \tag{3.33}$$

where T, E_{ee}, E_{en} and V_{ext} stand for the kinetic energy, electron-electron repulsion, nucleus-electron attraction and external potential respectively. Notice that T and E_{ee} are universal, while E_{en} depends on the actual system. Collecting the system independent terms into the so called Hohenberg-Kohn functional, $F_{HK}[\rho_0]$, E_0 in equation 3.33 reads as

$$E_0[\rho_0] = F_{HK}[\rho_0] + E_{en}[\rho_0] = F_{HK}[\rho_0] + \int \rho(\mathbf{r})\nu(\mathbf{r})d\mathbf{r} \tag{3.34}$$

where $\nu(\mathbf{r})$ is the external potential due to the nuclei, given by

$$\nu(\mathbf{r}) = -\sum_{\alpha} \frac{Z_\alpha}{r_{1\alpha}} \tag{3.35}$$

where Z_α is the nuclear charge of nucleus α and $r_{1\alpha}$ is the distance between electron 1 and nucleus α. The Hohenberg-Kohn functional $F_{HK}[\rho]$ is central to DFT. If it was known, the Schrödinger equation could be solved exactly. Moreover, it is universal and therefore, it applies equally to all the imaginable chemical systems. Unfortunately, neither $T[\rho]$ nor $E_{ee}[\rho]$ present in F_{HK} are known. $E_{ee}[\rho]$ could be divided into two

$$E_{ee}[\rho] = J[\rho] + E_{ncl}[\rho] \tag{3.36}$$

where $J[\rho]$ refers to the classical Coulomb part

$$J[\rho] = \frac{1}{2}\int \frac{\rho(\mathbf{r_1})\rho(\mathbf{r_2})}{r_{12}} d\mathbf{r_1} d\mathbf{r_2} \tag{3.37}$$

and $E_{ncl}[\rho]$ stands for the non-classical contributions to the electron-electron interaction, namely the self-interaction correction, and the exchange and Coulomb correlations.

The first theorem establishes that the ground state density $\rho_0(\mathbf{r})$ is sufficient to obtain all the properties of interest of a system. Nevertheless, it does not give a procedure to find out such $\rho_0(\mathbf{r})$. At this stage, the second theorem of Hohenberg-Kohn comes into play.

Theorem 2: *For any trial density $\widetilde{\rho}(\boldsymbol{r})$, the energy obtained from the Hohenberg-Kohn density functional represents an upper bound for the true ground state energy E_0.*

This means that the Hohenberg-Kohn functional delivers the lowest energy if and only if the input density is the true ground state density. Therefore, this second theorem shows a way to obtain $\rho_0(\mathbf{r})$ variationally. However, the variational $\widetilde{\rho}(\mathbf{r})$ has some conditions to be fulfilled. First, it has to be associated with some external potential $\nu(\mathbf{r})$ (ν-representavility). Second, it must be N-representable. It means that the density stems from an antisymmetric wave function, so that $\tilde{\rho}(\mathbf{r}) \geq 0$ and $\int \tilde{\rho}(\mathbf{r})dr = N$.

Kohn-Sham equation

The Hohenberg-Kohn theorems do not provide a explicit form of the density functional, nor do they show a way to obtain the density. In 1965 Kohn and Sham formulated an avenue to approximate the unknown Hohenberg-Kohn functional [62]. They realized that the toughest part to calculate the density functional laid on the kinetic energy. In this framework, since the orbital-based approaches like HF perform better, they introduced a non-interacting assistant system with the same density as the real system. Great part of the kinetic energy of such a system can be accurately computed. The motion of non-interacting particles is dependent on an effective one-particle potential, consisting of the external potential, the Coulomb interaction between electrons, and the exchange and correlation terms. Once the effective potential is known, Kohn-Sham (KS) method is solved in a self consistent way. In the HF approach, the ground state wave function is approximated as a single Slater determinant Ψ_{HF} constructed

from N spin orbitals χ_i. Ψ_{HF} would be the exact wave function of an assistant system of N non-interacting electrons, moving in the effective potential V_{HF}. The Hamiltonian for such system is

$$\hat{H_S} = -\frac{1}{2}\sum_i^N \Delta_i^2 + \sum_i^N V_S(\mathbf{r_i}) \tag{3.38}$$

where $V_S(\mathbf{r})$ stands for the effective local potential. Since $\hat{H_S}$ does not contain any electron-electron interactions, its ground state wave function can be described by a Slater determinant

$$\Psi_S(x_1, x_2, ..., x_N) = \frac{1}{\sqrt{N!}} \begin{vmatrix} \varphi_1(x_1) & \varphi_2(x_1) & ... & \varphi_N(x_1) \\ \varphi_1(x_2) & \varphi_2(x_2) & ... & \varphi_N(x_2) \\ ... & ... & & ... \\ \varphi_1(x_N) & \varphi_2(x_N) & ... & \varphi_N(x_N) \end{vmatrix} \tag{3.39}$$

and solved by the variational principle

$$\hat{f}^{KS}\varphi_i = \epsilon_i \varphi_i \tag{3.40}$$

where ϵ_i is the energy of the (φ_i) Kohn-Sham orbital and $\hat{f}^{KS}$ is the one-electron Kohn-Sham operator, defined as:

$$\hat{f}^{KS} = -\frac{1}{2}\Delta_i^2 + V_S(\mathbf{r}) \tag{3.41}$$

where we sum the kinetic energy to an effective potential $V_S(\mathbf{r})$. In the Kohn-Sham formulation, the effective potential $V_S(\mathbf{r})$ is chosen so that the density of the assistant non-interacting system, obtained from the Kohn-Sham orbitals (φ_i), is the same as the one of the real system:

$$\rho_s(r) = \sum_i^N \sum_s |\varphi_i(r,s)|^2 = \rho_0(r) \tag{3.42}$$

By analogy with the HF approach, the exact kinetic energy of the non-interacting reference system with the same density as the real one can be written as:

$$T_S = -\frac{1}{2}\sum_i^N \langle \varphi_i | \Delta^2 | \varphi_i \rangle \tag{3.43}$$

which is different from the real system. Therefore, Kohn and Sham rewrote the HK functional as:

$$F[\rho(\mathbf{r})] = T_S[\rho(\mathbf{r})] + J[\rho(\mathbf{r})] + E_{XC}[\rho(\mathbf{r})] \tag{3.44}$$

where the exchange-correlation energy is introduced, defined as:

$$E_{XC}[\rho(\mathbf{r})] = (T[\rho(\mathbf{r})] - T_S[\rho(\mathbf{r})]) + (E_{ee}[\rho(\mathbf{r}) - J[\rho(\mathbf{r})]) = T_C[\rho(\mathbf{r})] + E_{ncl}[\rho(\mathbf{r})] \tag{3.45}$$

T_C is the residual part of the kinetic energy between the real and the assistant systems and E_{ncl} is the non-classical electrostatic contribution. Therefore, the exchange-correlation term contains everything that is unknown. Let us rewrite the energy of the interacting system in terms of the quantities defined above:

$$\begin{aligned} E[\rho(\mathbf{r})] &= T_S[\rho(\mathbf{r})] + J[\rho(\mathbf{r})] + E_{XC}[\rho(\mathbf{r})] + E_{ne}[\rho(\mathbf{r})] \\ &= T_S[\rho(\mathbf{r})] + \frac{1}{2}\int\int \frac{\rho(\mathbf{r_1})\rho(\mathbf{r_2})}{r_{12}} d\mathbf{r_1} d\mathbf{r_2} + E_{XC}[\rho(\mathbf{r})] + \int V_{ne}[\rho(\mathbf{r})] d\mathbf{r} \\ &= -\frac{1}{2}\sum_i^N \langle\varphi_i|\Delta^2|\varphi_i\rangle + \frac{1}{2}\sum_i^N\sum_j^N \int\int |\varphi_i(\mathbf{r_1})|^2 \frac{1}{r_{12}} |\varphi_i(\mathbf{r_2})|^2 d\mathbf{r_1} d\mathbf{r_2} \\ &\quad + E_{xc}[\rho(\mathbf{r})] - \sum_i^N \int \sum_A^M \frac{Z_A}{\mathbf{r_{1A}}} |\varphi_i(\mathbf{r_1})|^2 d\mathbf{r_1} \end{aligned} \tag{3.46}$$

The variational minimization of this expression, applying the constraint $\langle\varphi_i|\varphi_j\rangle = \delta_{ij}$, leads to the following set of mono-electronic equations, known as Kohn-Sham equations:

$$\left(-\frac{1}{2}\sum_i^N \nabla^2 + \left[\int \frac{\rho(\mathbf{r_2})}{r_{12}} d\mathbf{r_2} + V_{xc}(\mathbf{r_1}) - \sum_A^M \frac{Z_A}{\mathbf{r_{1A}}}\right]\right)\varphi_i = \left(-\frac{1}{2}\sum_i^N \nabla^2 + V_{eff}(\mathbf{r_1})\right)\varphi_i = \epsilon_i\varphi_i \tag{3.47}$$

Comparing the above equation with the one-particle equations in the non-interacting reference system, we have that V_{eff} is identical to V_S:

$$V_S(\mathbf{r}) \equiv V_{eff}(\mathbf{r}) = \int \frac{\rho(\mathbf{r_2})}{r_{12}} d\mathbf{r_2} + V_{xc}(\mathbf{r_1}) - \sum_A^M \frac{Z_A}{\mathbf{r_{1A}}} \tag{3.48}$$

V_{xc} is due to the exchange-correlation energy E_{xc} which is unknown. So is the potential for which we have no clue to its explicit form. Therefore, V_{xc} is defined as the functional derivative of E_{xc} with respect to ρ:

$$V_{xc} \equiv \frac{\partial E_{xc}}{\partial \rho} \tag{3.49}$$

Unlike HF model, the Kohn-Sham approach is in principle exact. One would "just" need to know E_{xc} and V_{xc}. However, this is a daunting task and approximations are needed. The modern DFT is intended to find out the best approximation for these two terms.

Note that once V_S is known, the orbitals are determined, which dictate the ground state density and the ground state energy. However, V_S already depends on the density (and thus on the orbitals) through the Coulomb term $J[\rho]$. Therefore, the Kohn-Sham one-electron equations have to be solved iteratively, just like HF equations.

3.3 Time-dependent density functional theory

Time-dependent density functional theory (TDDFT) [63, 64], represents one of the prominent approaches to calculate excited-state properties (such as excitation energies, oscillator strengths, excited-state geometries, etc.), especially when excited states of medium-sized or large molecular systems are under investigation [65]. This is so beacuse it provides an excellent compromise between the computational cost and chemical accuracy [66]. Compared to wave function approximations, TDDFT accounts for dynamic correlation at relatively much lower computational cost. Therefore, the calculation of vertical excitation energies with TDDFT has become a sensible choice and the quality of the energies often lies within 0.1-0.5 eV [51] compared to exeperimental data. Nevertheless, one needs to be careful with TDDFT since results are quite sensitive to the choice of the exchange-correlation functional. Consequently, it is important to check the reliability of TDDFT calculations by having a wave function-based benchmark or comparing them to experimental data, as well as checking the sensitivity of the results to the choices of exchange-correlation functional.

3.3.1 Formal Foundations

The formal foundations of TDDFT rely on the Runge-Gross theorems [67], which in a sense are analogous to the Hohenberg-Kohn theorems for the ground state DFT. Runge-Gross theorem proves that densities $\rho(\mathbf{r}, t)$ and $\rho'(\mathbf{r}, t)$ of two systems evolving from the same initial state $\Psi(\mathbf{r}, t_0)$ under the influence of the scalar potentials $\nu(\mathbf{r}, t_0)$ and $\nu'(\mathbf{r}, t_0)$, both Taylor expandable about t_0 and differing by more than a purely time-dependent function, will always differ. Simply put, it states that for a given initial wave function, there exists a unique mapping between the time-dependent external potential and its time-dependent density. This theorem represents the time-dependent analogue of the first Hohenber-Kohn Theorem. The time-dependent density may be obtained from the time-dependent Schrödinger equation. This could be obtained via the popular Kohn-Sham approach. Excitation energies and other properties could then be obtained by solving the time-dependent KS equation via two different strategies (taking the strength of the time-dependent potential into consideration). One strategy, useful in case the potential is strong, is to propagate the KS wave function in real time. The second strategy, reasonable when the the potential is weak, is to use linear response TDDFT (LR-TDDFT). Within this approach, the time-dependent KS equation is solved perturbatively to first order in the frequency domain. This is appropriate for many practical situations in spectroscopy, in which the spectral response of a system to a weak probe is determined [64].

In the LR-TDDFT framework, the excitation energies (ω) and transition amplitudes are obtained from the following non-Hermitian eigenvalue equation (known as Casida's equation [64]), as eigenvalues and corresponding eigenvectors, respectively:

$$\begin{bmatrix} \mathbf{A} & \mathbf{B} \\ \mathbf{B}^* & \mathbf{A}^* \end{bmatrix} \begin{bmatrix} \mathbf{X} \\ \mathbf{Y} \end{bmatrix} = \omega \begin{bmatrix} \mathbf{1} & \mathbf{0} \\ \mathbf{0} & \mathbf{-1} \end{bmatrix} \begin{bmatrix} \mathbf{X} \\ \mathbf{Y} \end{bmatrix} \tag{3.50}$$

where the matrix elements depend on the exchange-correlation functional. For a hybrid exchange-correlation functional (incorporating part of exact exchange from Hartee-Fock theory), they are

are defined as follows:

$$A_{ar\sigma,bs\tau} = \delta_{\sigma,\tau}\delta_{a,b}\delta_{r,s}(\epsilon_{r,\sigma} - \epsilon_{a,\tau}) + (a_\sigma r_\sigma|j_\tau s_\tau) - \delta_{\sigma,\tau}c_{HF}(a_\sigma b_\sigma|r_\tau s_\tau) + (1 - c_{HF})(a_\sigma r_\sigma|f_{\sigma,\tau}|b_\tau s_\tau) \tag{3.51}$$

$$B_{ar\sigma,bs\tau} = (a_\sigma r_\sigma|s_\tau b_\tau) - \delta_{\sigma,\tau}c_{HF}(a_\sigma s_\sigma|r_\tau b_\tau) + (1 - c_{HF})(a_\sigma r_\sigma|f_{\sigma,\tau}|s_\tau b_\tau) \tag{3.52}$$

where indices a, b correspond to ground state occupied orbitals φ_a, φ_b, indices r, s correspond to virtual orbitals φ_r, φ_s and σ, τ represent spin variables. c_{HF} is the coefficient of the HF exchange in the hybrid functional and $\epsilon_{i,\sigma}$ is the energy of the spin-orbital φ_{i_σ}. The four index integrals expressed in Mulliken notation are

$$(a_\sigma r_\sigma|b_\tau s_\tau) = \int\int \varphi_a(\mathbf{r_1})\varphi_r(\mathbf{r_1})r_{12}^{-1}\varphi_b(\mathbf{r_2})\varphi_s(\mathbf{r_2})d\mathbf{r_1}d\mathbf{r_2} \tag{3.53}$$

$$(a_\sigma r_\sigma|f_{\sigma,\tau}|b_\tau s_\tau) = \int\int \varphi_a(\mathbf{r_1})\varphi_r(\mathbf{r_1})f_{\sigma,\tau}\varphi_b(\mathbf{r_2})\varphi_s(\mathbf{r_2})d\mathbf{r_1}d\mathbf{r_2} \tag{3.54}$$

where $f_{\sigma,\tau}$ is the time-independent non-local exchange-correlation kernel in the adiabatic approximation, which form depends on the chosen exchange-correlation functional.

The Tamm-Dancoff approximation (TDA) [68] was introduced as a further approximation to Casida's equation. It corresponds to neglecting the matrix $\mathbf{B}$, that is, all contributions to the excitation energies coming from de-excitation of the correlated ground state are decoupled from the ground state excitations. This leads to a Hermitian eigenvalue equation

$$\mathbf{AX} = \omega\ \mathbf{X} \tag{3.55}$$

Remarkably, TDA is often a very good approximation to TDDFT, because it is simpler and provides, in general, excitation energies of similar quality. The TDA equation is closely related to the the CIS method, but with the $\mathbf{A}$ matrix depending on the exchange-functional. This is because the TDA approximation leads in the Time Dependent Hartree Fock (TDHF) case (also known as random-phase approximation, RPA) to CIS, while in the TDDFT case one gets TDDFT/TDA equations. Therefore, the advantage of TDA is the connection it has with wave

functions, which facilitates the characterization of electronic excitations. In practice, ground state approximate exchange-correlation density functionals are used in TDDFT calculations, in the so-called adiabatic approximation [65, 69] with the assumption that the electronic density varies slowly in time.

3.3.2 Failures of TDDFT with standard exchange-correlation functionals

Charge Transfer Excited States

TDDFT performs very well to calculate low-lying valence excited states, however, it has a difficulties in describing Rydberg states and CT excitations [70, 71, 72, 73, 74]. The excitation energies for CT states are severely underestimated (if pure standard xc-functionals are employed), what is more, the potential energy curves of CT states do not exhibit the proper $1/R$ dependence along a charge separation coordinate R [72, 75, 76]. The positive and negative charges in a CT state electrostatically attract each other and, therefore, separation of these charges must result in an attractive $1/R$ dependence. Such asymptotic behaviour of the energy along the CT separation can be grasped by considering a donor system and an acceptor system separated by a distance R. In the case of an electron transfer from the donor to the acceptor, the donor needs at least the energy corresponding to its ionization potential (I_d) and there will be an energy gain of the acceptor's electron affinity (A_a). In addition, once the electron is transferred, there will be an electron at the acceptor and a hole in the donor, which will electrostatilcally be attracted to each other, leading to a Coulombic energetic gain of $-1/R$. Consequently, the energy required to create the CT state is

$$E(R) = I_d - A_a - \frac{1}{R} \tag{3.56}$$

From the above model, one would expect the excitation energy of a CT to increase as $-1/R$. However, this is not the case when pure xc functionals, i.e, with no HF exchange, are used [77].

Imagine a CT state, where an electron is transferred from an occupied orbital i of molecule A to a virtual orbital a of another molecule B. For simplicity, we will assume that the overlap between orbitals on molecule A and orbitals on molecule B is zero. For such a state, the only terms that do not vanish of matrix $\mathbf{A}$ (from equation 3.51) are the first and the third, which are the difference of one-particle energies of donor orbital i on A and the acceptor orbital a on B and the nonlocal HF exchange part of Kohn Sham operator. This last term is not zero since orbitals i and j are both on the molecule A and the orbitals a and b are on molecule B. This is a Coulomb-like term because the created holes (orbitals i and j corresponding to the positive charge in the CT state) interact with the electrons (orbitals a and b reflecting the negative charge in the CT state), which relates to the electrostatic attraction within the CT state. Consequently, this term is crucial for the correct $1/R$ asymptotic behaviour of the potential energy curve along the intermolecular separation of the donor and the acceptor units, hence, the presence of exact exchange is vital. Similarly, matrix $\mathbf{B}$ (equation 3.52) is zero if the two orbitals involved in the CT state do not overlap.

So, all in all, it is now obvious that pure xc functionals (that is, $c_{HF} = 0$) drastically underestimate excitation energies of CT states, because they are simply given by the difference between the energies of the acceptor and the donor MOs, ϵ_a and ϵ_i, respectively. Within HF theory this is already a rough estimate for the energy of the CT state at large distances, since Koopman's theorem states that, $-\epsilon_i$ and $-\epsilon_a$ correspond to the ionization potential of molecule A and to the electron affinity of molecule B. This is because the occupied orbitals are calculated for the N-electron system, while the virtual orbitals are formally evaluated for the (N+1)-electron system. This is not the case in density functional theory following the Kohn-Sham formalism, since the same potential is used to calculate the occupied and virtual orbitals. As a consequence, while the HOMO still corresponds to the ionization potential, the LUMO is generally more strongly bound in DFT than in HF theory and cannot be related to the electron affinity. Since the negative of the LUMO energy is therefore much larger than the true electron affinity, the orbital energy difference corresponding to a CT state is usually a drastic underestimation of its correct excitation energy [78]. Therefore, such self-interaction error in DFT leads to artificial underestimation of the HOMO-LUMO gap. In addition, this electron transfer self-interaction

error leads to a wrong asymptotic energy profile of CT states computed with standard functionals [79]. The energy of the accepting orbital contains the Coulomb repulsion of orbital a with all occupied orbitals of the ground state including orbital i, which is no more occupied in the CT state. This means that the transferred electron in orbital a experiences the electrostatic repulsion with itself being in orbital i. This can be cancelled by including exact exchange.

Long-range corrected (LRC) functionals [80, 81] have been shown to be a good solution to address the failure of TDDFT for CT states. Such functionals smoothly include long-range Hartree-Fock exchange [82, 83], hence, resulting to be successful for the calculation of CT states of diverse systems. The Coulomb operator of the Hamiltonian is split into short-range and long-range components, which can be obtained by the use of the error function:

$$\frac{1}{r_{12}} = \frac{1 - \mathrm{erf}(\omega r_{12})}{r_{12}} + \frac{\mathrm{erf}(\omega r_{12})}{r_{12}} \tag{3.57}$$

The first term of the right hand side is the short-range component and on a length of $\approx 1/\omega$ it decays to zero, while the one on the left hand side consists of a long-range component. The ω parameter determines the proportion between the two ranges depending on the value of r_{12} and it is determined empirically or by physical arguments [84], and the most commonly used values are in the 0.2-0.4 bohr^{-1} range [84]. The range-separated functional includes short-range exchange from a density functional and the long-range part is calculated with exact HF exchange. This solution of the CT problem has the clear advantage that one takes profit of the correct short-range behaviour of standard DFT xc functionals, while its incorrect long-range asymptotic behaviour due to the self-interaction error is replaced by the correct Hartree-Fock one.

3.4 Basis sets

The flexibility of the employed finite basis set is a critical aspect in order to obtain reliable results in electronic structure calculations. For instance, the basis set choice is very important for modeling chemical bonding, because the bonds are often polarized. The charge distribution

about an atom in a molecule is usually perturbed in comparison with the isolated atom. For example, the electron cloud in an isolated hydrogen atom is symmetrical, but when the hydrogen atom is present in a molecule the electrons are attracted towards the nuclei. The distortion can be considered to correspond to mixing p-type character into the 1s orbital of the isolated atom to give a form of sp hybrid. In a similar manner, the unoccupied d orbitals introduce asymmetry into p orbitals. The most common solution to this problem is to introduce polarisation functions into the basis set. The polarisation functions have a higher angular quantum number and so correspond to p orbitals for hydrogen and d orbitals for the first- and second-row elements. With these, one can model the correct shape of atomic orbitals which then become molecular orbitals within the typically applied LCAO (Linear Combination of Atomic Orbitals) approach.

The calculation of electronically excited states demands careful attention on the choice of the basis set. Polarization functions are mandatory when dealing with excited states. Also, the use of diffuse functions usually improves the computed transition energies and excited state properties. These are extended Gaussian basis functions with a small exponent, which give flexibility to the "tail" portion of the atomic orbitals, far away from the nucleus. Therefore, they are important for describing long-range interactions, as it is the case in electronically excited states, in which charge transfer processes may take place between far apart regions [85].

3.4.1 Basis set superposition error (BSSE)

The BSSE is a technical problem, specially notorious in dimers and molecular aggregates in general. The problem arises as a consequence of the sharing of basis set corresponding to each monomer, whenever they form a bigger system. Originally introduced by Liu and McLean in 1973 [86], it was firstly reported by Kestner in 1969 [87]. Let us consider a dimer (AB) formed by monomers A and B, each monomer being stabilized at the dimer since B donates basis functions to A and vice versa. This situation cannot occur in the separated monomers and, therefore, the dimer results to be overstabilized. The BSSE would be expected to be particularly significant when small, inadequate basis sets are used, e.g., the minimal basis STO-nG basis sets, which do not provide an adequate representation of the electron distribution far

from the nuclei, particularly in the region where non-covalent interactions are strongest. The counterpoise correction [88] is a rather simple technique to mitigate the BSSE. It includes the neighbour monomer's orbitals in the monomeric calculations so as to have "the same" basis set as in the dimer. In the general case:

$$A + B \rightarrow AB \tag{3.58}$$

$$\Delta E = E(AB) - [E(A) + E(B)] \tag{3.59}$$

The calculation of the energy of the individual species A is performed in the presence of 'ghost' orbitals of B; that is, without the nuclei or electrons of B. A similar calculation is performed for B using ghost orbitals on A. An alternative approach is to use a basis set in which the orbital exponents and contraction coefficients have been optimised for molecular calculations rather than for atoms. The relevance of the BSSE and its dependence upon the basis set and the level of theory employed remains a subject of much research.

3.5 Accounting for solvent effects. The polarizable continuum model

The vast majority of the experimental studies regarding the photophysical/photochemical properites of molecular systems are performed in solution. Therefore, it is important to mimic solvent effects in electronic structure calculations. When specific solute-solvent interactions, e.g., hydrogen bonds, non-covalent interactions, etc., are not relevant, the electrostatic interaction between the solute an the solvent could be modelled with implicit solvation models. Conceptually, a solvated molecule can be thought as a process in which first a cavity has to be created in the solvent in order to place the solute molecule. Then, the cavity is polarized due to the electric field created by the solvent. The produced cavity's polarization generates an electric field at the solvent molecule. It is this last effect that can be modelled as a perturbation operator that is added to the Hamiltonian of the solute in the gas phase.

The most popular implicit solvation model among standard quantum chemistry packages are polarizable continuum models (PCM) [89, 90, 91], also known as dielectric continuum models or "apparent surface charge" SCRF models, in which the quantum chemical description of a molecular system is coupled to a continuum description of the environment. Among this family, the most popular implemented versions are the conductor-like model (C-PCM) and the "integral equation formalism" (IEF-PCM). In such models, the solute is embedded in a polarizable continuum of dielectric ε. First a cavity is created in order to accommodate the solute. The free energy variation of this step is called cavitation energy. When the molecule of the gas phase geometry and electronic structure is placed inside the cavity, the electric field created by the molecule polarizes the continuum and an electrostatic potential arises in the cavity. Such electrostatic potential is called reaction potential and interacts with the molecule and generates a total free energy change. The free energy change arising from the solute-solvent, solvent-solvent and internal solute electrostatic interactions is called electrostatic contribution. Finally, the solute-solvent dispersion energy gives rise to the dispersion term. The solvation free energy is the free energy change to transfer a molecule from vacuum to solvent and can be defined as follows:

$$\Delta G_{sol} = \Delta G_{elec} + \Delta G_{disp} + \Delta G_{cav} \tag{3.60}$$

When the solvent is treated as a continuum, the Laplacian of the reaction potential ($\phi(r)$) is related to the free charge density ($\rho(r)$) by the Poisson's equation for a constant dielectric:

$$\varepsilon \Delta \phi(\mathbf{r}) = -4\pi\rho(\mathbf{r}) \tag{3.61}$$

The polarizable continuum model solves the electrostatic problem by introducing a charge distribution spread on the cavity surface [92, 93]. The cavity volume is obtained by adding the van der Waals spheres of the solute's atoms. Since the surfaces of these volumes are irregular, no analytic function could fit them and, therefore, ΔG_{elec} is calculated numerically. The cavity surface is divided into a large number of small surface elements, refered to as *tesserae*, and a point charge is associated with each surface element. The reaction potential is then added to

the solute Hamiltonian and it is solved iteratively by SCF.

$$\hat{H} = \hat{H}_0 + \phi(\mathbf{r}) \tag{3.62}$$

After each SCF iteration new values of the surfaces charges are calculated from the current wave function to update the reaction potential, which is used in the next iteration until the solute wave funtion and the surface charges are self-consistent. Overall, these models determine the total electrostatic potential arising from the given charge distribution by solving the classical Poisson equation with several approximations. The total potential consists of the solute's potential and the continuum's solvent one, the latter one being a reaction field potential arising from polarization of the solvent medium.

When considering an excited state, there is a sudden change in the solute's charge distribution. In that scenario, the solvent responds in two different ways to changes in the state of the solute: the solvent have time to polarize its electron distribution, this process is very rapid and only the electrons of the solvent can follow such a response. The remaining degrees of freedom (nuclei), follow a slow process and remain unchanged as in the initial state. Such splitting of the solvent response can be treated in two extreme time regimes: the non-equilibrium and the equilibrium regime. In the non-equilibrium regime, the fast and the slow processes are treated separately: the electronic polarization of the solvent is treated in equilibrium with the solute's excited state electronic density, while the slow degrees of freedom remain in equilibrium with the ground state electron density. An equilibrium calculation, on the other hand, describes a situation where all degrees of freedom (both the electronic and nuclear) of the solvent had time to fully respond to the solute, thus, they are considered equilibrated with the electron density of the electronic state that wants to be studied of the solute. It is important to know that the non-equilibrium solvation is appropriate for processes which are too rapid for the solvent to have time to fully respond to changes in the solute, this is the case of vertical excitations. However, the equilibrium solvation should be chosen for slower process, such as a geometry optimization (a process that takes place on the same time scale as molecular motion in the solvent). PCM is able to describe both situations because two different dielectric constants can be considered.

When dealing with non-equilibrium solvation, the dynamic (optical) dielectric constant of the solvent is used. While for equilibrium solvation, the static (zero-frequency) dielectric constant is considered. In the literature, two different approaches have been developed for describing nonequilibrium solvent effects: the linear response (LR) approach [94] and the state-specific (SS) [95]. In the LR formulation, the dynamic polarization of the solvent to the excitation is computed from the transition density. This means that the excitation energies are determined from the solvated ground state and the SCRF is included in the conventional excited state calculation. The LR is well-suited for transitions in which there is a small change of the electron density, because the electrostatic interaction between the solvent and the excited state density does not vary a lot compared to that of the ground state. By contrast, when excitations involving a large density rearrangement are computed, the SS approach should be used, since it considers the capability of part of the solvent degrees of freedom to instantaneously respond to changes in the solute wave function upon excitation and this effect is not accounted for in the LR approach. In the SS approach, a single excited state is modelled and its energy is determined by making the electrostatic potential generated by the excited state density self consistent with the solvent reaction field, that is, the solute is polarized self-consistently with respect to the solvent's reaction field. Consequently, in the SS approach, the excitation energies are calculated from the difference in the energy of each state, for which each electronic density is solved self consistently with the solvent reaction field.

3.6 Computational tools for the characterization of excited states

3.6.1 Transition dipole moment and oscillator strength

According to the electric dipole approximation, the probability for a transition between two electronic states (Ψ_i and Ψ_f) is proportional to the square of the transition dipole moment $\boldsymbol{\mu}$, which in the basis of adiabatic states (stationary states of the electronic Hamiltonian within

the Born-Oppenheimer approximation) is given as

$$\boldsymbol{\mu} = \langle \Psi_i | q\mathbf{r} | \Psi_f \rangle \tag{3.63}$$

This expression represents the effective electric dipole moment of the molecule in a transition between two electronic states. In this case, we have considered the Franck-Condon [96] approximation, taking $\boldsymbol{\mu}$ to be independent of the nuclear coordinates, that is, truncating the Taylor series of $\boldsymbol{\mu}$ about the equilibrium geometry of the initial state to first order.

The transition dipole moment is related to the oscillator strength f as follows:

$$f = \left(\frac{8\pi^2 m_e \nu}{3he^2} \right) |\boldsymbol{\mu}|^2 \tag{3.64}$$

where ν is the excitation frequency, m_e is the mass of the electron, e is the charge of the electron and h is the Planck constant.

The oscillator strength does not have any dimension and is also related to the intensity of an electronic transition by the area under the absorption band:

$$f = 4.135 \cdot 10^{-9} \int \epsilon(\bar{\nu}) d\bar{\nu} \tag{3.65}$$

where $\bar{\nu}$ is the mean absorption frequency and ϵ is the molar extinction coefficient measured experimentally when recording an absorption spectrum and the numerical prefactor is in units of cm^{-1}. Consequently, the oscillator strength is able join the macroscopic world (the experimental intensities of a spectrum) with a quantum mechanical observable, which accounts for the electronic structure of the absorbing molecules.

Within the Thomas-Reiche-Kuhn sum rule [69], the sum of the oscillator strengths of the transitions from one state to all the other states must be equal to the total number of electrons of the system. This rule is valid when calculations are performed with TDDFT and only if the basis set is complete (containing an infinite set of functions). However, this is not the case for

excitations in real systems. In addition, the rule is not satisfied for TDA calculations neither.

The probability of an excitation can be deduced from the expressions in 3.63 and 3.64. Since TDA is related to CIS, we could think of an excited state wave function as a linear combination of single excitations from the reference ground state Slater determinant. Imagine that the first excited state (S_1) of a system corresponds mainly to an HOMO-LUMO transition, because of the one-electron nature of the dipole moment operator in expression 3.63, the integral will only depend on these orbitals. Therefore, in this single-excitation picture, HOMO and LUMO orbitals need to overlap with each other, but because of the presence of the position operator, the larger it is the separation between them, the larger will be the transition dipole moment. As a result, the structure of Donor- π- Acceptor dyes suits perfectly to obtain large oscillator strengths, since the HOMO and LUMO are spatially separated, but still they overlap because of the π-conjugated bridge.

3.6.2 Charge Transfer Characterization

Mulliken charges come from the Mulliken Population Analysis (MPA) [97, 98] and give a good estimation of partial atomic charges from the density matrix. The method is very simple and, as a result, have become popular to provide qualitative interpretations. When excited states are calculated, Mulliken charges associated to an electronic transition can be estimated from hole and particle transition density matrices. In this way, one can easily measure the CT extent of an excited state: the difference in charge between the initial and final states (the transition charge) quantifies the number of electrons relocated in the molecule upon the excitation. However, the problem is that Mulliken charges are very sensitive to the basis set choice, since charges on atomic centers are assigned on the basis of the total electron density in basis functions located on each center. In addition, it is well accepted that MPA can result in unreasonable atomic charges due to incompleteness of atom-centred basis sets and the presence of diffuse functions that do not resemble atomic orbitals. Natural Population Analysis (NPA) proposed by Weinhold and Reed [99, 100] was designed to fix the problems existing in the Mulliken scheme by constructing a set of natural atomic orbitals (NAOs) in an arbitrary atomic basis set. The construction of

these natural orbitals begins with occupancy-weighted symmetric orthogonalization of atom-centred basis functions that are separated into a highly occupied natural minimal basis and a largely unoccupied natural Rydberg basis [101]. This procedure produces an orthonormal set of atomic orbitals that retain a great degree of their atom-centred features, thus ensuring that the shape of the strongly occupied orbitals is preserved better than that of the weakly occupied ones (referred to as Rydberg orbitals) that consist of many diffuse orbitals from using extended basis sets. The diagonal elements of the density matrix made from the NAOs represent the electron occupancies of each NAO summing exactly to the total number of electrons. The natural orbitals are known to be inherent to the wave function, rather the quality of the basis set. The NPA scheme has been recognized as a reliable tool for calculating atomic charges and has been widely used for studying donor–acceptor interactions [100]. Therefore, both MPA and NPA are an efficient way to quantify the CT character of electronic states.

Chapter 4

Optical properties of quadrupolar and bi-quadrupolar dyes: intra and inter chromophoric interactions

4.1 Introduction

The dynamics of charge and energy transport in biological systems and functional organic materials strongly rely on how chromophores interact in π-stacked assemblies [19, 20, 21, 22, 23, 24]. Because dye aggregation has important outcomes in the area of organic electronics and photonics, there is a strong need to establish reliable relationships between orbital overlap in organic solids and optical and electronic properties. However, this task remains extremely difficult owing to the manifold structural parameters that dictate exciton coupling in the crystal state. Moreover, three-dimensional organization of dye molecules in single crystals and thin films is very hard to predict [25], which makes it difficult to design new materials with tailored functions.

Boron difluoride complexes of curcuminoids represent a versatile class of dyes combining electron donor (D) and acceptor (A) units in a D-A-D quadrupolar-like architecture, in which A is

the central dioxaborine ring (DOB) and D are the terminal aromatic moieties [102, 103, 104, 105, 106]. Optical properties in the solid state are among the most interesting attributes of curcuminoids-BF_2 [107, 108]. Thin films of those dyes for example were shown to display an intense near infrared fluorescence emission, which led to the generation of electroluminescent and lasing materials with unprecedented performances [109]. Single-crystal X-ray diffraction studies have shown that curcuminoids-BF_2 molecules self-assemble into π-stacks in which the π-conjugated backbones are tightly packed and interact strongly [102, 107, 108]. These observations prompted us to undertake the design of model dimeric aggregates and the investigation of their UV-vis absorption properties in order to derive insights into exciton coupling in well-defined aggregate packings.

The work presented herein was performed within the framework of a collaboration with the group of Prof. Frédéric Fages in the University of Marseille, in which we were in charge of the computational part. Nevertheless, for the sake of completeness, we report in this Chapter the entirety of the results, including experimental syntheses and optical characterizations. The group of Fages synthesized a series of covalently-tethered bichromophoric dyes in which two curcuminoid-BF_2 units are connected through a polymethylenic chain that acts as a flexible transparent linker (Figure 4.1). Many examples can be found in literature that report folding-driven intramolecular interaction between polycyclic aromatic hydrocarbons and dyes in nonconjugated systems. They enabled the investigation of excimer and exciplex formation [110], exciton coupling [111, 112] photodimerization [113], electron and electronic energy transfer [114, 115]. Unlike aromatic compounds that generally form excited-state dimers (excimers) [110], dipolar dyes possessing a large value of the dipole moment have a strong ability to self-associate in the ground state [112]. In their bichromophores, the preference for the open vs. folded form is directly linked to the ability of the solvent to solvate the chromophore [112, 116]. Symmetrically substituted curcuminoid-BF_2 have a ground state dipole moment oriented perpendicularly to the long molecular axis and its value has been found between 5 and 12 D depending on the strength of the lateral electron D group [108]. Electrostatic dipole-dipole interactions are thus expected to provide a large contribution to noncovalent chromophore ground state self-assembly toward the folded form in solvents of low polarity. This behavior is

in agreement with that prevailing in dipolar chromophores, but the main difference in the latter systems relative to curcuminoids is that the dipole moment is aligned with the donor-acceptor molecular axis [117].

Here we describe the synthesis of bichromophoric compounds **1'-3'** (Figure 4.1) in which an oct-1,8-diyl chain linker has been chosen in order to limit geometrical constraints in the folding process. The optical properties of **1'-3'** are compared to those of the corresponding monomeric reference compounds **1-3**. Compound **1** is a symmetric chromophore with two para-methoxyphenyl (PMP) electron donor units while dye **2** is a nonsymmetric molecule containing PMP and triphenylamino (TPA) as donor groups. Compound **3** is the meso-phenyl (*m*Ph) derivative of dye **1**. We provide a theoretical investigation of monomers **1-3** and tethered dimers **1'-3'**, and correlate the calculated data with data obtained from UV-vis spectra in solvents of different polarity. We also bring useful insights into the electronic nature of the ground and singlet excited states.

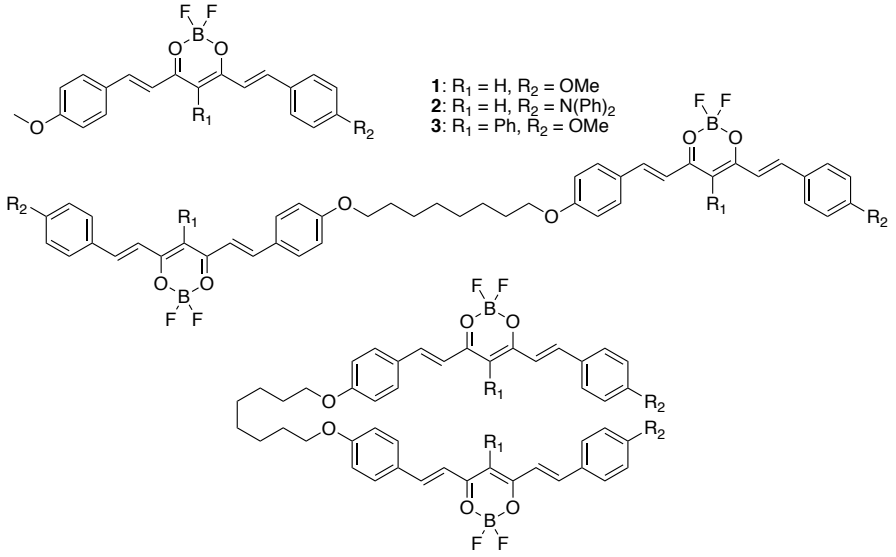

Figure 4.1: Borondifluoride curcuminoid monomers **1-3** (top), as well as open (middle) and folded (bottom) homodimers chemically linked through an octyl chain. Covalent dimers of **1-3** are labeled **1'-3'** in the text.

4.2 Experimental and computational details

4.2.1 UV-vis absorption measurements

The group of Prof. Fages recorded UV/Vis absorption spectra at room temperature (20-25 °C) on a Varian Cary 50. Solutions were prepared using spectroscopic grade solvents with concentrations ranging from 5×10^{-5} to 5×10^{-7} M in order to check the absence of any contribution of intermolecular aggregation. UV/Vis measurements were performed using quartz cuvettes with 1 cm and 5 cm optical path.

4.2.2 Quantum chemical calculations

Ground state geometry optimizations of curcumin derivative monomers and structural conformers of curcumin dimers were performed using DFT with the ωB97X-D exchange-correlation functional [118] (XCF) and the 6-31+G(d) basis set. The use of a long-range dispersion-corrected XCF was employed in order to accurately describe weak interactions, in particular the chromophore packing in the folded conformations of dimeric species. Basis set superposition error (BSSE) [119, 120] between energies of folded and open forms was corrected by means of the counterpoise (CP) scheme [121]. The computed CP energy correction is 3.7 kcal/mol (see Appendix A). Molecular structures of monomers were confirmed to be real minima on the potential energy surface by subsequent calculation of harmonic vibrational frequencies at the same level of theory. The structures showed positive force constants for all normal modes of vibration. Computed vibrational frequencies have been scaled by a 0.95 factor in order to correct the systematic slight overestimation obtained at the DFT level [122].

Molecular excitation energies were calculated using TDDFT (time-dependent density functional theory) with and without the Tamm-Dancoff approximation (TDA) [123]. The dependence of excitation energies and electronic character of low-lying transitions has been explored for different XCFs and basis sets (Tables A1-A10 and A19). The nature of computed states obtained with B3LYP, Coulomb-attenuating B3LYP (CAM-B3LYP) [124] and ωB97X-D [118] energy

functionals are qualitatively equivalent for the three considered monomers and the folded conformations of dimers **1'** and **3'**, as well as for the two lowest excited singlets of the V-shaped form of dimer **2'** (Figures A2 and A3, and Tables A5 and A10). In this chapter, we only discuss the results obtained with the B3LYP functional, which provides vertical excitation energies at the Franck-Condon region closer to experimental absorption maxima.
Solvent effects were taken into account by means of the conductor-like polarized continuum model (C-PCM) [125, 126, 127]. Transition energies in solution have been computed with the linear response (LR) approach [128, 129].

Computation of the diabatic states ($\{Z_i\}$) was performed for TDA states in vacuum and by means of the Edmiston-Ruedenberg localization scheme [130], since it is not available for TDDFT states. The number of adiabatic states considered correspond to the number of intra and inter-CT contributions in each case, i.e., 2 intra-CT in monomers **1** and **2**, and 3 intra-CT in monomer **3**. Curcumin dimers also include the 4 inter-CT excitations. Concretely, diabatization of curcumin monomers was obtained from 2 adiabatic states for dyes **1** and **2**, and 3 adiabats for molecule **3**, while the diabatization of the corresponding covalent homodimers was performed by considering the lowest 8 (**1'** and **2'**) and 10 (**3'**) excited singlets. Electronic interaction between diabatic states (electronic couplings) have been obtained as the off-diagonal elements of the diabatic Hamiltonian ($H_{ij} = \langle Z_i|\hat{H}|Z_j\rangle$). All calculations were performed with the Gaussian09 package [131] and the Q-Chem program [132].

4.3 Results and discussion

4.3.1 Synthesis

The synthetic routes to the compounds are described in Appendix A (Scheme A1). Monomers **1** and **3** were synthesized as described previously [102]. The synthesis of compound **2** was performed in two steps according to procedures reported for the preparation of nonsymmetric curcuminoids-BF_2.[133, 134] The BF_2 complex of hemicurcuminoid **H1** was subjected to an

aldol-type condensation reaction with 4-(N,N-diphenylamino)benzaldehyde (TPA-aldehyde) to give **2**.

Similarly, the synthesis of the bichromophoric dyes required dissymetrisation of the corresponding (acetylacetonato)difluoroboron to obtain a hemi-curcuminoid derivative. To this end, two synthetic routes have been followed (Scheme A1). Dimer **1'** was obtained in 12% yield from the condensation of hemicurcuminoid **H1** with 4,4'-[1,8-octanediylbis(oxy)]bis-benzaldehyde [135]. Synthesis of the dimers **2'** and **3'** involved instead the preparation of the bis-hemicurcuminoid dimers **H2** and **H3** (yields 35% and 15%, respectively) that were reacted in a second step with the corresponding aldehyde. Finally, **2'** and **3'** were obtained as pure solids after chromatography on silica gel (yields 11% and 18%, respectively). The structure of all compounds was confirmed by ^{1}H and ^{13}C NMR spectroscopy (for the soluble compounds) and by high resolution mass spectrometry (HRMS).

4.3.2 Low-lying excited singlets of curcuminoid monomers

Ground state optimized geometry of **1** exhibits all carbon and oxygen atoms on the same molecular plane, allowing for π-electron delocalization along the π-conjugated path containing an odd number of sp^2-hybridized carbon atoms. The conjugation extent in the other two molecules is similar, with tilted edge Ph groups of TPA in **2** and the mPh group orthogonal to the main molecular plain in **3**, i.e., dihedral angle $\theta = 90°$. Ground state potential energy profile along the torsion mode of the mPh moiety in **3** indicates that room temperature thermal energy should be enough to allow the rotation of the phenyl within a rather wide range, i.e. $60° \leq \theta \leq 90°$ (Figure A4). Therefore, in addition to the computationally most stable geometry of **3** ($\theta = 90°$), in the following study we also include the results for a non-orthogonal conformation with an energetically accessible rotation angle ($\theta = 62°$) [102]. Although occupied (virtual) molecular orbitals (MOs) are mostly localized on donor (acceptor) groups, the coplanarity between molecular fragments promotes important electron delocalization, as indicated by the shapes of the frontier MOs in Figure 4.2. Despite their structural similarities, MOs anticipate important differences between the three dyes. Namely, the asymmetric nature of the donor

groups in **2** results in the localization of the highest occupied MO (HOMO) and HOMO-1 on the TPA and PMP moieties, respectively. On the other hand, frontier MOs of monomer **3** anticipate the potential involvement of the *m*Ph π-electrons in the transition to the lowest excited states.

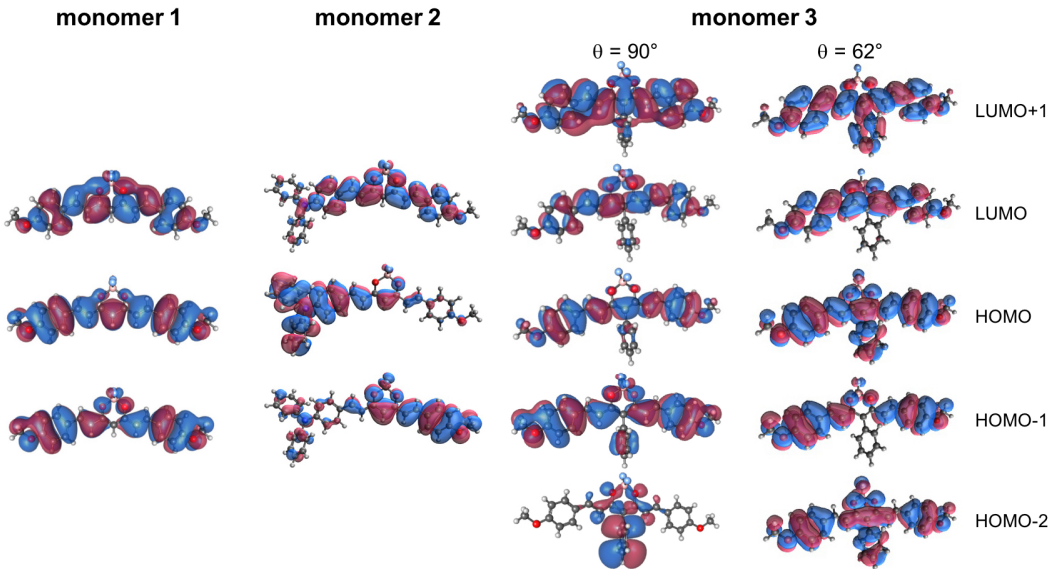

Figure 4.2: Frontier molecular orbitals of the curcumin monomers **1-3** calculated at the B3LYP/6-31+G(d) level.

Experimental absorption maxima (Figure 4.3) and computed singlet-singlet vertical transition energies and oscillator strengths of the three curcuminoids are shown in Table 4.1. TDDFT excitation energies to the lowest bright state (S_1 state) obtained for solvated molecules are in good quantitative agreement with experimental data. Besides, TDA yields excitation energies which are very close to the corresponding (full) TDDFT values, showing that the performance of TDA is essentially the same as TDDFT for this series of systems.

As shown in a previous study [134], the electronic excitation to the S_1 state of **1** at the Franck-Condon region corresponds to a $\pi \rightarrow \pi^*$ transition mainly described by the HOMO→LUMO electronic promotion. Moreover, as expected for symmetrical quadrupolar D-π-A-π-D chromophores [136], S_1 exhibits rather strong optical absorption (with large oscillator strength f), while the $S_0 \rightarrow S_2$ transition is dipole forbidden, i.e., dark state ($f \sim 0$). In the asymmetric monomer **2**, both S_1 and S_2 states are bright, and the magnitude of the computed strengths indicate larger transition probability to S_1 than to S_2, in agreement with the intensity of the

experimental absorption bands (Figure 4.3). Since the TPA moiety is a stronger electron donor group than PMP, the main contribution to the lowest excited singlet (HOMO→LUMO) corresponds to an intramolecular charge transfer (intra-CT) excitation from the TPA fragment to the central dioxaborine acceptor. The S_2 state of **2** is an intra-CT from the PMP unit. Finally, introducing a phenyl unit in the *meso* position (monomer **3**) brings out a new bright low-lying excited state, not present in **1** and **2**. At the ground state minimum ($\theta = 90°$), this new state arises as an intra-CT excitation from the *meso* substituent to the acceptor ring (S_2 state in Table 4.1). For the non-orthogonal disposition ($\theta = 62°$) the conjugated orbitals of the *m*Ph group mix with the π-system of the rest of the chromophore (Figure 4.2 and S5) and the lowest states correspond to mixings of intra-CT from both *m*Ph and the lateral PMP groups. The redshift of the main absorption band of **3** with respect to **1** is an indirect indication of the involvement of *m*Ph in the electronic transition.

Table 4.1: Vertical transition energies (eV), oscillator strengths (in parenthesis) and orbital contributions (in %) of curcumin monomers **1-3** in DCM solution calculated using the full-featured TDDFT and the TDA at the B3LYP/6-31+G(d) level, and experimental excitation energies corresponding to absorption maxima. Values in italics of **3** correspond to $\theta = 62°$. Orbital contributions correspond to TDA calculations. H = HOMO, L = LUMO.

Comp.	State	Exp.	TDDFT	TDA	Orbital contributions
1	S_1	2.54	2.50 (2.299)	2.60 (2.299)	87 H→L
	S_2	-	3.01 (0.004)	3.12 (0.004)	85 H-1→L
2	S_1	2.23	2.29 (0.982)	2.40 (0.990)	68 H→L, 18 H-1→L
	S_2	2.90	2.83 (0.746)	2.83 (0.747)	11 H→L, 72 H-1→L
3	S_1	2.46	2.60 (2.153)	2.67 (2.154)	90 H→L
			2.30 (0.799)	*2.36 (0.800)*	93 H→L
	S_2	-	3.01 (0.022)	3.15 (0.020)	97 H-2→L
			2.84 (1.007)	*2.90 (1.007)*	83 H-2→L
	S_3	-	3.33 (0.002)	3.38 (0.002)	87 H→L+1
			2.85 (0.017)	*2.87 (0.018)*	53 H-1→L, 37 H→L+1

To get a deeper insight on the nature of the various excited states in the three curcumin derivatives, we decompose the lowest (adiabatic) electronic transitions in terms of well defined contributions, referred to as diabatic states or diabats (Figure 4.4 and Table 4.2). Detailed description of the electronic diabats in terms of fragment Mulliken charges can be found as in Appendix A (Tables A13-A18). The lowest excited singlets of the symmetrical monomer **1** are built as the in-phase and out-of-phase combinations of two degenerated zwitterionic

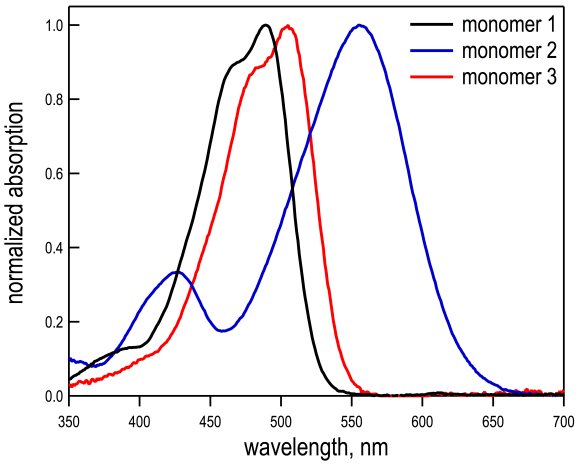

Figure 4.3: Normalized absorption spectra of molecules **1**-**3** recorded in DCM solution.

states ($S_{1,2} = Z_1 \pm Z_2$), respectively corresponding to intra-CT from each PMP moieties. The electronic coupling between the two diabats (Z_1 and Z_2) is strong ($H_{12} = 0.22$ eV), which results in a large computed gap between S_1 and S_2 (~ 0.4 eV). The different electron donating character of the terminal groups in compound **2** decouples the two diabatic states ($H_{12} = 0.02$ eV), and the two localized intra-CT diabats do not mix to form the adiabatic transitions. Diabatization of the three lowest states of the *meso*-substituted compound (**3**) at $\theta = 90°$ identifies S_1 and S_3 as being equivalent to the two lowest states in **1** (i.e. Z_1 and Z_2 symmetric mixings), while S_2 corresponds to the pristine excitation from mPh (Z_3). At $\theta = 62°$ the energy ordering of diabatic states changes, and the intra-CT from mPh (Z_3) becomes the lowest state (Figure 4.4). The non-orthogonality between mPh and PMP π-conjugated densities allows the mixing of Z_3 with the localized intra-CT from PMP units (Z_1 and Z_2), with Z_3 being the main contribution to S_1. Electronic couplings between diabatic states for **1**, **2** and the two explored conformations of **3** are shown in Appendix A (equations A6-A12).

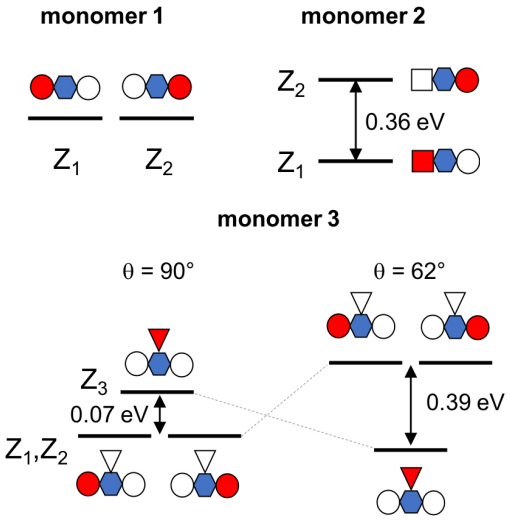

Figure 4.4: Diagramatic representation of diabatic (zwitterionic, Z_i) excited states and TDA/B3LYP/6-31+G(d) energy gaps (in eV) for curcumin monomers **1**-**3**. Different groups are indicated as circles (PMP), hexagons (DOB), squares (TPA) and triangles (mPh). Increase and decrease of fragment electron density upon excitation are indicated in blue and red, respectively.

Table 4.2: Weights (in %) of the diabatic states (Z_i) contributing to the adiabatic states (S_i) of **1**-**3**. Values in parenthesis of **3** correspond to $\theta = 62°$.

Comp.	State	Z_1	Z_2	Z_3
1	S_1	50	50	-
	S_2	50	50	-
2	S_1	100	0	-
	S_2	0	100	-
3	S_1	49	50	1
		(17)	(17)	(66)
	S_2	3	3	94
		(38)	(38)	(24)
	S_3	49	47	4
		(45)	(45)	(10)

4.3.3 Electronic absorption spectra

Solvatochromism of monomers

Comparison between excitation energies computed in gas phase and in different solvents informs of the relative stabilization of ground and excited states by means of solute-solvent dielectric

interactions (Table 4.3). In all three cases, increasing the solvent polarity induces a redshift of the transition energies to the lowest singlet in accordance with the intra-CT character of the excitation to S_1. It is also worth noticing that the largest solvatochromic effect, evaluated either by the relative position of absorption maxima recorded in different solvents (Figure A1) or as computed excitation energies, is observed for monomer **2**. This behavior can be rationalized by the dipolar nature of the transition to S_1 in **2**, while S_1 in **1** corresponds to a quadrupole [136].

Table 4.3: Excitation energies (eV) calculated at the TDDFT level (B3LYP/6-31+G*) and experimental absorption maxima for the curcumin derivatives **1-3** in solvents with different polarities: cyclohexane (CH, $\epsilon = 2.0$), di-*n*-butyl ether (DBE, $\epsilon = 3.1$) and dichloromethane (DCM, $\epsilon = 8.31$). (b) = bright state, (d) = dark state.

		gas	cyclohexane		di-*n*-butyl ether		dichloromethane	
comp.	state	TDDFT	TDDFT	Exp.	TDDFT	Exp.	TDDFT	Exp.
1	S_1 (b)	2.98	2.66	2.63	2.63	2.61	2.50	2.54
	S_2 (d)	3.42	3.07	-	3.05	-	3.01	-
2	S_1 (b)	2.94	2.41	2.34	2.33	2.33	2.29	2.23
	S_2 (b)	3.30	2.85	2.99	2.84	2.97	2.83	2.90
	S_1 (b)	2.56	2.33	2.54	2.31	2.51	2.30	2.45
3	S_2 (b)	3.18	2.81	2.71	2.85	2.68	2.84	-
$\theta = 62°$	S_3 (d)	3.21	2.83	-	2.80	-	2.85	-
	S_1 (b)	2.82	2.63	2.54	2.61	2.51	2.60	2.45
3	S_2 (d)	3.22	3.08	-	3.02	-	3.01	-
$\theta = 90°$	S_3 (d)	3.49	3.36	-	3.35	-	3.33	-

Vibronic absorption profile of monomers

Absorption profiles of monomers **1** and **3** in solution exhibit vibronic resolution with absorption peaks separated by about 1260 and 1320 cm^{-1}, respectively. Frequency calculations (Figures A7 and A8) allowed us to identify the different peaks of the spectrum with the coupling of the $S_0 \rightarrow S_1$ transition to in-plane vibrational modes computed within the 1260-1340 cm^{-1} (1340-1430 cm^{-1}) range for chromophore **1** (**3**). These modes are activated upon excitation to the S_1 state due to the $\pi \rightarrow \pi^*$ character of the transition. On the other hand, the more localized intra-CT nature of the two lowest singlets in **2** result in two absorption bands with no vibronic resolution.

4.3.4 Low-lying excited singlets of covalent curcumin dimers

Structural conformers

In the following we investigate the optical properties of covalent homodimers of borondifluoride curcuminoid derivatives **1-3** chemically linked through a polymethylenic chain (referred to as **1'-3'**, respectively). Since the length and flexibility of the polymethylenic bridge does not impose any particular arrangement between the two curcuminoid moieties, two possible structural conformations were considered: an open form in which the two curcuminoid monomers do not interact, and a folded form in which they are closely packed (Figure 4.1). The relative stability between the two structural forms is dictated by the strengths of the solvent-dye and π-stacking interactions, respectively favoring isolation of chromophores (open form) or the binding of the two dyes (folded form).

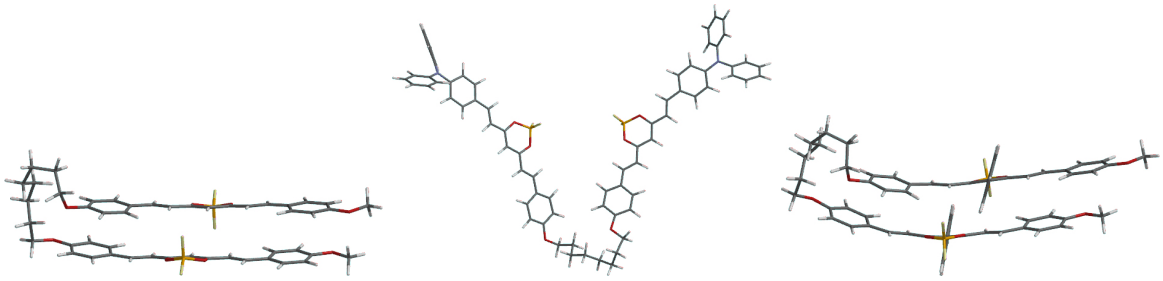

Figure 4.5: Optimized geometries for the folded form of dimers **1'** (left) and **3'** (right), and dimer **2'** (middle) in the V-shape conformation.

Electronic structure calculations of dimer **1'** (without taking into consideration entropic contributions or explicit solvent-solute interactions) predict the preference towards the folded conformer (Figure 4.5). The **1'** (folded) optimized geometry shows a sandwich-like structure of the two monomers very close to an eclipsed disposition (inter monomer slip of ~ 1.2 Å) with large superposition between equivalent PMP and DOB groups, and with the two BF_2 pointing to opposite directions in order to minimize steric hindrance and dipole-dipole interactions. The distance between the two monomeric planes is computed at 3.40 Å, i.e., within the range of typical π-π stacking interactions [137, 138, 139]. Relative energies between open and folded

conformers of **1'** computed in different solvents show how increasing the solvent's dielectric constant, which increases the chromophore's solubility, systematically reduces the relative stability of the folded form (Figure A6). Hence, increasing the strength of the dye-solvent interactions stabilizes the open form with respect to the folded conformation. This trend is in agreement with the change in experimental absorption profile measured in different solvents (Figure 4.6). The absorption spectrum of **1'** in dichloromethane (DCM) is virtually identical to the one recorded for the monomer. Decreasing the polarity of the solvent from DCM ($\epsilon = 8.3$) to di-*n*-butyl ether (DBE, $\epsilon = 3.1$) facilitates the coupling between the two chromophores within the dimer, modifying the absorption of **1'**. In particular, the absorption spectrum of **1'** in DBE exhibits a change in the relative intensity of the vibronic peaks, which might be related to the presence of H-aggregation between dyes [140]. In less polar solvents like cyclohexane (CH, $\epsilon = 2.0$), the solubility of **1'** decreases and the compounds tend to form intermolecular aggregates, resulting in a large broadening of the spectrum.

Similarly, the absorption profile of dimer **3'** in solution shows a progressive change in the relative intensity of the two main vibronic peaks upon variation of the solvent's dielectric constant, again suggesting the appearance of interactions between the two chromophoric moieties of the dimer. The computationally optimized folded form of **3'** resembles the geometry obtained for **1'**, with a similar inter-monomer separation and relative orientation, although the presence of the two *m*Ph groups induces a larger interchromophoric slip (~ 2.5 Å) along the long molecular axis (Figure 4.5).

Substitution of terminal PMP groups by TPA donors (**2'** dimer) substantially modifies the landscape of the ground state potential energy surface. The volume of the TPA group prevents the formation of the folded form and forces to decouple the two dyes, resulting in a strong preference for the open structure. Conformational search identifies a low-energy V-shaped structure of **2'** with weak inter-monomer interaction (Figure 4.5). The experimental absorption profiles of the monomer and dimer are almost identical. Moreover, the absorption coefficient of dimer **2'** measured in DCM solution ($\epsilon = 132200$ M^{-1} cm^{-1}) is, within uncertainties of the UV-Vis spectra of the two compounds, twice that of the monomer **2** ($\epsilon = 68000$ M^{-1} cm^{-1}), in accordance with a ground state open form with no detectable interaction between dyes. Only

the absorption of **2'** recorded in CH shows some deviation with respect to the spectrum of **2** pointing towards the presence of H-aggregation, *i.e.* the presence of vibronic peaks with $0 \rightarrow 2$ more intense than the $0 \rightarrow 1$ transition, which might indicate the presence of intradimer or intermolecular **2'**$\cdots$**2'** interactions due to low solubility.

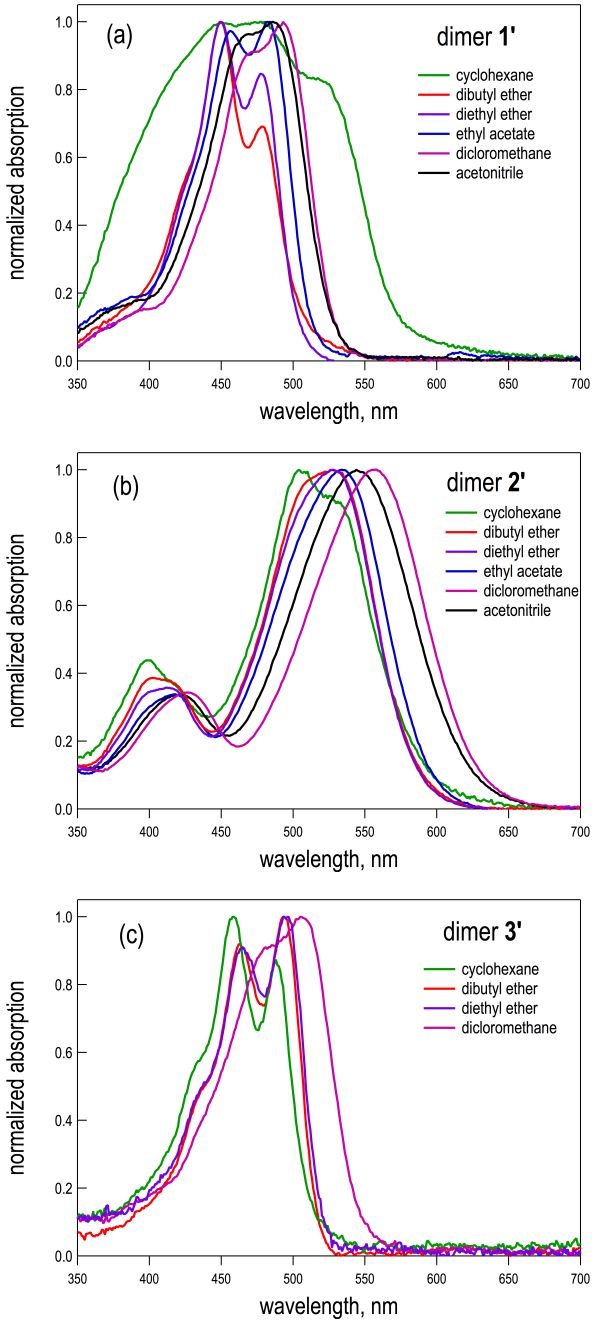

Figure 4.6: Normalized absorption spectra of dimers **1'-3'** recorded in different solvents.

Low-lying excited states of dimers

The ground state molecular geometry of the covalent curcumin derivative dimers has a large impact on their electronic properties. In the open conformations the two monomers are spatially well separated and, since the chromophores are linked through a saturated chain, the properties regarding low-energy electronic transitions correspond to two independent monomers as analyzed along the previous sections. On the other hand, the coupling of the two moieties in the folded and V-shape configurations, i.e., dimers in low-dielectric solvents, can sensibly modify the photophysical properties of dimers. In the following we characterize the low-lying electronic transitions for the folded conformation of **1'** and **3'**, and the V-shape of dimer **2'**, since they represent the most interesting and computationally challenging situations.

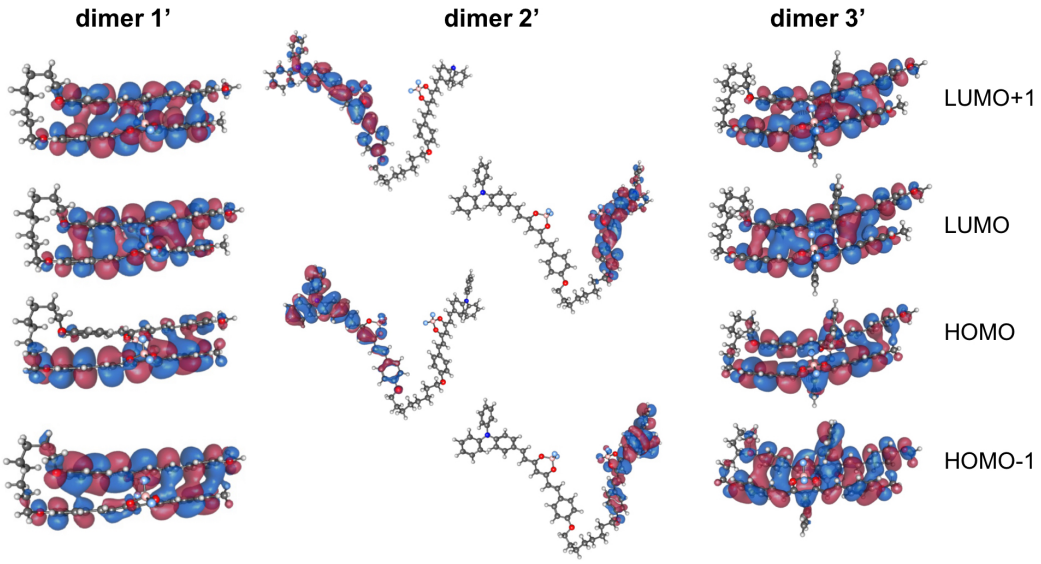

Figure 4.7: Frontier MOs of curcumin dimers **1'** and **3'** (folded conformer) and **2'** (V-shape form) computed at the B3LYP/6-31+G(d) level.

While frontier MOs of **1'** and **3'** are strongly delocalized over the two monomers, the lack of interchromophoric orbital interaction in **2'** results in a set of doubly degenerated localized MOs (Figure 4.7). In all cases, the polymethylenic bridge has merely a structural role, keeping the two monomers linked, without contributing to the photophysics of **1'-3'**. Computed excitation energies to the two lowest excited singlets of dimer **2'** (Table A.20) are very close to the value obtained for S_1 state of monomer **2** (Table 4.1). Analysis of excitation amplitudes and evaluation of charge displacements (Table A17) suggest that S_1 and S_2 of **2'** correspond to the

out-of-phase and in-phase combinations of intra-CT excitations from TPA, respectively. The gap between S_1 and S_2 in **2'** is in the order of 0.1 eV, in good agreement with the classical approximation of dipole-dipole Coulomb interactions (V_{dd}) between transition dipoles in oblique orientation [141].

$$V_{dd} = \frac{1}{4\pi\epsilon_0}\left[\frac{\boldsymbol{\mu}_1 \cdot \boldsymbol{\mu}_2}{|\mathbf{R}|^3} - 3\frac{(\boldsymbol{\mu}_1 \cdot \mathbf{R})(\boldsymbol{\mu}_2 \cdot \mathbf{R})}{|\mathbf{R}|^5}\right] = 0.11 \text{ eV} \tag{4.1}$$

where $\boldsymbol{\mu}_1$ and $\boldsymbol{\mu}_2$ are the transition dipole moments for each monomer and $\mathbf{R}$ is the distance vector between the two transition dipoles (see Appendix A for details). Computed excitation energies for **1'** predict H-type behavior, with a lowest optically inactive $S_0 \rightarrow S_1$ transition and a strongly dipole allowed $S_0 \rightarrow S_2$ transition at 2.19 and 2.59 eV, respectively. Approximately 0.1 eV above the bright S_2 state lie two nearly degenerated one-photon allowed transitions, which cannot be rationalized in terms of the Kasha's model [34] for the interaction of two chromophores. Similarly, the two lowest excited singlets of **3'** respectively correspond to dark and bright states. Transition energy to S_1 is very close to the energy obtained for dimer **1'**, while excitation to S_2 is computed at lower energy. The folded form of **3'** exhibits another low-lying dipole-allowed transition (S_3), while the rest of the computed spin-singlet transitions have rather small oscillator strengths (Tables A8 and A9).

Table 4.4: Excitation energies (in eV) and oscillator strengths (in parenthesis) computed at the TDDFT B3LYP/6-31+G* level in DCM solution for the folded forms of **1'** and **3'** dimers and the V-form of **2'**.

dimer	state	ΔE (strength)
1' (folded)	S_1	2.19 (0.008)
	S_2	2.59 (2.307)
	S_3	2.68 (1.196)
	S_4	2.71 (1.192)
2' (V-shape)	S_1	2.40 (1.171)
	S_2	2.49 (1.222)
3' (folded)	S_1	2.20 (0.009)
	S_2	2.23 (2.302)
	S_3	2.40 (1.489)
	S_4	2.55 (0.071)

Diabatic decomposition of dimers

Diabatization of the computed states for **1'** allows to describe low-lying singlet states in terms of intra- and inter-monomer CT contributions (Figure 4.8). Concretely, the lowest-energy diabats of dimer **1'** correspond to four degenerate (PMP→DOB) CT excitations in which electron density is transferred between monomers (Z_{inter}). The intra-monomer excitations (Z_{intra}) lie at slightly higher energies and they can be expressed as two doubly degenerated sets of diabats that split upon their symmetry and nature of the dipole-dipole interactions. Overall, computed excited state singlets for the folded form of **1'** exhibit large mixings between inter and intra CT diabats. In general, inter-monomer contributions dominate the composition of the lowest singlets, indicating strong electronic couplings (equation A10). The presence of important inter-CT suggests that the Kasha's rule does not hold for this system and allows for the presence of three low-lying optically active states (S_2, S_3 and S_4).

Table 4.5: Contributions (in %) of the diabatic states (Z_{inter}, Z_{intra} and Z_{meso}) for the four lowest adiabatic states (S_i, $i = 1, 4$) of dimers **1'** and **3'** (folded forms).

	1'		**3'**		
State	Z^a_{inter}	Z^b_{intra}	Z^c_{inter}	Z^d_{intra}	Z^e_{meso}
S_1	67	33	60	38	2
S_2	74	26	72	27	1
S_3	66	34	14	86	0
S_4	23	77	11	89	0

[a] $Z_{\text{inter}} = Z_1 + Z_2 + Z_3 + Z_4$, [b] $Z_{\text{intra}} = Z_5 + Z_6 + Z_7 + Z_8$,
[c] $Z_{\text{inter}} = Z_2 + Z_3 + Z_7 + Z_8$, [d] $Z_{\text{intra}} = Z_1 + Z_4 + Z_9 + Z_{10}$, [e] $Z_{\text{meso}} = Z_5 + Z_6$.

Low-energy states of **3'** are even more convoluted than in **1'** since they also include intra-monomer CT contributions from the *m*Ph group. Moreover, the interchromophoric longitudinal slip along the long molecular axis breaks the symmetry between the two PMP groups within the monomer, resulting in a lower degree of degeneracy of diabatic state energies. It is worth noticing that, since the *m*Ph substituents on each monomer are oriented opposite to the other monomer, inter-dye interactions can only stabilize CT states with PMP as the donor group. As a result, despite *m*Ph has a major role in the lowest states of monomer **3** (Table 4.2), the lowest diabats do not involve excitations from the *meso* group. The lowest diabat corresponds

to favorable dipole-dipole coupling of intra-CT from PMP, with the participation of two donor and two acceptor moieties (Figure 4.8, right).

Diabatization of electronic transitions of **2'** confirms the local character of the two lowest excited singlets corresponding to the linear combination of intra-CT from TPA, with no mixing with inter-monomer CT contributions ($Z_{\text{intra}} \sim 100\%$ for S_1 and S_2). This result is in agreement with the presence of weak electronic interaction between monomers in the excited state manifold due to the large spatial interchromophoric separation in the V-form. Higher states computed at the B3LYP level do not correspond to pristine linear combinations of the S_2 state of monomer **2** and hold strong inter monomeric CT character. On the other hand, the nature of the S_3 and S_4 states computed with exact exchange at long inter-electronic distances (CAM-B3LYP) do not show sizable inter-CT mixings, and seems to indicate that the large inter-CT presence for S_3 and S_4 obtained with B3LYP is a spurious effect due to the large excitation energy underestimation of electronic transitions with strong CT character (small overlap between hole and electron) by standard hybrid functionals [142]. Diabatic decomposition of low-energy excited singlet states of **2'** computed with different exchange-correlation functionals can be found in Appendix A (Table A19).

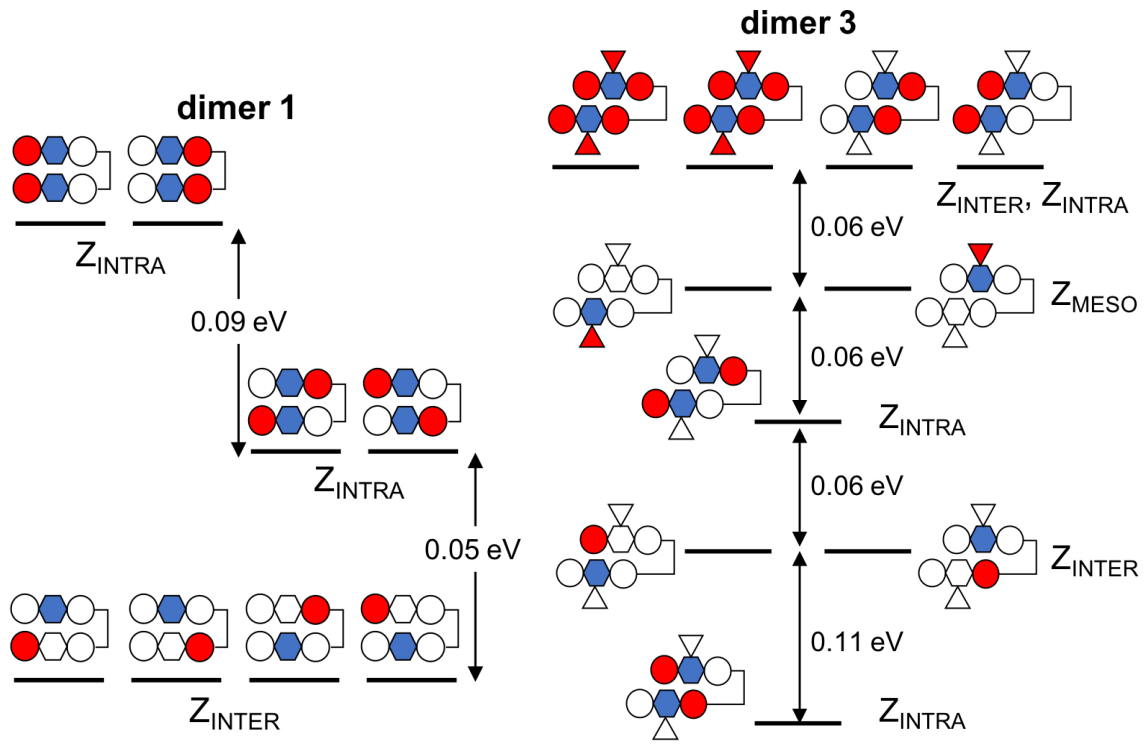

Figure 4.8: Diagramatic representation of diabatic (Z_{INTER}, Z_{INTRA} and Z_{MESO}) excited states and TDA/B3LYP/6-31+G(d) energy gaps (in eV) for curcumin dimers **1'** (left) and **3'** (right). Different groups are indicated as circles (PMP), hexagons (DOB) and triangles (mPh). Increase and decrease of fragment electron density upon excitation are qualitatively indicated in blue and red, respectively. Numerical charges can be found in the Tables A.13-A.18.

4.4 Conclusions

Three curcumin derivatives and their covalent dimers with a polymethylenic chain as the linker have been synthesized and characterized through absorption spectroscopy in solution and with a variety of theoretical calculations and computational tools. Deconvolution of the computed excitations in terms of diabatic states quantifies the involvement of the different chromophoric unities and helps to characterize the nature of the low-lying excited singlet states of the three molecules and their homodimers.

Computed vertical transition energies of molecules **1-3** are in very good agreement with experimental absorption maxima in solution. Despite the similarities of the recorded absorption spectra for the three chromophores, the different nature of the donor moieties imposes rather distinct electronic properties. The symmetric arrangement of the two PMP donor groups in

1 results in a bright lowest excited state (S_1) and a higher dark state (S_2) corresponding to the out-of-phase and in-phase combinations of the two intra-CT donor-acceptor (PMP→DOB) electronic transitions. The stronger donor character of TPA with respect to PMP breaks the left/right symmetry of chromophore **2**, which presents two (localized) optically active excitations. The phenyl substitution in the *meso* position (molecule **3**) introduces a new low-energy transition that can mix with the two lowest states of the pristine **1** molecule. In fact, TDDFT calculations suggest that the lowest excited singlet has a strong participation of *m*Ph as a donor group.

Molecular structures of covalent dimers **1'** and **3'** exhibit a solvent dependent equilibrium between the open conformation (no interaction between chromophores) and a folded form (stacking of monomers), while the bulkyness of the TPA group in **2'** prevents the stabilization of the stacking interactions characteristic of the folded dimer. A larger spatial separation between the two π-clouds in **2'** stems from the favored occurrence of the V-form and induces much weaker electronic interactions. In this case, low-lying excitations can be rationalized in terms of classical dipole-dipole interaction models. The situation is different for **1'** and **3'**. Conclusions drawn from quantum chemical calculations and experimental data converge to show the formation of a H-aggregate species when the two curcuminoid-BF_2 chromophores are linked via a long alkyl chain. Computational characterizations of low-lying transitions in the folded dimers reveal strong interchromophoric coupling and important inter-CT contributions. The latter feature is very interesting in the context of the photophysics of aggregated D-A-D chromophores. More particularly, it is likely that the radiative deactivation of such inter-CT excited states underpins the strongly redshifted fluorescence of curcuminoid-BF_2 derivatives in the solid state. Investigating this hypothesis by characterizing the full photophysical of **1'** and related derivatives containing a linker of different length and chemical nature constitutes an important perspective of this work.

Chapter 5

Flavylium fluorophores as near-infrared emitters

5.1 Introduction

Organic fluorophores exhibiting bright emission in the 1000-2000 nm optical range, referred to as the second near-infrared (NIR-II) window or shortwave infrared (SWIR), present high interest for biological imaging. Compared to far-red visible or NIR-I wavelengths (700-900 nm), NIR-II wavelengths offer important advantages for *in vivo* applications, such as deeper penetration, reduced autofluorescence, higher spatial resolution and lower optical absorption and scattering [143]. Despite the library of organic dyes emitting in the NIR-II window has expanded in the past few years [144, 145, 146, 147, 148, 149, 150, 151, 152], the design of exogenous contrast agents for NIR-II fluorescence imaging remains challenging. In fact, the current strategy to design SWIR-emissive fluorophores relies on making structural modifications to molecular dyes already used for optical imaging emitting at the visible and NIR-I region [39]. Among them, polymethine dyes constitute a promising class of bright and tunable fluorophores. These dyes are charged quadrupolar molecules that contain two heterocycles such as indolenines linked by a methine chain. Lengthening the polymethine linker, extending the electron conjugation or adding electron-donating groups onto the lateral heterocycles in order to enhance the quadrupo-

lar donor-acceptor-donor (D-A-D) character of the structure, have been shown to be promising strategies to bathochromically shift the emission properties of this class of fluorophores. In a recent work, Cosco *et al.* reported the synthesis of polymethines composed of dimethylamino flavylium heterocycles linked by methine chains of different length (**F1-5** and **F7a**, Figure 5.1), whose emission ranges from far-red to shortwave infrared wavelengths [29]. Notably, **F7a** was used to visualize the vasculature of the hind limb of a mouse, and was reported as the brightest SWIR polymethine probe employed so far for fluroescence imaging.

Since they provide insights on the relationships linking the chemical structure of the chromophores to their absorption and emission properties, computational approaches are also useful to design novel SWIR-emissive materials, by providing rational guidelines for eventual syntheses. In this Chapter, we report density functional theory (DFT) calculations on the absorption and emission properties of flavylium polymethine fluorophores reported by Cosco *et al.* Decomposition of the computed excitations in terms of diabatic states is also carried out in order to identify and quantify the nature of the relevant electronic transitions. In the light of these results, chemical functionalization patterns are proposed to further improve the absorption and emission capabilities of these compounds in the NIR-II optical window.

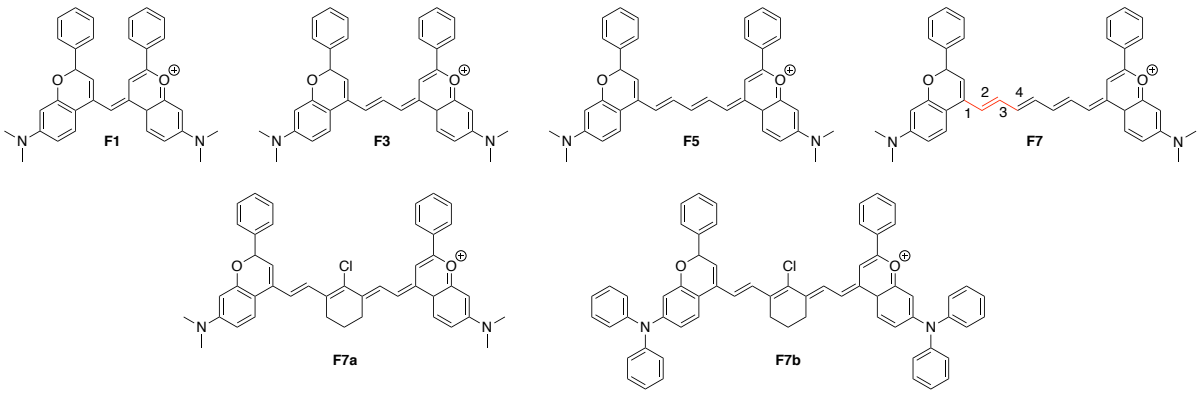

Figure 5.1: Flavylium derivatives investigated in this study. The conjugated segment used to calculate the bond length alternation is shown in red for **F7**.

5.2 Computational details

Geometry optimizations of the ground (S_0) and first excited singlet (S_1) states of flavylium molecules were performed using density functional theory (DFT) and its time-dependent (TDDFT) version respectively, together with the B3LYP functional and the 6-31+G(d,p) basis set. Molecular structures were confirmed to be real minima of the S_0 and S_1 potential energy surfaces on the basis of their real harmonic vibrational frequencies.

Electronic excitation energies were calculated by means of the (full) TDDFT, as well as its implementation using the Tamn-Dancoff approximation (TDA) [123]. The dependence of $S_0 \rightarrow S_1$ transition energies on different exchange-correlation functionals (XCFs) and basis sets has been addressed for the **F3** and **F7a** molecules (Annex B). Since B3LYP provides vertical excitation energies at the Franck-Condon region closer to experimental absorption maxima, this XCF was selected to characterize the optical properties of the investigated fluorophores. The computation of electronic transitions with important electron/hole spatial separation represents a challenge for TDDFT, which requires the use of energy functionals with the correct $1/R$ asymptotic behavior, e.g., range-separated XCFs [153, 79]. Despite that, it is important to notice that the charge transfer (CT) character of low-lying singlet-singlet excitations in the studied chromophores is not severe, as can be deduced from the sizeable HOMO/LUMO overlaps. As a result, in this case, the intramolecular CT character of low-lying states is well recovered by a hybrid functional with a 20% of exact exchange, i.e., B3LYP. The suitability of the B3LYP functional has been confirmed by comparing the results with other functionals (Tables B.2 and B.3), and in particular to range-separated functionals (CAM-B3LYP and ωB97X-D). But, even more importantly, the nature of the lowest excited singlets does not change between B3LYP and CAM-B3LYP or ωB97X-D. Moreover, the suitability of B3LYP to characterize electronic excitations in quadrupolar dyes has been recently demonstrated [28].

The effects of structural relaxation on the electronic structure of the S_1 state were also addressed by calculating the adiabatic transition energies, defined as the energy difference of the S_1 and S_0 states in their respective minimum ($E_{adia} = E_{S_1}^{opt} - E_{S_0}^{opt}$). The 0-0 energies were then evaluated as the sum of the adiabatic contribution and the difference of zero-point vibrational

energy (ZPVE) between S_1 and S_0 ($E_{0-0} = E_{adia} + \Delta E_{ZPVE}$).

Solvent effects were taken into account by means of the conductor-like polarized continuum model (C-PCM) [154, 155, 156], both in the geometry optimizations and calculations of the optical properties. Vertical transition energies were computed with the linear response (LR) approximation [157, 158] within a non-equilibrium state specific (SS) approach. Dichloromethane was used in all calculations, since this solvent was used for the experimental characterizations. The character of the electronic adiabatic excited states was analyzed using a deconvolution in terms of diabatic states or *diabats*, computed in dichloromethane by means of the Edmiston-Ruedenberg localization scheme [46] at the TDA level. As discussed below, two adiabatic states were considered in the diabatization scheme, corresponding to the donor-to-acceptor charge transfer contributions along the two branches of the molecules. Diabatization from two (adiabatic) transitions has been shown to be a reasonable approximation to describe the lowest singlet states in quadrupolar chromophores [28]. Electronic interactions between diabatic states are defined as the off-diagonal elements of the diabatic Hamiltonian. All calculations presented in this chapter were performed with the Q-Chem package [132].

5.3 Results and Discussion

5.3.1 Impact of polymethine chain length

Ground state (S_0) molecular structures exhibit a high degree of planarity across the entire conjugated system (Annex B). Despite the different molecular length, bond lengths, angles and dihedrals are very similar along the **F1-7** series (Table 5.1). Molecular geometries optimized on the first excited state (S_1) potential energy surface (PES) preserve molecular planarity and do not present major structural changes with respect to S_0. The main structural differences between S_0 and S_1 minima are found for some bond distances along the central polyene linker. In particular, bond length alternation (BLA) is systematically larger in the first excited state, indicating that π-electron conjugation decreases upon relaxation on the S_1 PES.

Table 5.1: Bond distances and bond length alternation (BLA = $(d_1+d_3-2d_2)/2$, all values in Å) along the polymethine linker of the flavylium derivatives calculated at the C-PCM:B3LYP/6-31+G(d,p) level in dichloromethane. See Figure 5.1 for bond labels.

	d_1		d_2		d_3		d_4		BLA	
molecule	S_0	S_1	S_0	S_1	S_0	S_1	S_0	S_1	S_0	S_1
F1	1.433	1.427	-	-	-	-	-	-	-	-
F3	1.420	1.434	1.411	1.414	1.412	1.413	-	-	0.005	0.010
F5	1.425	1.435	1.410	1.412	1.411	1.419	-	-	0.008	0.014
F7	1.425	1.436	1.410	1.420	1.413	1.436	1.411	1.423	0.009	0.016
F7a	1.413	1.421	1.395	1.407	1.407	1.429	1.397	1.412	0.015	0.018
F7b	1.427	1.412	1.408	1.420	1.420	1.410	1.427	1.433	0.016	0.009

Natural (NPA) and Mulliken populations reported in Tables 5.2 and B.1 show that the positive charge is equally distributed over the two lateral electron-donating groups in the electronic ground state of the molecules, with negligible delocalization on the central polyenic chain. Upon electronic excitation and relaxation on the S_1 PES, electron density is transferred from the donor extremities to the central linker, whose charge amounts to about $-0.2|e|$ independently of its size.

Table 5.2: Sum of the NPA charges for the atoms in the donor (D) and acceptor (A) groups for the S_0 and S_1 states of **F1**-**7**, **F7a** and **F7b** molecules in their respective energy minimum. Charge at D column corresponds to the average between D_1 and D_2 moieties.

	S_0		S_1	
molecule	D	A	D	A
F1	0.491	0.018	0.598	-0.195
F3	0.489	0.022	0.598	-0.195
F5	0.492	0.017	0.602	-0.203
F7	0.494	0.012	0.604	-0.209
F7a	0.481	0.038	0.596	-0.193
F7b	0.485	0.029	0.603	-0.206

As illustrated in Figure 5.2, the highest occupied and lowest unoccupied molecular orbitals (HOMO and LUMO) of the **F1**-**7** derivatives are largely delocalized over the entire molecule, with slightly more electron density on the two donor and the acceptor moieties in HOMO and LUMO, respectively. Adding methine units at the central fragment from **F1** to **F7** increases the

molecular conjugation length, resulting in energetically higher HOMO and lower LUMO. Consequently, the HOMO-LUMO energy gap shrinks considerably with the length of the molecule (Table 5.3).

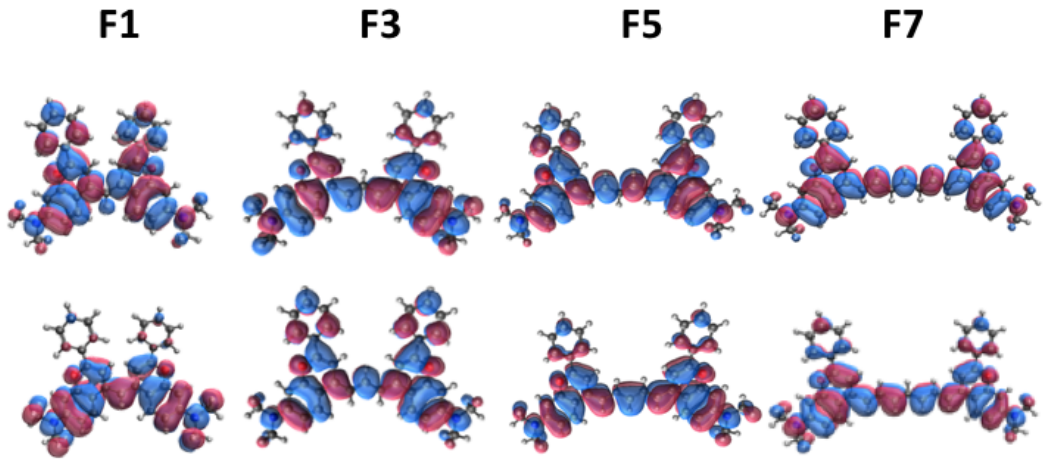

Figure 5.2: HOMO (bottom) and LUMO (top) of **F1-7** computed at the C-PCM:B3LYP/6-31+G(d,p) level in dichloromethane.

Table 5.3: HOMO and LUMO energies (ε_H and ε_L), and HOMO-LUMO gaps ($\Delta\varepsilon_{HL}$) computed at the C-PCM:B3LYP/6-31+G(d,p) level in dichloromethane for the falvylium derivatives. All values in eV.

molecule	ε_H	ε_L	$\Delta\varepsilon_{HL}$
F1	-5.578	-3.277	2.33
F3	-5.415	-3.326	2.09
F5	-5.279	-3.417	1.86
F7	-5143	-3.462	1.68
F7a	-5.143	-3.510	1.63
F7b	-5.070	-3.510	1.56

Table 5.4 reports the Franck-Condon vertical excitation energies (E_{GS}^{vert}) and de-excitation energies from the excited state minima (E_{ES}^{vert}), as well as the adiabatic (E_{adia}) and 0-0 transition energies (E_{0-0}) calculated at the TDDFT level for the investigated compounds.

As shown in previous studies [159, 28], the $S_0 \rightarrow S_1$ electronic excitation at the Frank-Condon region corresponds to a $\pi \rightarrow \pi^*$ electronic transition between the HOMO and LUMO. Although

they systematically overestimate the experimental absorption energies, vertical $S_0 \rightarrow S_1$ energies computed at the TDDFT level fairly reproduce the experimental redshifts of the absorption maximum when increasing the polymethine chain length. The evolution of theoretical $S_1 \rightarrow S_0$ de-excitation energies is also in good qualitative agreement with the experimental data, as well as that of 0-0 energies, which can be related to experimental crossing points between the absorption and fluorescence curves (from Ref. [29], ∼1.87 eV, ∼1.63 eV and ∼1.40 eV for **F1**, **F3** and **F5**, respectively).

Computed oscillator strengths are rather large, suggesting intense photo absorption and emission capabilities, and in agreement with the strong optical responses experimentally obtained. The $S_0 \rightarrow S_1$ (and $S_1 \rightarrow S_0$) transition dipole moments are aligned along the long molecular axis (Figure B.1 and Table B.5), as typically obtained in quadrupolar dyes [28].

As shown in Table B.8, TDA yields excitation energies which are very close to values provided by full-featured TDDFT calculations (as it is usually a good approximation to low-lying singlet-singlet excitations [123, 160]), showing that TDA, used in the following for electronic states diabatization, performs similarly as TDDFT for this series of systems.

Table 5.4: Vertical excitation energies to the excited state (S_1) at the ground state geometry (E_{GS}^{vert}) and de-excitation energies from the S_1 minima (E_{ES}^{vert}) for the series of derivatives, as well as adiabatic (E_{adia}) and 0-0 transition energies (E_{0-0}) calculated at the TDDFT/B3LYP/6-31+G(d,p) level in dichloromethane. Oscillator strengths are reported in parentheses. The experimental absorption and emission band maxima [29] are given in the last two columns. All energy values are in eV.

molecule	E_{GS}^{vert}	E_{ES}^{vert}	E_{adia}	E_{0-0}	E_{abs}^{exp}	E_{em}^{exp}
F1	2.09 (2.059)	1.83 (2.049)	1.89	1.86	1.91	1.80
F3	1.89 (2.783)	1.66 (2.930)	1.79	1.77	1.66	1.62
F5	1.73 (2.382)	1.44 (2.302)	1.62	1.54	1.44	1.36
F7	1.59 (2.948)	1.31 (2.669)	1.48	1.47	-	-
F7a	1.57 (2.963)	1.19 (2.801)	1.45	1.44	1.21	1.19
F7b	1.44 (2.956)	1.06 (2.996)	1.37	1.35	-	-

The low-lying transitions of linear quadrupolar dyes with the donor-acceptor-donor (D_1-A-D_2) pattern, are obtained as the combination of two intramolecular charge transfer (CT) states defined as donor-to-acceptor electronic excitations, that is CT_1 and CT_2 corresponding to $D_1 \rightarrow$A and $D_2 \rightarrow$A electronic transitions, respectively [161]. For symmetric systems, i.e., D_1

equal to D_2, the two CT states are degenerated and the two lowest (adiabatic) spin-singlet transitions are built as the in-phase (S_+) and out-of-phase (S_-) combinations of CT states:

$$|S_\pm\rangle = \frac{1}{\sqrt{2}}(|CT_1\rangle \pm |CT_2\rangle). \tag{5.1}$$

Typically, the lowest excitation is optically bright, as seen in the previous section for the **F1-7** family, and corresponds to the S_- eigenstate, in agreement with the favorable head-to-tail alignment of transition dipole moments of CT_1 and CT_2 (Figure 5.3). The energy separation between $S_1 \equiv S_-$ and $S_2 \equiv S_+$ is obtained as the interaction between CT_1 and CT_2. Therefore, the energy of the lowest excited singlet, directly related to the emission wavelength, will be dictated by the CTs diabatic energy and their electronic coupling $V \equiv \langle CT_1|\hat{H}|CT_2\rangle$.

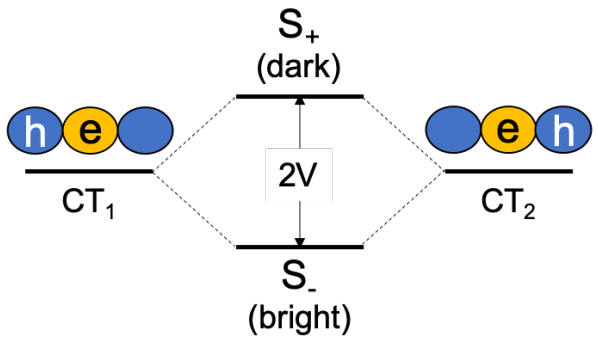

Figure 5.3: Diagramatic representation of the diabatization of the two lowest singlet excitations in flavylium molecules as the antisymmetric (S_-, bright) and symmetric (S_+, dark) combinations of the two CT states (CT_1 and CT_2). Localization of hole and electron upon excitation indicated as h and e respectively.

Diabatization of S_1 and S_2 states in flavilyum derivatives allows to decompose them in terms of CT_1 and CT_2, and transforms the (diagonal) adiabatic Hamiltonian into the (non-diagonal) diabatic Hamiltonian, with degenerate diabatic energies at the diagonal and electronic coupling as the off-diagonal term. The obtained energies and couplings for the **F1-7** series are shown in Table 5.5. Characterization of the two intramolecular CT states for each molecule in terms of the variation of Mulliken fragment charges can be found in Annex B (Table B.6).

Diabatic energy of the intramolecular CT state decreases with the length of the linker, approximately 0.2 eV for each additional methine unit, in agreement with computed adiabatic energies and the experimental bathochromic shift observed for the emission frequencies. Electronic cou-

Table 5.5: Vertical excitation energies to the first excited state ($S_1 \equiv S_-$), CT diabats (CT_i, $i = 1, 2$) energies and electronic couplings ($V \equiv \langle CT_1|\hat{H}|CT_2\rangle$) computed at the (TDA) B3LYP/6-31+G(d,p) level at the S_1 optimized geometry. State energies and couplings are given in eV and meV, respectively.

molecule	$E(S_1)$	$E(CT_i)$	V
F1	1.98	2.16	247
F3	1.75	2.00	209
F5	1.53	1.82	171
F7	1.39	1.52	145
F7a	1.28	1.50	295
F7b	1.14	1.20	280

plings between the two diabats (V) are rather strong for all molecules, and slightly decrease from **F1** to **F7**. This behavior results from larger delocalization of the negative charge in longer acceptor moieties, diminishing the overlap integral between the CT_1 and CT_2 diabats. Overall, while the CT energy is the main factor controlling the energy of the emitter in the flavylium series, electronic coupling further tunes the stabilization of the bright excitation with respect to ground state.

5.3.2 Impact of chemical substitution

The computational results in the previous section help to rationalize the trend in the fluorescent emission properties of the flavylium family, that is the increase in emission wavelength with the length of the molecule. Following, we attempt to further redshift the photoluminescence of these fluorophores. To that aim we consider two different chemical substitutions at the acceptor (**F7a**) and donor (**F7b**) moieties of the longest **F7** compound (Figure 5.1).

With a view to enhancing the electron withdrawing strength of the polymethine bridge, we introduce a chlorine atom at the central methylene unit of the **F7** molecule. Moreover, we slightly modify the linker with the formation of a six-membered non-conjugated ring, as it precisely corresponds to a flavylium dye recently synthesized for SWIR imaging [29].

The increased acceptor character of the central moiety of **F7a** with respect to **F7** stabilizes the energy of the LUMO, while the energy level of the HOMO does not change (Table 5.3, see

Figure 5.4 for MO shapes). Such reduction in the occupied-virtual gap results in a 0.12 eV red shift in the $S_1 \rightarrow S_0$ de-excitation energy (from 1.31 to 1.19 eV), while the strength of the transition slightly increases (Table 5.4).

Computed diabatic energy in **F7a** is barely lower than in **F7**. On the other hand, the coupling between the two diabats is approximately 2 times larger (Table 5.5). Since the coupling between CT_1 and CT_2 strongly depends on the overlap of the two states at the shared acceptor moiety, we argue that the improved electron acceptor character of the chlorine-substituted polyene bridge increases the diabatic interaction, which further stabilizes the lowest excited singlet (and destabilizes the S_2 state).

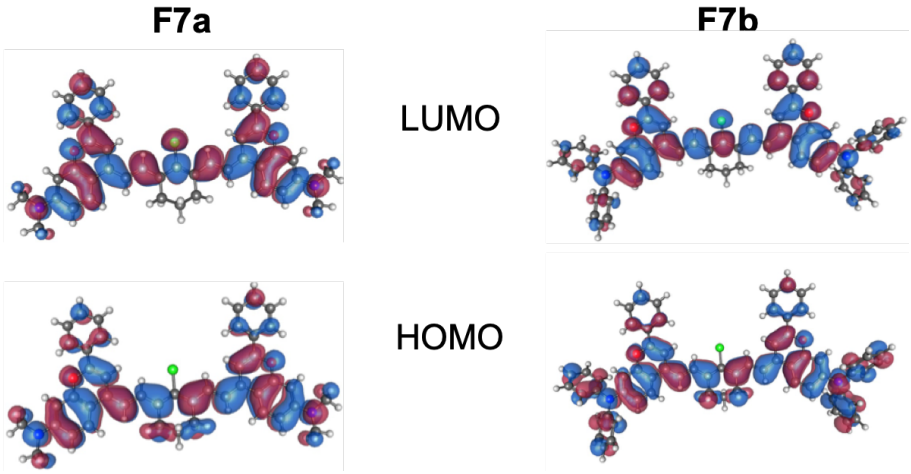

Figure 5.4: Frontier molecular orbitals, HOMO (bottom) and LUMO (top), of **F7a** and **F7b** calculated at the C-PCM:B3LYP/6-31+G(d,p) level.

Next, we aim to bring the emission band to even shorter wavenumbers by increasing the electron-donor ability of the two side fragments. In consequence, we propose the replacement of the dimethylamino groups in **F7a** by diphenylamino (**F7b**).

The stronger donor character of diphenylamino pushes the HOMO to a less negative energy, while the energy of the LUMO does not change with respect to **F7a**, reducing the HOMO-LUMO gap (Table 5.3). In accordance, the S_1 state in **F7b** shows smaller excitation and de-excitation energies and strong oscillator strengths (Table 5.4), making it an excellent candidate for SWIR imaging.

From a diabatic point of view, the redshift of excited state energy is mainly obtained as the

result of a large decrease of the CT diabatic state energy (Table 5.5). On the other hand, the electronic coupling remains nearly as strong as in **F7a**, in accordance with the fact that V is mainly tuned by the properties of the electron-acceptor moiety.

5.4 Conclusions

The absorption and emission properties of recently reported flavylium fluorophores were rationalized by means of TDDFT calculations and subsequent decomposition of the computed excitations in terms of diabatic charge transfer states. Diabatization of the lowest-energy excited state evidenced that the bathochromic shift of the emission wavelength observed when elongating the polymethine chain in the **F1-7** series mainly originates from the decrease of the diabatic CT energy. Enhancing the electron-withdrawing strength of the polymethine bridge by chlorine substitution of the linker in **F7a** was shown to further redshift the photo-luminescence of the fluorophore, as a result of the increase of the coupling between the diabatic states, which stabilizes the lowest (bright) excited singlet. Finally, increasing the electron-donor ability of the two lateral fragments by replacing the dimethylamino groups in **F7a** by diphenylamino substituents (**F7b**) was found to induce a large decrease of the CT diabatic state energy, which further stabilizes the emitting excited state. This new theoretically-designed fluorophore is thus expected to exhibit unprecedented bright emission in the shortwave infrared region, with high potential for biological imaging.

Chapter 6

Photophysics of molecular aggregates from excited state diabatization

6.1 Introduction

The computational characterization of electronic transitions becomes specially appealing in the study of molecular aggregates, molecular crystals, or thin films of organic chromophores, where excited states hold recognizable properties of the electronic transitions of its molecular constituents, but also novel features may appear as a result of the interchromophoric interactions. The detailed understanding of the electronic states in photoactivated aggregates and the properties emerging from interchromophoric couplings allows to rationalize the nature of low-lying transitions, e.g., the formation of the H- and J-aggregation phenomena [162, 163, 33, 164, 35, 36], and can help to disentangle the mechanism of novel photophysical events resulting from the interaction of two or more optically active molecules, such as singlet fission [40, 41, 42], triplet-triplet annihilation [165, 166, 167, 168], or aggregation induced emission [169].

The theoretical and computational description of photophysics in molecular aggregates is typically tackled by the use of exciton models [170], where excitonic states are obtained by combining well defined monomeric (diabatic) states through the definition of an effective Hamiltonian build as state energies and inter-state couplings. The excitonic model approach directly propor-

tionates physical characterization of excitons in terms of local excitations (LE), charge transfer (CT) configurations, or even multiexcitons (ME); and allows the computation of complex systems with a moderate cost. However, the results are strongly dependent on the choice of important diabatic states (diabats), which requires good pre-knowledge of the system under study. Alternatively, the description of electronic states of aggregates in terms of different electronic contributions can be achieved by the deconvolution of computed eigenstates from the employed model chemistry using a diabatization scheme. This procedure does not pre-impose the nature of states and only relies on the strategy employed to define the adiabatic-to-diabatic transformation. Despite these advantages, the characterization of excitons from the computation of adiabatic states is not as trivial and direct as in the exciton model.

The present study focuses on the development of the theoretical framework and implementation of a computational algorithm for the description and rationalization of excitonic states based on the diabatization of electronic eigenstates in molecular aggregates. In this manuscript we present the general equations for the description of excitonic states and deconvolute their energies in different types of contributions for equivalent and non-equivalent molecular dimers. Then we apply these tools to the study of low-energy excitations for different conformations of the ethylene-ethylene and ethylene-tetrafluoroethylene dimers as model systems.

6.2 Theory

6.2.1 Excited state diabatization

Let us first recall the principle of excited state diabatization already introduced in Chapter 3. By definition, electronic diabatic states $\{\Phi_i\}$ are those with zero derivative coupling elements:

$$d_{ij}^{\alpha} = \langle \Phi_i | \nabla_{\alpha} | \Phi_j \rangle = 0 \tag{6.1}$$

where α index corresponds to a nuclear coordinate. In practice, ideal diabats for which all derivative couplings perfectly vanish cannot be obtained from a finite number of adiabatic

states [45]. One possible path to obtain a basis of diabatic (or quasi-diabatic) states eluding a direct (*arbitrary*) definition is through the diabatization of eigenstate solutions of model chemistries, i.e., adiabatic states. Diabatization of a finite set of adiabatic electronic states ($\{\Psi_i\}; i = 1, N$) can be achieved through the action of a rotation matrix $\mathbf{U}$ (equation 6.3).

$$\hat{H}\Psi_i = E_i\Psi_i \tag{6.2}$$

$$\Phi_i = \sum_{j=1}^{N} U_{ji}\Psi_j \tag{6.3}$$

Then, an orthonormal basis of diabatic states ($\{\Phi_i\}; i = 1, N$) is constructed as linear combinations of adiabats. Such approach is not free from human input, since final diabatic states might depend on the size of adiabatic basis considered and the procedure employed to define $\mathbf{U}$. Decomposition of adiabatic wave functions as a sum of well characterized diabatic configurations (equation 6.4) provides a direct analysis of the nature of the electronic (adiabatic) states, and it has shown to be a valuable tool in the characterization of electronic excitations of complex systems such as in covalent dimers [171, 172], or in the aggregation of quadrupolar dyes [28].

$$\Psi_i = \sum_{j=1}^{N} c_j^{(i)}\Phi_j, \qquad i = 1, N. \tag{6.4}$$

Several strategies and procedures exist in order to construct diabatic states: (i) explicit minimization of derivative couplings [173, 174, 175], (ii) implicit minimization by designing diabatic states according to specific physical and/or mathematical properties [176], and (iii) through the use of a physical observable, e.g., dipole moment [177].

In addition to the information derived from the decomposition of adiabatic states (equation 6.4), the (non-diagonal) diabatic Hamiltonian contains very useful information. Diagonal pieces represent the energy level of diabats, while off-diagonal elements $H_{ij} \equiv \langle\Phi_i|\hat{H}|\Phi_j\rangle$ correspond to interstate electronic couplings, which upon the electronic nature of the coupled states can be related to different processes, e.g., exciton or electron (hole) transfer [178].

6.2.2 Diabatic states in aggregates

The diabatization of electronic states is particularly appealing in aggregates of interacting chromophores. Typically, electronic excitations in the presence of two or more chromophores can be deconvoluted in terms of monomeric excitations (LE) and possibly novel excitations emerging as the result of dye-dye interactions, such as CT excitations found in extended structures of organic chromophores, and ME states corresponding to the concomitant excitation of two or more chromophores.

Excitonic models rely on the use of a basis of well defined (diabatic) states to describe electronic excitations in aggregates. In this diabatic basis, the eigenstates of an aggregate of M molecular species is generally expressed as:

$$\Psi_i = \sum_{j \in \mathrm{LE}} c_j^{(i)} \Phi_j + \sum_{k \in \mathrm{ME}} c_k^{(i)} \Phi_k + \sum_{q \in \mathrm{CT}} c_q^{(i)} \Phi_q \tag{6.5}$$

where j, k, and q indexes run over LE, ME, and CT excitations, respectively. Comparison of equation 6.5 to equation 6.4 gives a direct connection between excitonic models and diabatization of excited states. In other words, the electronic nature of the diabatic states and their role as pieces of the excited states weighted by the amplitudes of the different contributions in equation 6.5 could be in principle obtained through diabatization of adiabatic states.

6.2.3 Excitonic model for symmetric dimers

The general wave function expression of molecular aggregates largely simplifies in the case of molecular dimers. Furthermore, when the two lowest molecular singlet-to-singlet excited states are energetically well separated ($E(S_1) << E(S_2)$) and disregarding ME excitations, equation 6.5 reduces to:

$$\Psi_i = c_{10}^{(i)} \Phi_{10} + c_{01}^{(i)} \Phi_{01} + c_{AC}^{(i)} \Phi_{AC} + c_{CA}^{(i)} \Phi_{CA} \tag{6.6}$$

where subindices indicate local excitation in either monomer (10 and 01), and charge separation cation/anion (CA) and anion/cation (AC) diabats. If the two monomers in the dimer are

equivalent, i.e. homodimers in a symmetric disposition, it is possible to express states $\{\Psi_i\}$ as symmetric (+) and antisymmetric (−) combinations of LE and CT diabats, that is Frenkel excitions (FE) and charge resonances (CR), respectively.

$$\Phi_{FE}^{(\pm)} = \frac{1}{\sqrt{2}}(\Phi_{10} \pm \Phi_{01}) \tag{6.7}$$

$$\Phi_{CR}^{(\pm)} = \frac{1}{\sqrt{2}}(\Phi_{AC} \pm \Phi_{CA}) \tag{6.8}$$

Since symmetric (antisymmetric) FE can only mix with CR with the same symmetry, excited states of equivalent dimers can be also written as:

$$\Psi_i = c_{FE}^{(i)}\Phi_{FE}^{(\pm)} + c_{CR}^{(i)}\Phi_{CR}^{(\pm)}; \quad \text{for} \quad i = 1, 4 \tag{6.9}$$

in which $c_{FE}^{(i)} = \pm\sqrt{1 - c_{CR}^{(i)2}}$ by normalization of the electronic wave function, $\langle\Psi_i|\Psi_i\rangle = 1$. Expanding eigenenergy expressions $E_i = \langle\Psi_i|\hat{H}|\Psi_i\rangle$ for the two symmetric and two antisymmetric states allows to decompose them in different types of contributions as:

$$E_i^{(\pm)} = E_{LE} \pm V_{DC} + 2\ \mathrm{sign}_{h,e}^{(i)}\ \lambda_i\sqrt{1-\lambda_i^2}(V_e \pm V_h) + \lambda_i^2[E_{CT} - E_{LE} \pm (V_{CT} - V_{DC})] \tag{6.10}$$

where super-indices (+)/(−) indicate symmetric/antisymmetric states, $\lambda_i = |c_{CR}^{(i)}|$, $\mathrm{sign}_{h,e}^{(i)}$ is the sign resulting from the product of FE and CR amplitudes (equation 6.11), E_{LE} and E_{CT} correspond to diabatic state energies:

$$\mathrm{sign}_{h,e}^{(i)} = \frac{c_{FE}^{(i)}c_{CR}^{(i)}}{|c_{FE}^{(i)}c_{CR}^{(i)}|} \tag{6.11}$$

$$E_{LE} = \langle\Phi_{10}|\hat{H}|\Phi_{10}\rangle = \langle\Phi_{01}|\hat{H}|\Phi_{01}\rangle \tag{6.12}$$

$$E_{CT} = \langle\Phi_{AC}|\hat{H}|\Phi_{AC}\rangle = \langle\Phi_{CA}|\hat{H}|\Phi_{CA}\rangle, \tag{6.13}$$

and V_{DC}, V_{CT}, V_e, and V_h are the direct, CT, electron, and hole couplings, respectively:

$$V_{DC} = \langle \Phi_{10} | \hat{H} | \Phi_{01} \rangle \tag{6.14}$$

$$V_{CT} = \langle \Phi_{AC} | \hat{H} | \Phi_{CA} \rangle \tag{6.15}$$

$$V_e = \langle \Phi_{10} | \hat{H} | \Phi_{CA} \rangle = \langle \Phi_{01} | \hat{H} | \Phi_{AC} \rangle \tag{6.16}$$

$$V_h = \langle \Phi_{01} | \hat{H} | \Phi_{CA} \rangle = \langle \Phi_{10} | \hat{H} | \Phi_{AC} \rangle \tag{6.17}$$

Notice that adiabatic state energies in terms of diabatic energies and couplings can be also achieved through explicit diagonalizaton of the diabatic Hamiltonian (Appendix C).

For high energy CT states ($E_{CT} >> E_{LE}$) charge separated configurations do not mix with LE states and the two lowest-lying transitions correspond to the symmetric and antisymmetric FE ($\lambda_1, \lambda_2 = 0$), in agreement with the Kasha's model for weakly interacting chromophores [33]. The sign and magnitude of V_{DC}, which depend on the spatial disposition of the two chromophores, controls the energy splitting between FE states. Approximating electronic states within the (minimal) HOMO-LUMO orbital space of each chromophore, V_{DC} can be obtained as:

$$V_{DC} \approx 2(h_A l_A | l_B h_B) - (h_A h_B | l_B l_A) \tag{6.18}$$

where h_X and l_X indicate HOMO and LUMO orbitals of chromophore X, and $(ij|kl)$ is the two electron integral between spatial orbitals:

$$(ij|kl) = \int d\mathbf{r}_1 d\mathbf{r}_2 \phi_i^*(\mathbf{r}_1) \phi_j(\mathbf{r}_1) r_{12}^{-1} \phi_k^*(\mathbf{r}_2) \phi_l(\mathbf{r}_2) \tag{6.19}$$

In the case of the long-range coupling between dipole allowed transitions, Coulomb interaction dominates and the direct coupling is often further approximated to the classical (through space) expression for dipole-dipole interactions,

$$V_{DC} \approx J_{Coul} = \frac{\mu^2 (1 - 3cos^2\theta)}{4\pi\varepsilon R^3} \tag{6.20}$$

where μ is the norm of the molecular transition dipole moment, R is the intermolecular distance,

θ is the angle between $\boldsymbol{\mu}$ and $\mathbf{R}$, and ε is the dielectric constant.

The direct coupling approximation in equation 6.20 is often employed in the Föster theory of exciton energy transfer [179], which produces very good results within the weak coupling regime found in spatially separated chromophores (typically for $R >> 4$ Å), but as soon as the electron density of different molecules overlap, short-range interactions, such as exchange or V_e and V_h, need to be taken into account. Short-range LE/CT couplings are typically written as the electron and hole transfer integrals (equations 6.21 and 6.22), which result from the HOMO-LUMO orbital space approximation, likewise for the V_{DC} term in equation 6.18.

$$V_h \approx t_h \equiv -\langle h_A|\hat{H}|h_B\rangle \tag{6.21}$$

$$V_e \approx t_e \equiv \langle l_A|\hat{H}|l_B\rangle \tag{6.22}$$

In the perturbative limit, and considering intermediate normalization of the perturbed wave function, the CT amplitudes are computed as $-(V_e \pm V_h)/(E_{CT} - E_{LE})$ and the super-exchange energy contributions of the two lowest states are approximated as the sum of the self-energy Δ_{CT} and the short-range coupling J_{CT} [180]:

$$E_{1,2}^{(\pm)} \simeq E_{LE} \pm V_{DC} + \Delta_{CT} \pm J_{CT} \tag{6.23}$$

$$\Delta_{CT} = -\frac{V_e^2 + V_h^2}{E_{CT} - E_{LE}} \tag{6.24}$$

$$J_{CT} = -\frac{2V_eV_h}{E_{CT} - E_{LE}} \tag{6.25}$$

Equation 6.23 indicates that the relative magnitude of J_{CT} with respect to V_{DC} and the signs of V_e and V_h control the nature of the lowest transitions and selectively stabilize either the symmetric or antisymmetric solution, eventually inducing the formation of H- or J-aggregation [37].

6.2.4 Connection between diabatization and the excitonic model

Diabatization of low-lying states directly produces the pieces, i.e., diabatic energies and couplings, corresponding to energy contributions of different nature. Concretely, the terms contributing to the eigenenergies of dimer states (equation 6.10) in different orders of CR amplitudes can be directly correlated to the state energies and couplings defined in excitonic models.

In general, the application of a diabatization scheme does not ensure the generation of electronic configurations with a well defined relative phase, e.g., using a phase convention based on the system's symmetry, as assumed in equations 6.14-6.17. As a result, the off-diagonal elements of the diabatic Hamiltonian (H_X) correspond to electronic couplings (equations 6.14-6.17) with a sign uncertainty, $H_X = \pm V_X$. On the other hand, the overall sign of the product between amplitudes and couplings for each contribution is well defined and independent of the employed convention, i.e. the sign of amplitudes and couplings are linked to each other. Therefore, in order to avoid the definition of relative phases between diabatic states, we include the state specific sign of each energy contribution in equation 6.10 to each corresponding coupling term and rewrite the adiabatic excitation energy of state i as:

$$E_i = E_{LE} + W_{DC}^{(i)} + 2\lambda_i\sqrt{1-\lambda_i^2}(W_e^{(i)} + W_h^{(i)}) + \lambda_i^2(E_{CT} - E_{LE} + W_{CT}^{(i)} - W_{DC}^{(i)}) \quad (6.26)$$

$$W_{DC}^{(i)} = \mathrm{sign}_{DC}^{(i)}\langle\Phi_{10}|\hat{H}|\Phi_{01}\rangle \quad (6.27)$$

$$W_h^{(i)} = \mathrm{sign}_h^{(i)}\langle\Phi_{10}|\hat{H}|\Phi_{AC}\rangle \quad (6.28)$$

$$W_e^{(i)} = \mathrm{sign}_e^{(i)}\langle\Phi_{10}|\hat{H}|\Phi_{CA}\rangle \quad (6.29)$$

$$W_{CT}^{(i)} = \mathrm{sign}_{CT}^{(i)}\langle\Phi_{CA}|\hat{H}|\Phi_{AC}\rangle \quad (6.30)$$

where we define couplings $W_X^{(i)}$ as the product between off-diagonal elements of the diabatic Hamiltonian (H_X) and the sign of the contribution obtained as the normalized product of amplitudes (Appendix C). Finally, we reorganize energy contributions upon the nature of the state-state couplings in terms of diagonal energy shifts (Δ_i), direct couplings ($\Omega_{DC}^{(i)}$), super-exchange *hole* ($\Omega_h^{(i)}$) and *electron* ($\Omega_e^{(i)}$) contributions as the ones arising from $W_h^{(i)}$ and $W_e^{(i)}$,

and inter-CT couplings ($\Omega_{CT}^{(i)}$) as:

$$
\begin{aligned}
E_i &= E_{LE} + \Delta_i + \Omega_{DC}^{(i)} + \Omega_{SX}^{(i)} + \Omega_{CT}^{(i)} && (6.31)\\
\Delta_i &= \lambda_i^2 (E_{CT} - E_{LE}) && (6.32)\\
\Omega_{DC}^{(i)} &= (1-\lambda_i^2) W_{DC}^{(i)} && (6.33)\\
\Omega_{CT}^{(i)} &= \lambda_i^2 W_{CT}^{(i)} && (6.34)\\
\Omega_{h}^{(i)} &= 2\lambda_i \sqrt{1-\lambda_i^2}\; W_{h}^{(i)} && (6.35)\\
\Omega_{e}^{(i)} &= 2\lambda_i \sqrt{1-\lambda_i^2}\; W_{e}^{(i)} && (6.36)\\
\Omega_{SX}^{(i)} &= \Omega_{h}^{(i)} + \Omega_{e}^{(i)} && (6.37)
\end{aligned}
$$

In equation 6.26 the contributions arising from the LE/CT interaction, i.e. $W_e^{(i)}$ and $W_h^{(i)}$, appear as the lowest order in the CT mixings, and for the typical case in which $E_{LE} < E_{CT}$ the two lowest singlet excitations still have a predominantly LE (or FE) character (small λ_i). At the $\lambda_i \to 0$ limits the energies of the two lowest states can be expressed (to the first order) as:

$$E_i \simeq E_{LE} + W_{DC}^{(i)} + 2\lambda_i (W_e^{(i)} + W_h^{(i)}) + O(\lambda_i^2);\ i = 1, 2 \tag{6.38}$$

The linear term in λ_i in the r.h.s of equation 6.38 is directly related to second order perturbative correction to FE energies employed to include the main effects arising from LE/CT mixings (super-exchange) [180]. Equation 6.38 closely resembles the perturbative exciton model in equation 6.23, although it explicitly contains the CR amplitude λ_i. The terms corresponding to the product of λ_i with $W_e^{(i)}$ and $W_h^{(i)}$ can be directly related to the J_{CT} term (equation 6.25), and their overall contribution can eventually control the nature of the lowest lying excited singlet, resulting in H- or J-aggregation properties.

The construction of an excitonic model from a diabatization scheme presents several advantages over the standard approaches based on the initial calculation of diabatic states. The diabatization scheme does not rely on an arbitrary definition of diabatic states and all interstate couplings are obtained free of approximations such as the ones in equations 6.18-6.22. Moreover, contrary to the standard perturbative approach in the diabatic approximation that is only

valid for weak LE/CT couplings, the state energy expressions obtained as the diabatization of eigenstates in terms of explicit CR amplitudes are applicable to the entire range of LE/CT mixings, i.e., weak and strong couplings.

6.2.5 Non-equivalent chromophores

So far, the performed analysis has considered the interaction of chemically and structurally equivalent molecules. If the two coupled chromophores are non-equivalent, either due to non-symmetrical disposition of homodimers or in heterodimers, the general energy equation 6.31 remains valid, but the symmetry relationships in equations 6.7 and 6.8 can no longer be applied. In those situations, the explicit expression for each of the energy contributions needs to be modified according to the asymmetry between LE and CT states:

$$\begin{aligned}
\Delta_i &= \lambda_i^2(E_{CT}-E_{LE}) + \delta_{LE}^{(i)2}\Delta E_{LE} + \delta_{CT}^{(i)2}\Delta E_{CT} && (6.39)\\
\Omega_{DC}^{(i)} &= \left[(1-\lambda_i^2)^2 - \delta_{LE}^{(i)4}\right]^{1/2} W_{DC}^{(i)} && (6.40)\\
\Omega_{CT}^{(i)} &= \left[\lambda_i^4 - \delta_{CT}^{(i)4}\right]^{1/2} W_{CT}^{(i)} && (6.41)\\
\Omega_{h}^{(i)} &= \left[\lambda_i^2(1-\lambda_i^2) + \lambda_i^2\delta_{LE}^{(i)2} + (1-\lambda_i^2)\delta_{CT}^{(i)2} + \delta_{LE}^{(i)2}\delta_{CT}^{(i)2}\right]^{1/2} W_{h}^{(i)} \\
&+ \left[\lambda_i^2(1-\lambda_i^2) - \lambda_i^2\delta_{LE}^{(i)2} - (1-\lambda_i^2)\delta_{CT}^{(i)2} + \delta_{LE}^{(i)2}\delta_{CT}^{(i)2}\right]^{1/2} W_{h'}^{(i)} && (6.42)\\
\Omega_{e}^{(i)} &= \left[\lambda_i^2(1-\lambda_i^2) + \lambda_i^2\delta_{LE}^{(i)2} - (1-\lambda_i^2)\delta_{CT}^{(i)2} - \delta_{LE}^{(i)2}\delta_{CT}^{(i)2}\right]^{1/2} W_{e}^{(i)} \\
&+ \left[\lambda_i^2(1-\lambda_i^2) - \lambda_i^2\delta_{LE}^{(i)2} + (1-\lambda_i^2)\delta_{CT}^{(i)2} - \delta_{LE}^{(i)2}\delta_{CT}^{(i)2}\right]^{1/2} W_{e'}^{(i)} && (6.43)
\end{aligned}$$

where E_{LE} and E_{CT} are the LE and CT average energies, ΔE_{LE} and ΔE_{CT} correspond to half the diabatic energy gaps, $\delta_{LE}^{(i)2}$ and $\delta_{CT}^{(i)2}$ are the squared amplitude asymmetries:

$$E_{LE} = \frac{E_{10}+E_{01}}{2};\ E_{CT} = \frac{E_{AC}+E_{CA}}{2} \quad (6.44)$$

$$\Delta E_{LE} = \frac{E_{10}-E_{01}}{2};\ \Delta E_{CT} = \frac{E_{AC}-E_{CA}}{2} \quad (6.45)$$

$$\lambda_i^2 = c_{AC}^{(i)2} + c_{CA}^{(i)2};\ \delta_{LE}^{(i)2} = c_{10}^{(i)2} - c_{01}^{(i)2};\ \delta_{CT}^{(i)2} = c_{AC}^{(i)2} - c_{CA}^{(i)2} \quad (6.46)$$

$W_{DC}^{(i)}$ and $W_{CT}^{(i)}$ are defined in equations C.10 and C.15, and the *hole* and *electron* (non-symmetric) signed couplings are defined as:

$$W_h^{(i)} = \text{sign}_h^{(i)} \langle \Phi_{10} | \hat{H} | \Phi_{AC} \rangle; \; W_{h'}^{(i)} = \text{sign}_{h'}^{(i)} \langle \Phi_{01} | \hat{H} | \Phi_{CA} \rangle \tag{6.47}$$

$$W_e^{(i)} = \text{sign}_e^{(i)} \langle \Phi_{10} | \hat{H} | \Phi_{CA} \rangle; \; W_{e'}^{(i)} = \text{sign}_{e'}^{(i)} \langle \Phi_{01} | \hat{H} | \Phi_{AC} \rangle. \tag{6.48}$$

Notice that if we consider the case with no asymmetries, that is $W_h^{(i)} = W_{h'}^{(i)}$, $W_e^{(i)} = W_{e'}^{(i)}$ and $\Delta E_{LE} = \Delta E_{CT} = \delta_{LE}^{(i)} = \delta_{CT}^{(i)} = 0$, then equations 6.39-6.43 converge to equations 6.32-6.36. While ΔE_{LE} and ΔE_{CT} can be seen as direct energy measurements of the asymmetry between chromophores, $\delta_{LE}^{(i)2}$ and $\delta_{CT}^{(i)2}$ can be used to evaluate the asymmetry resulting from electronic interactions, i.e. they quantify the degree of LE and CT coherence in the i-th excited state, with $\delta_X^{(i)2} = 0$ indicating perfect resonance.

6.3 Computational details

Molecular geometries have been optimized at the MP2/cc-pVTZ level. Calculations of molecular dimers have been done considering the (frozen) optimized geometries at the molecular level. Excited states of molecules and dimers have been computed at the configuration interaction singles (CIS) level with the 6-31G basis set. Calculation of excitation energies and electronic couplings with a larger basis set (6-31G(d)) do not show significant differences (Figures C1 and C2). Diabatization of electronic states was performed with the Edmiston-Ruedenberg (ER) localization scheme [46] for the four electronic states with participation of the $\pi \rightarrow \pi^*$ electronic promotions, that is excitations between the molecular HOMOs and LUMOs.

All calculations discussed in this chapter were performed with the Q-Chem program [132].

6.4 Examples

In the following, we exemplify the use of excited state diabatization in the analysis of transition energies and electronic properties of low-lying singlet-to-singlet excitations in molecular dimers. We explore a variety of stacked conformations of symmetric and non-symmetric dimers corresponding to a wide range of electronic couplings, and rationalize the origin of the electronic nature of low-lying excited states in molecular dimers.

6.4.1 Eclipsed ethylene dimer

In order to exemplify the methodology described above, we investigate singlet-singlet electronic transitions in the ethylene dimer in different relative conformations. The employed molecular orientation and π-frontier molecular orbitals (MOs) of the ethene molecule involved in the studied electronic states are indicated in Figure 6.1.

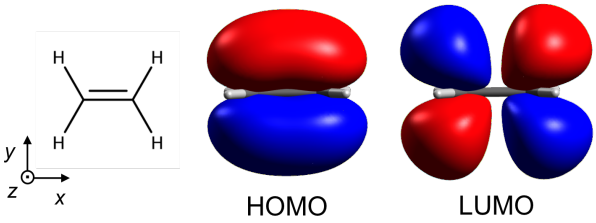

Figure 6.1: Molecular orientation of ethene molecule employed along the study (left), and higher occupied MO (HOMO) and lower unoccupied MO (LUMO) computed at the CIS/6-31G level.

First we consider the case of two ethylene molecules in the eclipsed (D_{2h}) disposition at different intermolecular (z-axis) separations, which results in H-aggregation. The energy profiles for the two singlet states emerging from the ($\pi \rightarrow \pi^*$) 1^1B_{3u} state of the monomer are shown in Figure C.1, corresponding to the lowest S_1 dark state belonging to the B_{2g} representation, and the bright S_2 state with B_{3u} symmetry.

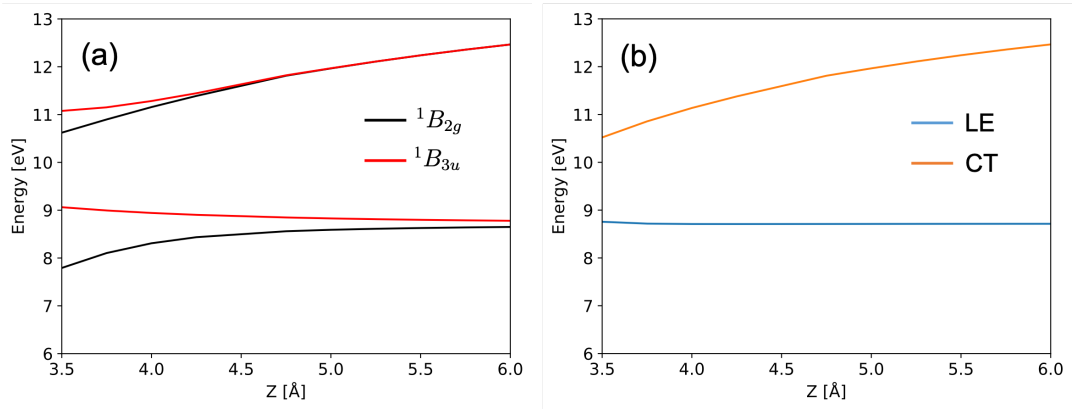

Figure 6.2: (a) Energy profiles (in eV) of the four lowest $\pi \rightarrow \pi^*$ excited singlet states and (b) diabatic LE and CT energies for the eclipsed ethylene dimer at different intermolecular separations (z in Å) computed at the CIS/6-31G level.

At large molecular separations the energies of the two lowest singlets (1^1B_{2g} and 1^1B_{3u}) converge towards the excitation energy of the monomer, which is equivalent to the (constant) LE diabatic energy. The two states resulting from the symmetric and antisymmetric $\pi \rightarrow \pi^*$ CT mixings ($\Phi_{CR}^{(\pm)}$) involving the highest and lowest molecular orbitals (HOMO and LUMO) of the two monomers belong to the same irreducible representations of S_1 and S_2 ($S_3 \in B_{3u}$ and $S_4 \in B_{2g}$) and appear at higher energy. For $z > 4.5$ Å both states are virtually degenerated to the CT (diabatic) energy, which exhibits the expected $1/R$ dependence.

At shorter distances the interaction induced by orbital overlap and LE/CT mixings results in an important stabilization and destabilization of the dark (B_{2g}) S_1 and S_4 states, while S_2 and S_3 profiles present mild deviations with respect to LE and CT energies, indicating weaker interchromophoric interactions.

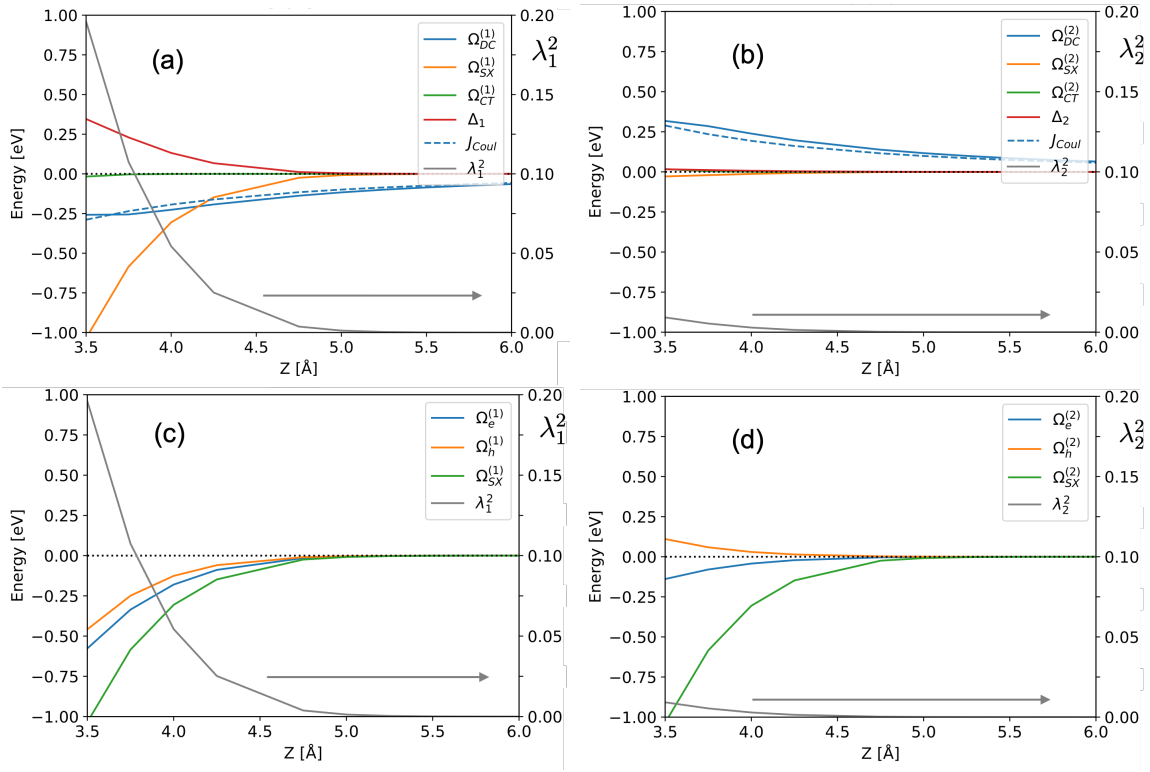

Figure 6.3: Contributions to the (a) dark S_1 and (b) bright S_2 excitation energies (in eV); (c,d) decomposition of the super-exchange $\Omega_{SX}^{(i)}$ in electron ($\Omega_e^{(i)}$) and hole ($\Omega_h^{(i)}$) parts, and λ_i^2 of both excited singlets for the eclipsed ethylene dimer at different intermolecular separations computed at the CIS/6-31G level. J_{Coul} corresponds to the classical dipole-dipole Coulomb interaction (equation 6.20).

In order to rationalize the excitation energies along the intermolecular separation coordinate R (in the z-direction), in the following we explore the different terms and contributions as described in equation 6.31. As shown in Figure C.3a, along the entire D_{2h} distortion the direct coupling and super-exchange terms contribute to lower the energy of the 1^1B_{2g} state with respect to the lowest monomer transition (E_{LE}), while the second order contribution in LE/CT mixings (Δ_1) is positive since its sign is defined by $E_{CT} - E_{LE}$ difference.

As expected, the absolute magnitude of all interaction terms increases as R decreases. At large R, $\lambda_{1,2} \to 0$ and the two lowest singlets mainly correspond to the symmetric and antisymmetric combinations of the two LE diabats (Frenkel excitons $\Phi_{FE}^{(\pm)}$). In that region, the S_1/S_2 energy splitting is controlled by the direct coupling, which is the predominant interaction for the excitation energy to 1^1B_{2g} at long distances ($R > 4.5$ Å), and along the entire separation range

for the 1^1B_{3u} state. The $\Omega_{DC}^{(i)}$ contribution exhibits opposite signs for the two lowest excitons, in agreement with the Kasha's rule [33]. The classical expression for the dipole-dipole interaction (J_{Coul} in equation 6.20) matches very well with $\Omega_{DC}^{(i)}$ energies at the long range, while slightly deviates from it as the two molecules approach to each other (Figure C3).

At lower distances the orbital overlap between the two monomers becomes significant and the magnitude of LE/CT mixing (λ_1^2) and of the super-exchange $\Omega_{SX}^{(1)}$ coupling (and Δ_1) increase rapidly compared to $\Omega_{DC}^{(1)}$. As a result, super-exchange becomes the most important (stabilizing) contribution to the energy of S_1 for $R < 4.3$ Å, and the Δ_1 term turns out to be also very important. Notice that both hole and electron pieces of $\Omega_{SX}^{(1)}$ contribute to lower the energy of S_1 (Figure C.3c). On the other hand, super-exchange and second order contributions for the 1^1B_{3u} bright state, i.e., $\Omega_{SX}^{(2)}$ and Δ_2 respectively, are rather small compared to the 1^1B_{2g} counterparts. Moreover, the hole and electron contributions emerging from the LE/CT interaction ($\Omega_h^{(2)}$ and $\Omega_e^{(2)}$) virtually cancel each other (Figure C.3d) resulting in a marginal role of the super-exchange energy contribution to the overall transition to 1^1B_{3u}. Consequently, the blue-shifting $\Omega_{DC}^{(2)}$ term dominates the energy change with respect to the excitation in the monomer, that is H-aggregation (Figure C.3b), in agreement with small λ_2 values and with the rather constant energy profile of 1^1B_{3u} (Figure C.1).

6.4.2 Slip-stacked ethylene dimer

In this section we will discuss the energies, couplings and contributions for coplanar ethylene dimers with different in-plane displacements for two fixed intermolecular distances, corresponding to weak ($z = 4.7$ Å) and strong ($z = 3.5$ Å) LE/CT interaction regimes. Slip-stacked distortions of the ethylene dimer reduce the D_{2h} symmetry of the eclipsed conformation and, in general, only the inversion center remains as a symmetry element (C_i symmetry). Hence, the two lowest excited singlets belong to the A_g and A_u representations. For linear displacements ($x = 0$ Å or $y = 0$ Å) the dimer holds C_{2h} symmetry ($S_1 \in A_g$ and $S_2 \in B_u$), with the two-fold rotational symmetry axis corresponding to the x- and y-axis for $x = 0$ and $y = 0$ linear displacements, respectively.

Excitation energy surfaces in the xy-plane at $z = 3.5$ Å ($z = 4.7$ Å) for the 2^1A_g and 1^1A_u states are shown in Figure C.4 (Figure C4). The excitation energy to the dark 2^1A_g state has a minimum at the eclipsed conformation ($x = y = 0$ Å), which continuously increases towards E_{LE} when slipping the molecules along the short molecular axis y. On the other hand, slip-stack displacement in the x-direction exhibits two shallow energy maxima at $x \simeq \pm 3.0$ Å ($y = 0.0$ Å). The PES of 1^1A_u is rather smoother than the 2^1A_g one, with transition energy maximum and minima at the displacements corresponding to the minimum and maxima of 2^1A_g. Again, the energy of the two states converge to E_{LE} at large intermolecular distances. Moreover, it is worth noticing that the energy ordering of the two states swaps along the long-axis (x) displacement, corresponding to the transition from H- to J-aggregation (Figure C.4c), while the ethylene dimer remains as H-aggregate for y-distortions (Figure C.4d). For $y = 0.0$ Å the energy crossings are located at $x = \pm 2.0$ Å .

At larger separation between the molecular planes (z) the two PESs qualitatively exhibit the same characteristics as in Figure C.4, although with weaker stabilizations (destabilizations) with respect to E_{LE}. The crossing between the two states in the x-direction appears at larger displacements ($x = 3.0$ Å in Figure C4b).

Likewise along the symmetry preserving z-distortion, the computed energy for the LE diabat remains constant in the xy-plane, that is flat PES, while the PES of the pristine CT configuration presents the $1/R$ topology with larger well depths for shorter inter-planar z-distances (Figure C5).

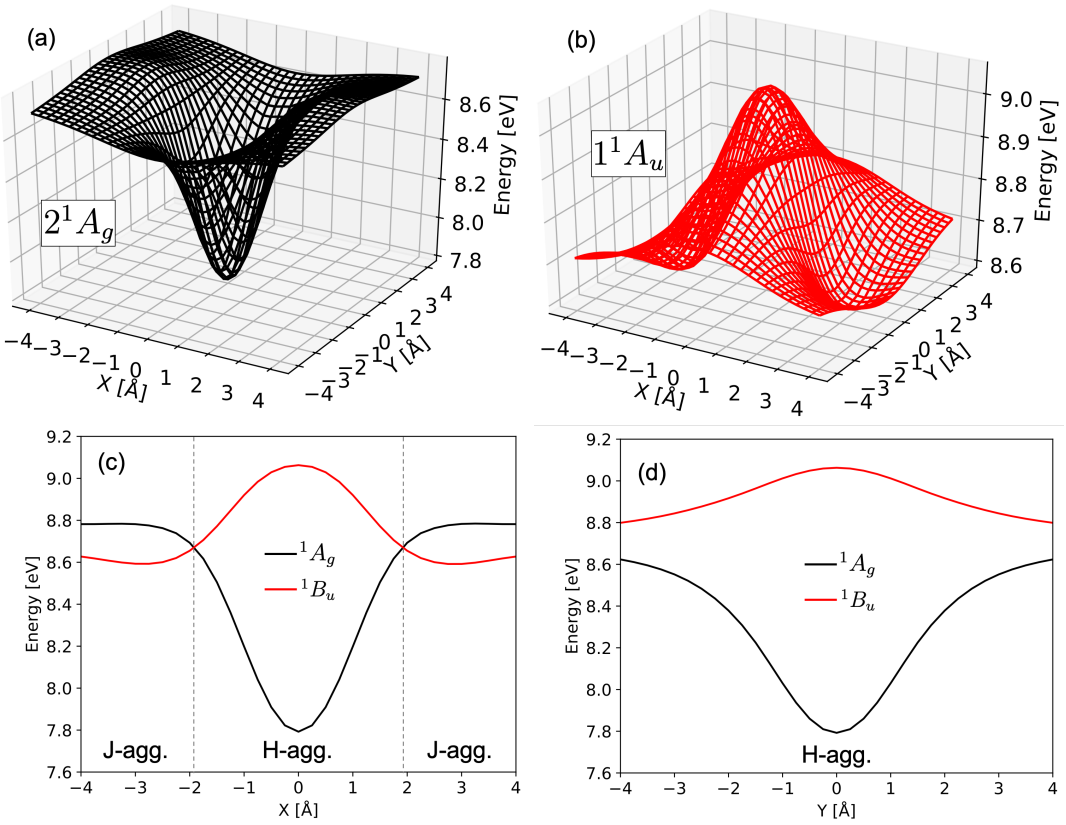

Figure 6.4: Adiabatic energies (in eV) of the two lowest excited singlet states in the xy-plane (a,b), and corresponding energy profiles along the long (c) and short (d) axes for the coplanar ethylene dimer at $z = 3.5$ Å, computed at the CIS/6-31G level.

Decomposition of the adiabatic energies of dark and bright states in diabatic contributions within the strong electronic coupling regime ($z = 3.5$ Å) is shown in Figure C.6. The direct coupling term for 2^1A_g (1^1A_u) state exhibits and intense minimum (maximum) at the D_{2h} symmetry origin with vertical nodes crossing the x-axis at the H- to J-aggregation transition region. Super-exchange energy stabilizes both S_1 and S_2 states, although they hold highly different profiles and magnitudes. In the 2^1A_g state, $\Omega_{SX}^{(1)}$ has a deep minimum at the eclipsed disposition that, in conjunction with $\Omega_{DC}^{(1)}$, promotes the formation of the excimer state. As evaluated along the D_{2h}-symmetry distortion (Figure C.3a), $\Omega_{SX}^{(1)}$ dominates over $\Omega_{DC}^{(1)}$ for small (x, y) slip-stacking distortions at $z = 3.5$ Å, but it vanishes faster than the direct coupling as the distance between the molecules increases.

As shown in Figure C.3, the LE/CT mixing in the 1^1A_u state is much weaker than in 2^1A_g, resulting in smaller super-exchange energy. The $\Omega_{SX}^{(2)}$ term has minima at the long-axis displaced

geometries ($x \simeq \pm 2.5$ Å), for which super-exchange accounts for approximately ~ 0.2 eV stabilization energy (at $z = 3.5$ Å) with respect to the monomeric excitation energy (E_{LE}). Hence, the LE/CT coupling also acts as the driving force for the stabilization of the bright state at slightly long-axis displaced structures, while the direct coupling imposes a rather strong energy penalty for $x \to 0$ coplanar arrangements on the bright state PES.

Like $\Omega_{SX}^{(i)}$, the destabilizing Δ_i terms for the two excited singlets are also controlled by LE/CT mixing degree (λ_i^2) and their contributions to the transition energies hold the same topologies as their super-exchange counterparts, but with small absolute values since they correspond to second order corrections. Energy contributions $\Omega_{DC}^{(i)}$, $\Omega_{SX}^{(i)}$ and Δ_i at larger inter-planar separation exhibit qualitatively similar landscapes as the ones in Figure C.6, but with rather weaker intensities (Figure C6).

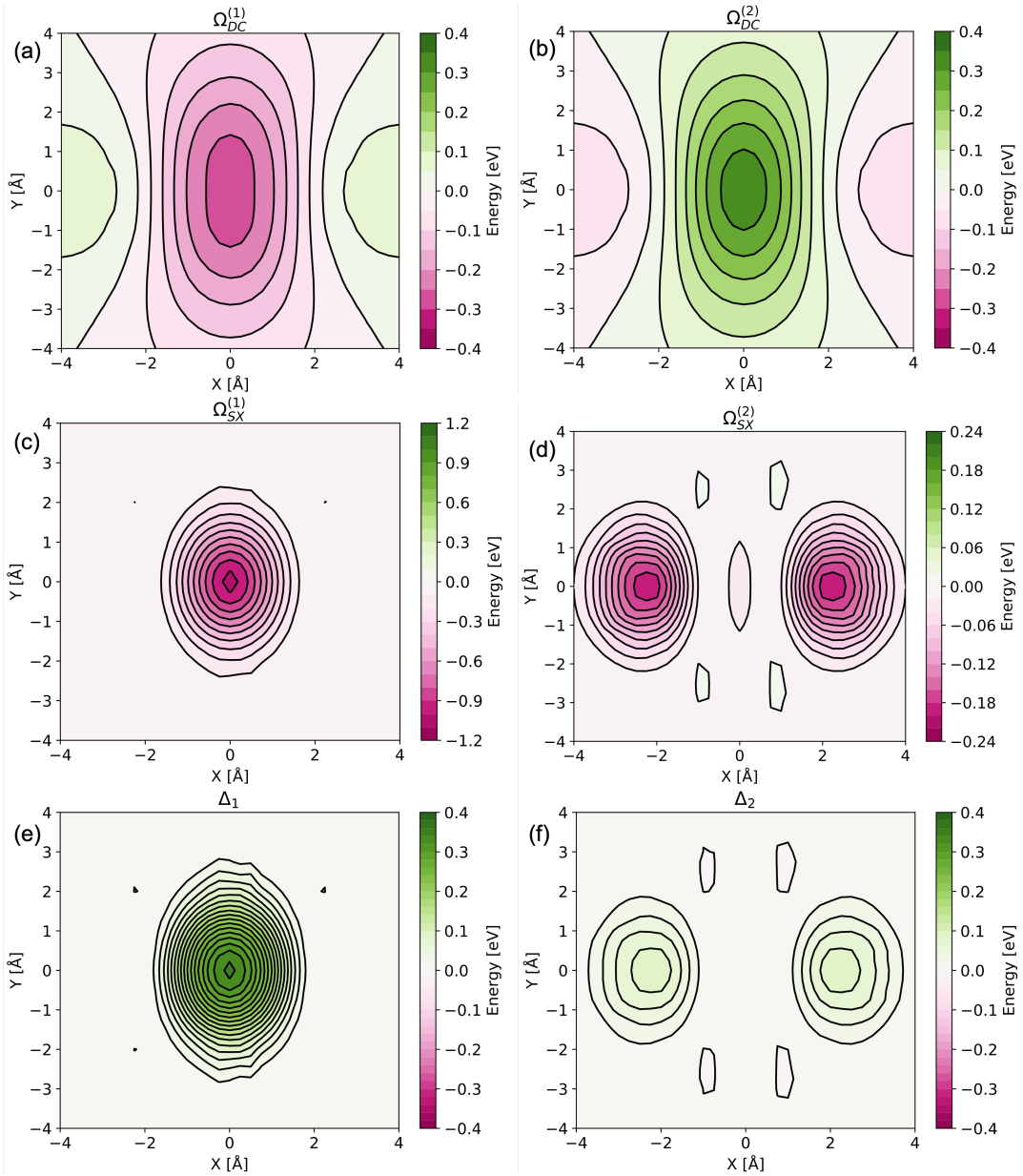

Figure 6.5: Contributions (in eV) to the excitation energies for the two lowest excited singlets in the xy-plane at $z = 3.5$ Å computed at the CIS/6-31G level. (a,b) Direct couplings ($\Omega_{DC}^{(i)}$); (c,d) super-exchange ($\Omega_{SX}^{(i)}$); and (e,f) second order energy term Δ_i.

To clearly evaluate the relative role of direct, LE/CT and CT/CT couplings we represent their profiles along the x and y mono dimensional slip-stacking displacements for the weak and strong interaction regimes for the 2^1A_g state (Figure C.7). Equivalent representations for the bright state can be found as Appendix C (Figure C7). Individually, the profiles of $\Omega_{DC}^{(1)}$, $\Omega_{SX}^{(1)}$, $\Omega_{CT}^{(1)}$ and Δ_1 show similar behaviors in both regimes ($z = 3.5$ and 4.7 Å), but there are important quantitative differences, as mainly indicated by the degree of LE/CT mixing (λ_1^2), which eventually

controls the relative magnitude of the electronic couplings beyond the direct exciton-exciton term.

At the D_{2h} geometry, for relatively short vertical intermolecular separation ($z = 3.5$ Å) the lowest dark state holds a sizable LE/CT mixing accounting for 20% of the transition. This contribution rapidly diminishes as we break the D_{2h} symmetry and the $\Omega_{SX}^{(1)}$ contribution becomes smaller than the direct coupling. Following the long-axis displacement, the H to J transition occurs at the displacement ($x = \pm 2.0$ Å) where $\Omega_{SX}^{(1)}$ (and λ_1^2) go to zero, and very close where there is a sign inversion of $\Omega_{DC}^{(1)}$. Along the y-distortion the dimer remains as an H-aggregate with $\Omega_{SX}^{(1)}$ and $\Omega_{DC}^{(1)}$ contributions always negative and crossing each other at $y = \pm 2.0$ Å.

The absolute magnitude of all the couplings diminishes at larger vertical separations ($z = 4.7$ Å), specially for λ_1^1 and λ_1^2 terms, since they strongly depend on the effective inter-monomer orbital overlaps. As a result, $\Omega_{DC}^{(1)}$ controls the chromophoric interaction in the excited state at all (x, y) points for $z = 4.7$ Å.

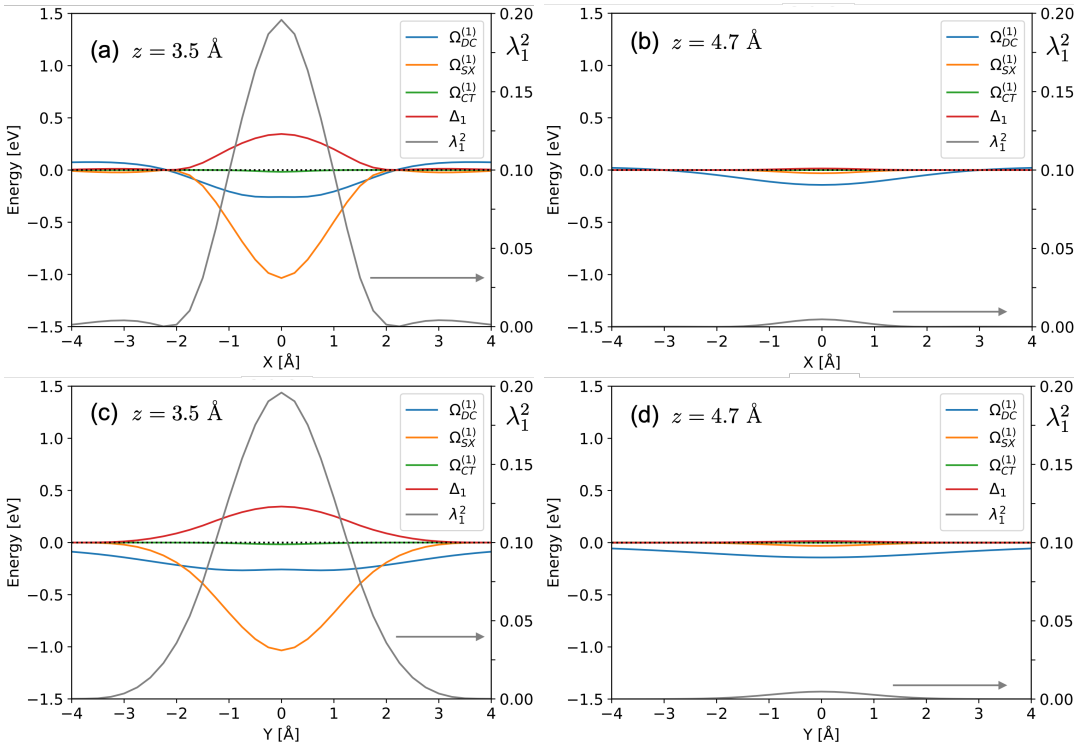

Figure 6.6: Energy contributions (in eV) and LE/CT mixings (λ_1^2) to the excitation energies to the 2^1A_g state along the long molecular x-axis with $y = 0.0$ Å and at (a) $z = 3.5$ Å and (b) $z = 4.7$ Å, and along the short molecular y-axis with $x = 0.0$ Å and at (c) $z = 3.5$ Å and (d) $z = 4.7$ Å, computed at the CIS/6-31G level.

6.4.3 Ethylene-tetrafluoroethylene dimer

In the last example we explore the nature of electronic excitations and couplings in non-equivalent chromophores. To that end we consider the coplanar ethylene-tetrafluoroethylene dimer. In this dimer the LE and CT pairs of diabats are no longer degenerate, with the lowest singlet-singlet excitation on C_2H_4 and the lowest charge separation configuration corresponding to the electronic transfer from C_2H_4 to C_2F_4 (Figure 6.7).

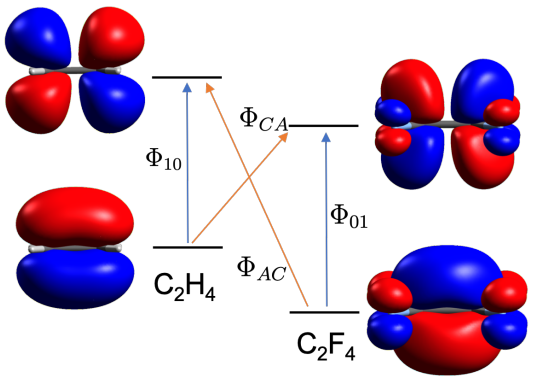

Figure 6.7: Frontier molecular orbital diagram of ethylene (left) and tetrafluoroethylene (right). HOMO to LUMO arrows indicate LE (orange) and CT (blue) diabatic transitions.

At the coplanar C_{2v} conformation the four $\pi\pi^*$ singlet adiabatic states of the dimer belong to the same irreducible representation (B_1), with their energies at dissociation tending to the C_2H_4 and C_2F_4 LE states, and $C_2H_4{}^+\cdots C_2F_4{}^-$ and $C_2H_4{}^-\cdots C_2F_4{}^+$ CT energies, respectively (Figure 6.8). The profiles of the average LE and CT energies (equation 6.44) are very close to the symmetric case (Figure C.1b), with constant E_{LE} and $1/R$ dependence of E_{CT}.

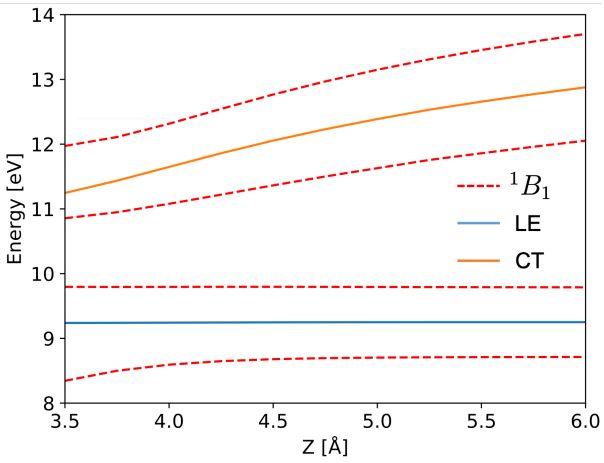

Figure 6.8: Energy profiles (in eV) of the four lowest $\pi \rightarrow \pi^*$ excited singlet states (red dashed lines) and diabatic LE (blue) and CT (orange) average energies for the C_{2v} ethene-tetrafluoroethene dimer at different intermolecular separations (z in Å) computed at the CIS/6-31G level.

The dependence of electronic couplings with R for the S_1 state is similar to the symmetrical case, but with much lower LE/CT mixings (λ_1^2). At large separation ($z > 5$ Å) S_1 corresponds to the pristine LE on C_2H_4 with no mixings with other diabats ($\lambda_1^2 = 0, \delta_{LE}^{(1)2} = 1$) and with

$\Omega^{(1)}_{DC} = \Omega^{(1)}_{SX} = \Omega^{(1)}_{CT} = 0$ (Figure 6.9a). At shorter distances the π-orbitals of the two molecules effectively interact, mixing the transition on C_2F_4 into the lowest adiabatic singlet ($1-\delta^{(1)2}_{LE} > 0$). The coupling of the two LE states stabilize the lowest singlet ($\Omega^{(1)}_{DC} < 0$). Simultaneously, super-exchange contribution becomes a stabilizing factor as λ_1^2 grows, while CT configurations play virtually no role to the S_1 energy. It should be noticed that, due to the localized nature of the lowest singlet at dissociation in the asymmetric case, the direct exciton coupling is effective in a rather shorter range than in the D_{2h} ethylene dimer. Both hole and electron LE/CT couplings contribute to $\Omega^{(1)}_{SX}$ (Figure 6.9b), which is directly related to the interaction of both frontier monomeric orbitals, HOMOs and LUMOs, respectively.

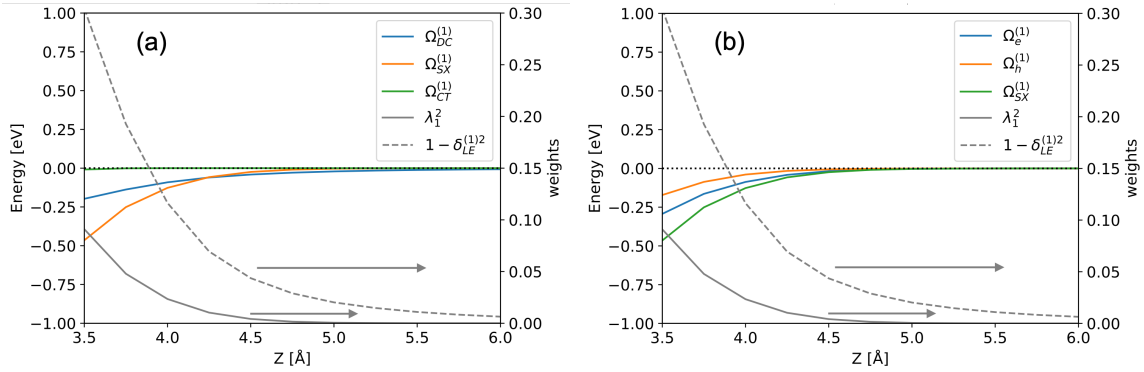

Figure 6.9: (a) Excitation energy coupling contributions (in eV) to the S_1 state and (b) decomposition of the super-exchange $\Omega^{(1)}_{SX}$ in electron ($\Omega^{(1)}_e$) and hole ($\Omega^{(1)}_h$) parts, and λ_1^2 and $1-\delta^{(1)2}_{LE}$ of the lowest excited singlets for the $C_2H_4\cdots C_2F_4$ dimer at different intermolecular separations computed at the CIS/6-31G level.

6.5 Conclusions

In this chapter we have presented a connection between excited states diabatization schemes and energy expressions derived from excitonic models. Such relationships allow to characterize the properties of electronic transitions in molecular aggregates and decompose their excitation energies in contributions issued from couplings with different physical origin. Moreover, the methodology presented in this work is able to quantify the weight of the different contributions from *ab initio* electronic structure calculations of the super system, avoiding both the use of pre-defined diabatic states and strong (potentially unjustified) approximations for the calculations

of electronic couplings.

Our methodology has been tested in symmetric and non-symmetric molecular dimers. The present results show how, in symmetric systems, super-exchange is the most important exciton stabilization driving force in strongly interacting chromophores (short range) controlling the nature of the lowest transition, e.g., H- or J-aggregation, while direct coupling prevails at the weakly coupling regime. The localized character of low-lying states in non-symmetric dimers can also hinder the LE/LE interaction at long range, only allowing the presence of short range effective couplings.

It is worth noticing that the methodology introduced is variational within the window of chosen adiabats and can be applied to the entire range of coupling regimes, while approximations based on perturbation theory typically employed in the construction of excitonic Hamiltonians are ill-defined in the strong coupling regime, which might drive to incorrect interpretations. On the other hand, like in any methodology based on the diabatization of a finite number of adiabatic states, the presented scheme depends on the set of adiabatic states. The selection of the space of adiabatic states is not unique and in some cases might not appear as straightforward as in the examples explored in this manuscript. At the same time, we believe that our analysis might help to identify problematic diabatization schemes and can be also used to better select or improve the space of adiabatic states.

The presented theory and methodological approach for the characterization of electronic transitions in interacting chromophores has been developed for the case of two interacting molecules based on the diabatization of four singlet excitons, but it can be generalized to the presence of multiple chromophores and/or to the case of more than four adiabatic (and diabatic) states. Moreover, beyond the detailed characterization of electronic transitions in aggregates, the present approach could eventually be used to check the validity of diabatic state energies and interstate couplings employed in excitonic models, determine their range of applicability or to obtain *ab initio* diabatic state energies and interstate couplings that can be eventually plugged into model excitonic Hamiltonians to explore electronic transition in large aggregates or in molecular solids.

Chapter 7

General conclusions

In the present thesis, different computational approaches for the characterization of electronic excited states have been implemented and applied to the study of different organic systems. In particular, we have seen that the computational characterization of electronic transitions becomes specially appealing in the study of molecular aggregates, where excited states hold recognizable properties of the electronic transitions of its molecular constituents, but also novel features may appear as a result of the interchromophoric interactions. This thesis is largely devoted to understand such interchromophoric interactions in order to characterize the electronic states in photoactivated aggregates and to study their properties. The specific conclusions for each project have already been stated in the respective Chapters. Accordingly, the following lines are intended to give an end to the manuscript by highlighting the main results of the work and providing some directions for future work.

As discussed in the previous Chapters, the theoretical and computational description of photophysics in molecular aggregates is typically tackled by the use of exciton models. However, these approaches are based on the definition of relevant diabatic states, which requires good pre-knowledge of the system under study. One of the main achievements of this work was the use of an alternative strategy, which enables a connection between excited states diabatization schemes and energy expressions derived from excitonic models. Such relationships allow to characterize the properties of electronic transitions in molecular aggregates and decompose their

excitation energies in contributions issued from couplings with different physical origin. The methodology presented in this work is able to quantify the weight of the different contributions from *ab initio* electronic structure calculations of the super system, avoiding both the use of pre-defined diabatic states and strong (potentially unjustified) approximations for the calculations of electronic couplings. This methodology, tested on model symmetric and non-symmetric molecular dimers in Chapter 6, allowed to identify the important exciton stabilization driving forces in interacting chromophores.

As reported in Chapter 4, deconvolution of the computed excitations in terms of diabatic states also allowed quantifying the involvement of the different chromophoric unities and characterizing the nature of the low-lying excited singlet states of three curcumin derivatives and their covalent dimers linked through a polymethylenic chain. With the example of flavylium fluorophores, we demonstrated in Chapter 5 that such a methodology is also highly helpful for gaining clear physical insights on the nature of the excited states of isolated conjugated dyes. Here, diabatization of the lowest-energy excited state evidenced that the bathochromic shift of the emission wavelength observed when elongating the polymethine chain in the investigated series of compounds mainly originates from the decrease of the diabatic charge transfer energy. The clear and intuitive rationalizing picture offered by the diabatization scheme allowed us to propose new theoretically-designed fluorophores, which are expected to exhibit unprecedented bright emission in the shortwave infrared region, with high potential for biological imaging.

From a global viewpoint of computational chemistry, this work has thus demonstrated that the relevance of developing simple characterization tools, close to the chemist's intuition, for rationalizing the nature of excited states in organic (supra)molecular systems and better understanding and control of their optical properties.

Appendix A

Optical properties of quadrupolar and bi-quadrupolar dyes: intra and interchromophoric interactions

A.1 Synthesis of the curcumin derivatives

All solvents for synthesis were of analytic grade. NMR spectra were recorded at room temperature on a JEOL JNM ECS 400 (400 and 100 MHz for ^{1}H and ^{13}C, respectively) spectrometer. Data are listed in parts per million (ppm) and are reported relative to tetramethylsilane (^{1}H and ^{13}C); residual solvent peaks of the deuterated solvents were used as internal standards. High resolution mass spectra were obtained in Spectropole, Marseille (http://www.spectropole.fr). 1,8-Bis(4-formylphenoxy)octane was obtained according a previously described procedure.[135] All starting chemical products and solvents were purchased from Sigma-Aldrich or TCI and used without further purification.

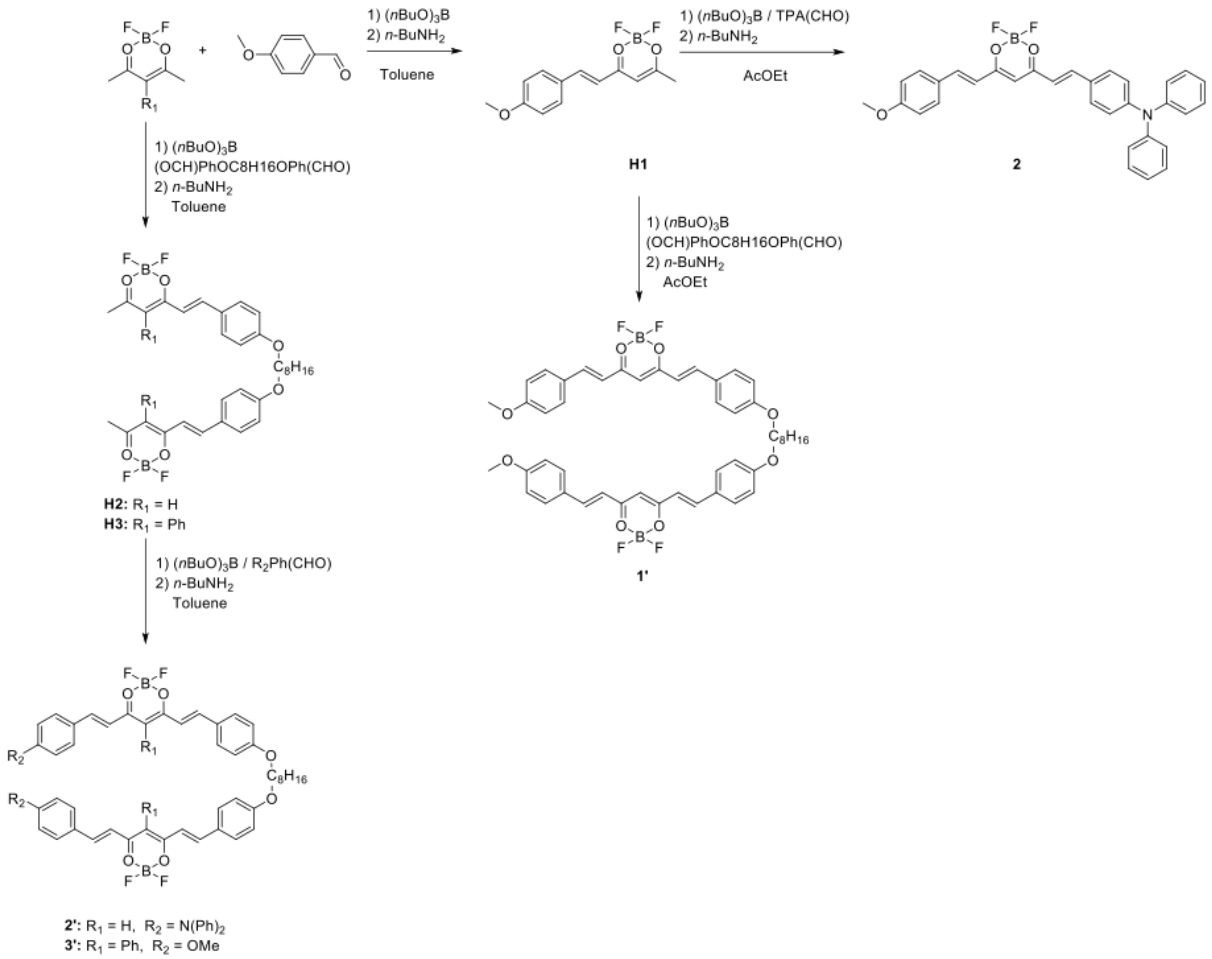

A.1.1 Difluoro(3-phenylpentane-2,4-dionato)boron

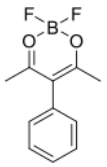

Boron trifluoride diethyletherate (3.51 mL, 27.92 mmol) was added dropwise to a solution of 3-phenylpentane-2,4-dione (4.1 g, 23.27 mmol) in dichloromethane (100 mL). The reaction mixture was stirred at 40 °C overnight. After cooling, solvents were removed under vacuum and the crude was purified on silica gel column with dichloromethane/cyclohexane (1/1 v:v) as eluent. The result product was obtained as a white solid (5.01 g, 96 %). ^{1}H NMR (400 MHz, $CDCl_3$, ppm): $\delta = 7.50 - 7.40$ (m, 3H), $7.20 - 7.14$ (m, 2H), 2.11 (s, 6H). ^{13}C NMR (100 MHz, CDCl3, ppm): δ = 191.2, 133.1, 130.7, 129.7, 129.1, 23.8.

A.1.2 BF_2-hemicurcuminoid H1

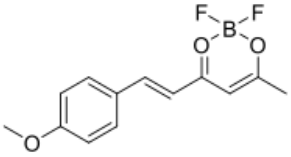

(Acetylacetonato)difluoroboron (5.38 g, 36.40 mmol) was dissolved into 100 mL of toluene and stirred at reflux for 30 min under argon. Then a solution of p-anisaldehyde (1.11 mL, 9.10 mmol) and tri-*n*-butylborate (2.71 mL, 10.01 mmol) in 100 mL of toluene was added dropwise and the reaction mixture was stirred for 30 min under reflux. A first portion of *n*-butylamine (450 μL, 4.55 mmol) was added and after 2 h a second portion of *n*-butylamine (450 μL, 4.55 mmol) was added and the reaction mixture was stirred under reflux overnight. Solvent was removed under vacuum and the crude was purified on silica gel column with cyclohexane/dichloromethane (1/1 v:v) as eluent. The product was obtained as a yellow powder (1.47 g, 61 %). ^{1}H NMR (400 MHz, $CDCl_3$, ppm): $\delta = 8.05$ (d, $J = 15.5$ Hz, 1H), 7.58 (d, $J = 8.8$ Hz, 2H), 6.96 (d, $J = 8.8$ Hz, 2H), 6.51 (d, $J = 15.5$ Hz, 1H), 5.96 (s, 1H), 3.88 (s, 3H), 2.32 (s, 3H). ^{13}C NMR (100 MHz, CDCl3, ppm): $\delta = 190.5$, 180.9, 163.2, 148.7, 131.6, 126.7, 117.2, 115.0, 101.2, 55.7, 24.4.

A.1.3 Bis(BF_2-hemicurcuminoid)-α,ω-octane H2

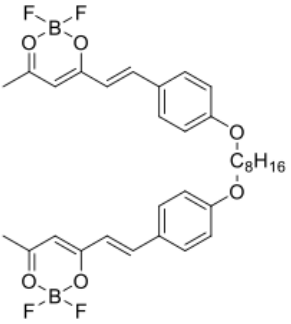

(Acetylacetonato)difluoroboron (3.33 g, 22.56 mmol) was dissolved into 50 mL of toluene and stirred at reflux for 30 min under argon. 1,8-Bis(4-formylphenoxy)octane (1.0 g, 2.82 mmol) and tri-*n*-butylborate (763 μL, 2.82 mmol) were dissolved into 100 mL of toluene and the solution was added dropwise to the reaction mixture. After stirring for 30 min at reflux, a first portion

of n-butylamine (139 μL, 1.41 mmol) was added. A second portion of n-butylamine (139 μL, 1.41 mmol) was added after 3h and the reaction mixture was stirred at reflux overnight. After cooling, the reaction mixture was filtered and the solvent was removed under vacuum. The crude was purified on silica gel column with dichloromethane/cyclohexane (1/1 v:v) as eluent. The product was obtained as an orange powder (601 mg, 35 %). 1H NMR (400 MHz, $CDCl_3$, ppm): $\delta = 8.04$ (d, $J = 15.5$ Hz, 2H), 7.56 (d, $J = 8.8$ Hz, 4H), 6.92 (d, $J = 8.8$ Hz, 4H), 6.50 (d, $J = 15.5$ Hz, 2H), 5.96 (s, 2H), 4.02 (t, $J = 6.4$ Hz, 4H), 2.32 (s, 6H), $1.87 - 1.75$ (m, 4H), $1.53 - 1.36$ (m, 8H). ^{13}C NMR (100 MHz, $CDCl_3$, ppm): $\delta = 180.9$, 162.9, 148.8, 131.6, 129.0, 126.5, 117.0, 115.4, 101.2, 28.4, 29.3, 29.1, 26.0, 24.4.

A.1.4 BF_2-hemicurcuminoid H3

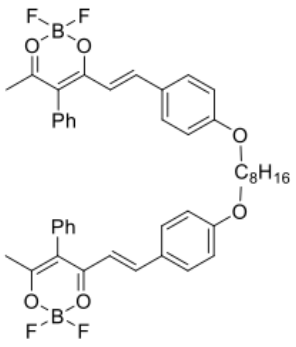

Difluoro(3-phenylpentane-2,4-dionato)boron (4.0 g, 17.86 mmol) was dissolved into 50 mL of toluene and stirred at reflux for 30 min under argon. Solution of 1,8-bis(4-formylphenoxy)octane (1,58 g, 4.47 mmol) and tri-n-butylborate (1.45 mL, 5.36 mmol) in 100 mL of toluene was added dropwise into the reaction mixture. After stirring for 30 min at reflux, a first portion of n-butylamine (221 μL, 2.24 mmol) was added to the reaction mixture. A second portion of n-butylamine (221 μL, 2.24 mmol) was added after 2h and the reaction mixture was stirred at reflux overnight. After cooling, the precipitate was filtered under vacuum. The product was purified on silica gel column with cyclohexane/dichloromethane (7/3 v:v) as eluent to give the product as an orange powder (452 mg, 15 %). ^{1}H NMR (400 MHz, $CDCl_3$, ppm): $\delta = 8.07$ (d, $J = 15.4$ Hz, 2H), $7.54 - 7.42$ (m, 6H), 7.34 (d, $J = 8.8$ Hz, 4H), $7.26 - 7.21$ (m, 4H), 6.83 (d, $J = 8.8$ Hz, 4H), 6.26 (d, $J = 15.4$ Hz, 2H), 3.96 (t, $J = 6.5$ Hz, 4H), 2.13 (s, 6H), $1.82 - 1.71$

(m, 4H), 1.51 − 1.31 (m, 8H). ^{13}C NMR (100 MHz, CDCl3, ppm): δ = 178.8, 162.8, 149.1, 133.2, 131.8, 131.5, 129.5, 128.9, 126.9, 115.9, 115.2, 114.3, 68.4, 29.4, 29.1, 26.0, 23.9.

A.1.5 Monomer 2

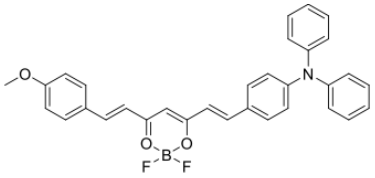

BF_2-hemicurcuminoid **H1** (0.5 g, 1.88 mmol) was dissolved into 30 mL of ethyl acetate and heated to 60 °C. A solution of 4-(*N*, *N*-diphenylamino)benzaldehyde (0.62 g, 2.26 mmol) and tri-*n*-butylborate (612 μL, 2.26 mmol) in 30 mL of ethyl acetate was added to the reaction mixture and stirred for a further 30 min at 60 °C. Then, *n*-butylamine (74.3 μL, 0.75 mmol) was added to the solution. A second portion of the *n*-buthylamine was made (37.2 μL, 0.38 mmol) after 4h. The reaction mixture was stirred at 60 °C overnight. After cooling, the solvent was removed under vacuum and the crude was purified on silica gel column with cyclohexane/dichloromethane (1/1 v:v) as eluent. Precipitation from cyclohexane/dichloromethane gave the product as a brown powder (122 mg, 12 %). ^{1}H NMR (400 MHz, $CDCl_3$, ppm): δ = 7.99 (d, J = 15.6 Hz, 1H), 7.98 (d, J = 15.3 Hz, 1H), 7.57 (d, J = 8.8 Hz, 2H), 7.44 (d, J = 8.8 Hz, 2H), 7.37 − 7.30 (m, 4H), 7.20 − 7.12 (m, 6H), 6.98 (d, J = 8.8 Hz, 2H), 6.94 (d, J = 8.8 Hz, 2H), 6.57 (d, J = 15.6 Hz, 1H), 6.53 (d, J = 15.3 Hz, 1H), 5.98 (s, 1H), 3.87 (s, 3H). ^{13}C NMR (100 MHz, $CDCl_3$, ppm): δ = 179.5, 178.8, 162.8, 151.6, 147.2, 146.4, 146.3, 131.2, 131.0, 129.8, 127.3, 126.7, 126.2, 125.1, 120.6, 118.4, 117.2, 114.9, 101.9, 55.7. HRMS (ESI): Calcd. For $C_{32}H_{26}NO_3F_2BNa^+$ $[M+Na]^+$: 544.1871. Found: 544.1872 (-0.2 ppm).

A.1.6 Dimer 1

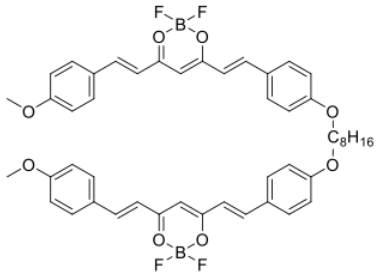

BF_2-hemicurcuminoid **H1** (1.0 g, 3.76 mmol) was dissolved into 15 mL of ethyl acetate and heated to 60 °C. 1,8-Bis(4-formylphenoxy)octane (0.48 g, 1.50 mmol) and tri-*n*-butylborate (810 μL, 3.00 mmol) were dissolved into 10 mL of ethyl acetate and the solution was added to the reaction mixture. After 30 min at 60°C, a first portion of *n*-butylamine (75 μL, 0.75 mmol) was added to the solution. A second portion of *n*-butylamine (75 μL, 0.75 mmol) was made after 2 h. After cooling, the precipitate was filtered under vacuum. The product was purified on silica gel column with dichloromethane as eluent (0.37 g, 32 %). ^{1}H NMR (400 MHz, DMSO, ppm): $\delta = 7.97$ (d, $J = 15.6$, 4H), 7.85 (d, $J = 8.8$, 4H), 7.83 (d, $J = 8.8$, 4H), $7.10 - 7.01$ (m, 12H), 6.50 (s, 2H), 4.06 (t, $J = 6.4$, 4H), 3.84 (s, 6H), $1.80 - 1.67$ (m, 4H), $1.48 - 1.31$ (m, 8H). HRMS (ESI): Calcd. For $C_{48}H_{48}O_8F_4B_2Na^+$ $[M+Na]^+$: 873.3380. Found: 873.3379 (+ 0.1 ppm).

A.1.7 Dimer 2

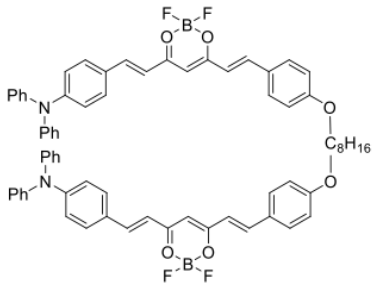

BF_2-hemicurcuminoid **H2** (0.78 g, 1.27 mmol) was dissolved into 20 mL of toluene and stirred at reflux. 4-(*N*, *N*-Diphenylamino)-benzaldehyde (0.70 g, 2.54 mmol) and tri-*n*-butylborate (687 μL, 2.54 mmol) were dissolved into 40 mL of toluene and added to the reaction mixture.

n-Butylamine (62.0 μL, 0.63 mmol) was added after 30 min at reflux. A second addition of the n-buthylamine (62.0 μL, 0.63 mmol) was made after 2 h. The reaction mixture was stirred at reflux overnight. After cooling, the solvent was removed under vacuum and the crude was purified on silica gel column with cyclohexane/dichloromethane (1/1 v:v) as eluent. The precipitation from cyclohexane/dichloromethane gave the product as a brown powder (144 mg, 11 %). ^{1}H NMR (400 MHz, $CDCl_3$, ppm): $\delta = 7.97$ (d, $J = 15.4$ Hz, 2H), 7.95 (d, $J = 15.4$ Hz, 2H), 7.53 (d, $J = 8.7$ Hz, 4H), 7.43 (d, $J = 8.8$ Hz, 4H), $7.37 - 7.29$ (m, 8H), $7.20 - 7.12$ (m, 12H), 6.97 (d, $J = 8.7$ Hz, 4H), 6.90 (d, $J = 8.8$ Hz, 4H), 6.54 (d, $J = 15.4$ Hz, 2H), 6.51 (d, $J = 15.4$ Hz, 2H), 5.97 (s, 2H), 4.01 (t, $J = 6.4$ Hz, 4H), $1.88 - 1.74$ (m, 4H), $1.49 - 1.36$ (m, 8H). ^{13}C NMR (100 MHz, $CDCl_3$, ppm): $\delta = 162.4$, 151.6, 150.9, 147.1, 146.4, 131.2, 131.0, 129.8, 127.0, 126.7, 126.2, 125.1, 120.5, 118.2, 117.2, 115.3, 115.0, 101.8, 68.3, 29.2, 27.1, 25.9. HRMS (ESI): Calcd. For $C_{70}H_{62}N_2O_6F_4B_2Na^+$ $[M+Na]^+$: 1147.4644. Found: 1147.4648 (+0.3 ppm).

A.1.8 Absorption spectra of monomers 1 and 2 in different solvents

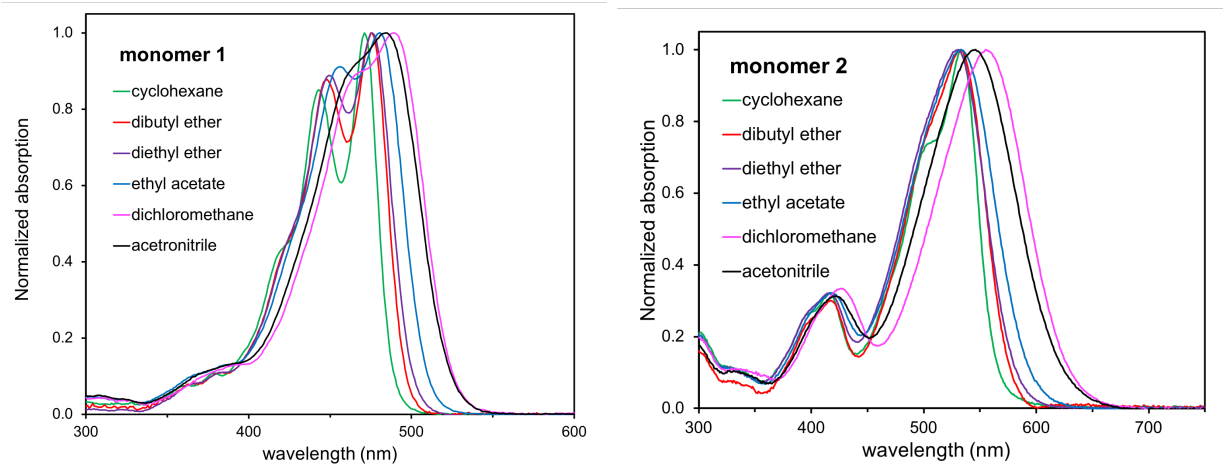

Figure A.1: Normalized absorption spectra of curcumin monomers **1** (left) and **2** (right) recorded in different solvents.

A.2 Excitation energies: functional and basis set

A.2.1 Curcumin monomers

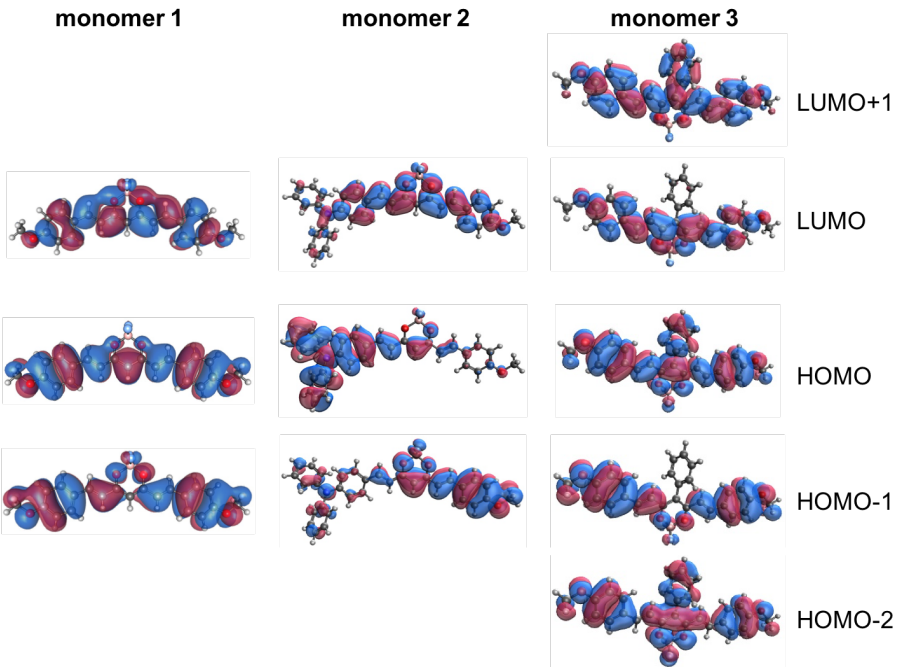

Figure A.2: Frontier molecular orbitals of the curcumin monomers **1**-**3** calculated at the ωB97X-D/6-31+G(d) level. Molecular orbitals of **3** corresponds to the $\theta = 62°$ case.

	ωB97X-D		BLYP		B3LYP		CAM-B3LYP	
state	TDA	TDDFT	TDA	TDDFT	TDA	TDDFT	TDA	TDDFT
S_1	3.43	3.32	2.58	2.47	2.98	2.86	3.37	3.26
	(2.47)	(2.13)	(1.75)	(1.42)	(2.30)	(2.25)	(2.48)	(2.11)
S_2	4.34	4.15	2.74	2.68	3.42	3.33	4.24	4.05
	(0.10)	(0.08)	(0.02)	(0.02)	(0.00)	(0.02)	(0.09)	(0.07)

Table A.1: Excitation energies (in eV) of monomer **1** obtained with different energy functionals and the 6-31+G(d) basis set in vacuum. Oscillator strengths indicated in parenthesis.

	6-31+G(d)		6-311++G(d,p)	
state	TDA	TDDFT	TDA	TDDFT
S_1	3.43 (2.47)	3.32 (2.13)	3.42 (2.46)	3.30 (2.13)
S_2	4.34 (0.10)	4.15 (0.08)	4.32 (0.10)	4.13 (0.08)

Table A.2: Excitation energies (in eV) of monomer **1** computed with the ωB97X-D functional and different basis sets. Oscillator strengths indicated in parenthesis.

	ωB97X-D		B3LYP		CAM-B3LYP	
	TDA	TDDFT	TDA	TDDFT	TDA	TDDFT
S_1	3.82 (1.33)	3.73 (1.32)	2.94 (0.98)	2.82 (0.98)	3.75 (1.28)	3.72 (1.28)
S_2	4.00 (0.99)	3.91 (1.00)	3.30 (0.75)	3.18 (0.78)	3.97 (0.98)	3.93 (0.97)

Table A.3: Excitation energies (in eV) of monomer **2** obtained with different energy functionals and the 6-31+G(d) basis set in vacuum. Oscillator strengths indicated in parenthesis.

	ωB97X-D		B3LYP	
	TDA	TDDFT	TDA	TDDFT
S_1	3.07 (1.02)	3.00 (0.92)	2.56 (0.80)	2.43 (0.79)
S_2	4.04 (1.20)	3.96 (1.19)	3.18 (1.01)	3.14 (0.96)
S_3	4.14 (0.02)	4.08 (0.01)	3.21 (0.02)	3.16 (0.20)

Table A.4: Excitation energies (in eV) of monomer **3** obtained with different energy functionals and the 6-31+G(d) basis set in vacuum. Oscillator strengths indicated in parenthesis.

comp.	state	ωB97X-D	B3LYP	transition
1	S_1	88	87	H→L
	S_2	83	85	H-1→L
2	S_1	63	68	H→L
		23	18	H-1→L
	S_2	70	20	H-1→L
		12	11	H→L
3	S_1	94	92	H→L
	S_2	78	83	H-2→L
	S_3	56	51	H-1→L
		39	37	H→L+1

Table A.5: Main orbital contributions (in %) for the low-lying singlet excitations of monomers **1-3** computed at the TDA level with B3LYP and ωB97X-D energy functionals and the 6-31+G(d) basis set in vacuum. H and L indicate HOMO and LUMO, respectively.

A.2.2 Curcumin derivative dimers

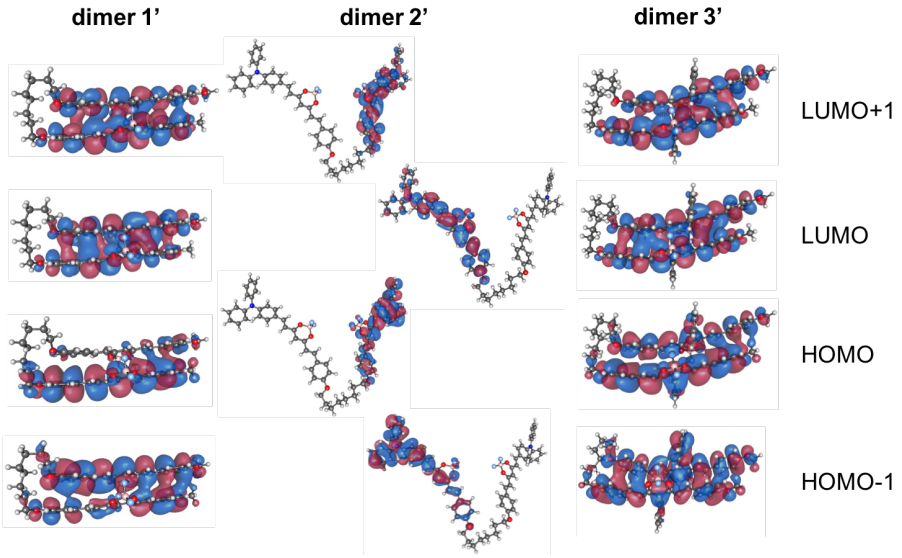

Figure A.3: Frontier molecular orbitals of the curcumin dimers **1'-3'** calculated at the ωB97X-D/6-31+G(d) level.

	ωB97X-D		B3LYP	
state	TDA	TDDFT	TDA	TDDFT
S_1	3.03 (0.02)	2.96 (0.02)	2.48 (0.01)	2.35 (0.02)
S_2	3.39 (2.56)	3.27 (3.22)	2.90 (2.34)	2.78 (2.30)
S_3	3.52 (1.27)	3.47 (0.56)	3.03 (1.08)	2.86 (1.18)
S_4	3.64 (1.27)	3.57 (0.37)	3.10 (1.08)	2.97 (1.18)
S_5	4.02 (0.09)	3.94 (0.06)	3.28 (0.06)	3.06 (0.01)
S_6	4.11 (0.01)	4.05 (0.01)	3.33 (0.01)	3.16 (0.04)
S_7	4.31 (0.02)	4.28 (0.02)	3.39 (0.00)	3.26 (0.00)
S_8	4.41 (0.01)	4.38 (0.01)	3.41 (0.00)	3.32 (0.00)

Table A.6: Excitation energies (in eV) of dimer **1'** (folded) obtained with different energy functionals and the 6-31+G(d) basis set in vacuum. Oscillator strengths indicated in parenthesis.

	ωB97X-D		B3LYP		CAM-B3LYP	
state	TDA	TDDFT	TDA	TDDFT	TDA	TDDFT
S_1	3.81 (1.46)	3.80 (1.45)	2.92 (1.17)	2.91 (1.17)	3.73 (1.96)	3.71 (1.95)
S_2	3.81 (1.46)	3.80 (1.45)	2.95 (1.22)	2.95 (1.21)	3.73 (1.91)	3.71 (1.94)
S_3	4.00 (0.96)	3.99 (0.96)	2.98 (0.40)	2.96 (0.41)	4.00 (0.90)	3.99 (0.89)
S_4	4.00 (0.96)	3.99 (0.96)	3.04 (0.41)	3.04 (0.41)	4.00 (0.87)	3.99 (0.87)
S_5	4.32 (0.01)	4.33 (0.01)	3.22 (0.02)	3.22 (0.02)	4.34 (0.01)	4.32 (0.01)
S_6	4.34 (0.01)	4.34 (0.01)	3.24 (0.03)	3.24 (0.03)	4.35 (0.01)	4.32 (0.01)
S_7	4.45 (0.02)	4.42 (0.01)	3.25 (0.02)	3.25 (0.02)	4.45 (0.02)	4.42 (0.02)
S_8	4.45 (0.03)	4.43 (0.02)	3.28 (0.00)	3.28 (0.00)	4.46 (0.07)	4.43 (0.04)

Table A.7: Excitation energies (in eV) of dimer **2'** (V-shape) obtained with different energy functionals and the 6-31+G(d) basis set in vacuum. Oscillator strengths indicated in parenthesis.

	ωB97X-D		B3LYP	
state	TDA	TDDFT	TDA	TDDFT
S_1	2.78 (0.02)	2.76 (0.01)	2.39 (0.01)	2.37 (0.01)
S_2	3.28 (2.51)	3.26 (2.50)	2.40 (2.32)	2.39 (2.32)
S_3	3.43 (1.58)	3.40 (1.58)	2.58 (1.49)	2.55 (1.59)
S_4	3.71 (0.11)	3.68 (0.09)	2.69 (0.08)	2.69 (0.06)
S_5	3.88 (0.28)	3.79 (0.19)	2.73 (0.12)	2.70 (0.09)
S_6	4.12 (0.07)	4.10 (0.05)	2.75 (0.03)	2.73 (0.02)
S_7	4.16 (0.07)	4.14 (0.06)	2.77 (0.03)	2.76 (0.03)
S_8	4.26 (0.02)	4.24 (0.02)	2.89 (0.02)	2.88 (0.01)
S_9	4.27 (0.01)	4.25 (0.01)	2.91 (0.01)	2.90 (0.01)
S_{10}	4.28 (0.00)	4.25 (0.00)	2.93 (0.00)	2.92 (0.01)

Table A.8: Excitation energies (in eV) of dimer **3'** (folded) obtained with different energy functionals and the 6-31+G(d) basis set in vacuum. Oscillator strengths indicated in parenthesis.

dimer	state	gas phase		DCM	
		TDDFT	TDA	TDDFT	TDA
	S_1	2.35 (0.016)	2.48 (0.009)	2.19 (0.008)	2.28 (0.009)
	S_2	2.78 (2.301)	2.90 (2.342)	2.59 (2.307)	2.63 (2.307)
	S_3	2.86 (1.178)	3.03 (1.083)	2.68 (1.196)	2.74 (1.076)
1'	S_4	2.97 (1.182)	3.10 (1.085)	2.71 (1.192)	3.80 (1.091)
(folded)	S_5	3.06 (0.010)	3.28 (0.059)	2.87 (0.022)	2.96 (0.032)
	S_6	3.16 (0.045)	3.33 (0.005)	2.98 (0.007)	3.04 (0.004)
	S_7	3.26 (0.002)	3.39 (0.001)	3.03 (0.001)	3.13 (0.001)
	S_8	3.32 (0.001)	3.41 (0.000)	3.11 (0.000)	3.20 (0.000)
	S_1	2.91 (1.172)	2.92 (1.169)	2.40 (1.171)	2.41 (1.170)
	S_2	2.95 (1.211)	2.95 (1.221)	2.49 (1.222)	2.49 (1.220)
	S_3	2.96 (0.401)	2.98 (0.401)	2.58 (0.402)	2.60 (0.400)
2'	S_4	3.04 (0.406)	3.04 (0.389)	2.59 (0.401)	2.63 (0.399)
(V-shape)	S_5	3.22 (0.017)	3.22 (0.009)	2.67 (0.013)	2.67 (0.009)
	S_6	3.24 (0.028)	3.27 (0.028)	2.70 (0.026)	2.73 (0.021)
	S_7	3.25 (0.021)	3.28 (0.010)	2.80 (0.023)	2.82 (0.019)
	S_8	3.28 (0.002)	3.28 (0.012)	2.82 (0.002)	2.84 (0.002)
	S_1	2.37 (0.009)	2.39 (0.010)	2.20 (0.009)	2.29 (0.011)
	S_2	2.39 (2.319)	2.40 (2.320)	2.23 (2.302)	2.30 (2.324)
	S_3	2.55 (1.487)	2.58 (1.488)	2.40 (1.489)	2.49 (1.490)
3'	S_4	2.69 (0.063)	2.69 (0.076)	2.55 (0.071)	2.63 (0.074)
(folded)	S_5	2.70 (0.086)	2.73 (0.120)	2.56 (0.089)	2.64 (0.096)
	S_6	2.73 (0.021)	2.75 (0.026)	2.60 (0.021)	2.69 (0.022)
	S_7	2.76 (0.028)	2.77 (0.027)	2.61 (0.026)	2.71 (0.029)
	S_8	2.88 (0.014)	2.89 (0.019)	2.71 (0.021)	2.79 (0.017)
	S_9	2.90 (0.012)	2.91 (0.009)	2.75 (0.011)	2.81 (0.010)
	S_{10}	2.92 (0.006)	2.93 (0.003)	2.78 (0.001)	2.82 (0.001)

Table A.9: Excitation energy (in eV) and oscillator strengths (in parenthesis) at B3LYP/6-31+G(d) level of theory in the gas phase and in DCM solution for the three different curcumin covalent dimers.

comp.	state	ωB97X-D	B3LYP	transition
1'	S_1	78	75	H-1→L
		18	19	H→L
	S_2	56	55	H→L
		26	27	H-1→L
	S_3	58	62	H→L+1
		20	30	H→L
	S_4	83	78	H-1→L+1
2'	S_1	76	80	H-1→L
	S_2	82	85	H→L+1
3'	S_1	41	43	H→L
		7	6	H-1→L
	S_2	49	47	H→L
		32	36	H-1→L
	S_3	47	45	H→L+1
		28	31	H→L
	S_4	34	31	H→L+1
		13	15	H-1→L

Table A.10: Main orbital contributions (in %) for the low-lying singlet excitations of dimers **1'-3'** computed at the TDA level with B3LYP and ωB97X-D energy functionals and the 6-31+G(d) basis set in vacuum. H and L indicate HOMO and LUMO, respectively.

A.3 Rotation of the *meso*-phenyl in monomer 3

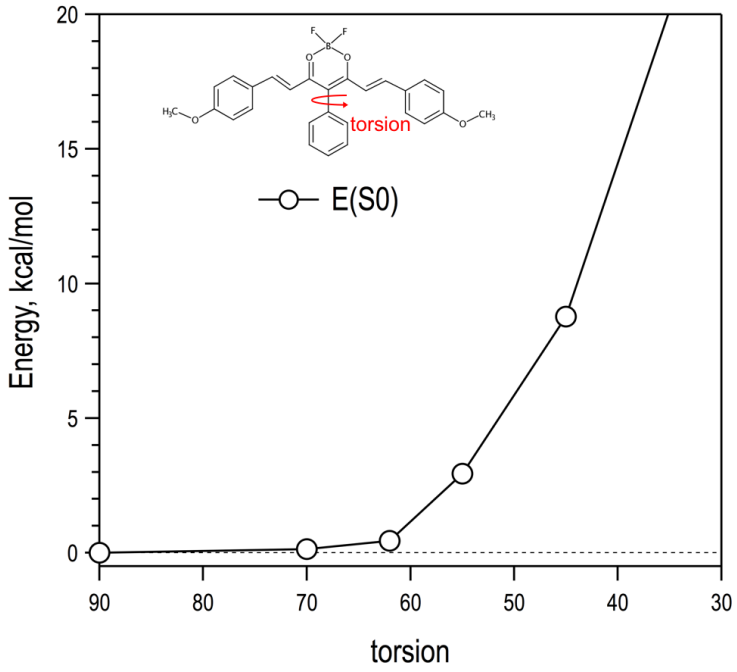

Figure A.4: Ground state potential energy profile along the torsion of the *m*Ph group of monomer **3** computed at the B3LYP/6-31+G(d) level in DCM solution.

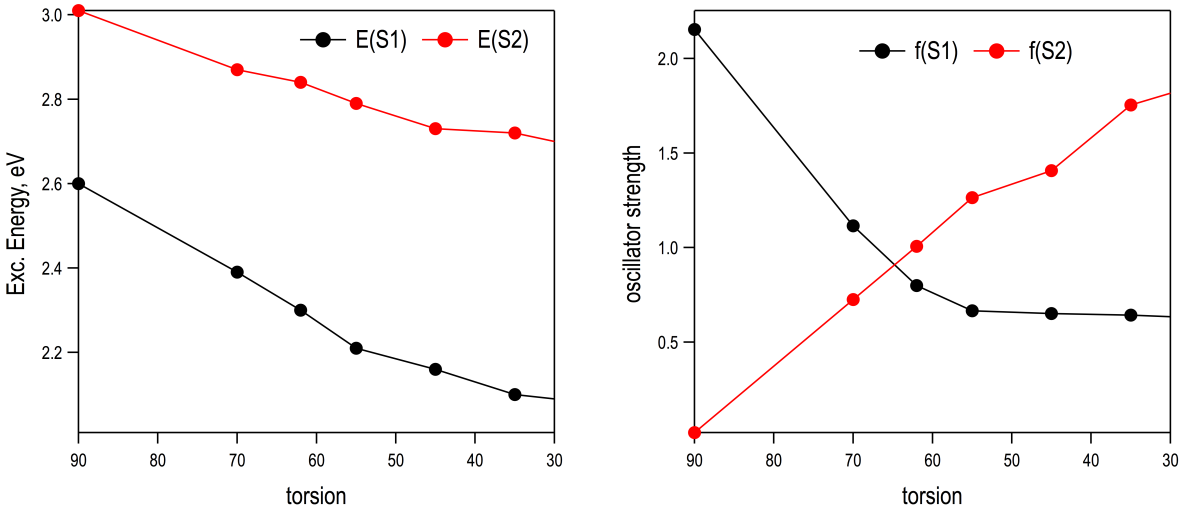

Figure A.5: Excitation energies (left) and oscillator strengths (right) for the two lowest excited singlet states of **3** along the torsion of the *m*Ph group computed at the B3LYP/6-31+G(d) level in DCM solution.

A.4 Relative energies between open/folded conformers

The relative stability between opened and folded structural conformations of curcumin derivative covalent dimers is dictated by the competition between the solvent-chromophore interactions and the π-stacking between the two monomers. As a result, apolar solvents like cyclohexane show a higher preference towards the folded form compared with more polar solvents.

The relative energy between the two forms ($\Delta E = E(open) - E(folded)$) has been computed in different solvents. Basis set superposition error (BSSE) have been corrected through the counterpoise procedure. To perform CP in covalent dimers we evaluate the CP correction at the folded from without the linker as:

$$E_{cp} = 2(E^*(mono)) - E(mono)) \tag{A.1}$$

where $E(mono)$ is the energy of the monomer, and $E^*(mono)$ is the energy of the monomer in the presence of basis set functions in the positions of the second monomer in the folded form. Then, the corrected energy for the open conformer is obtained as:

$$E^c(open) = E(open) + E_{cp} \tag{A.2}$$

Relative energies in different solvent are shown in Figure A.6.

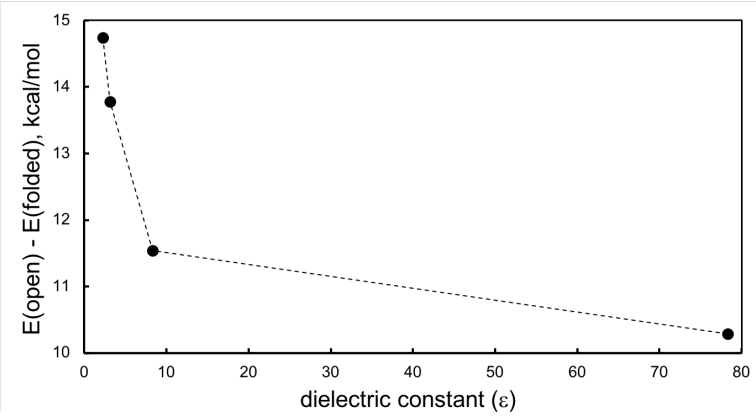

Figure A.6: Computed relative stability (in kcal/mol) between the open and folded conformers of dimer **1'** as a function of the polarity of the solvent. Points at the graph correspond to the dielectric constants of benzene, Bu_2O, DCM and water (in increasing order of ϵ).

Our results systematically indicate a preference for the folded conformation of dimer **1'**. These results should not be taken quantitatively, since entropic effects (stabilizing the open form) are not included. On the other hand, the trend of relative energies demonstrates how increasing the solvent's polarity shifts the equilibrium between the two forms towards the open conformation.

A.5 Absorption spectra: vibronic resolution

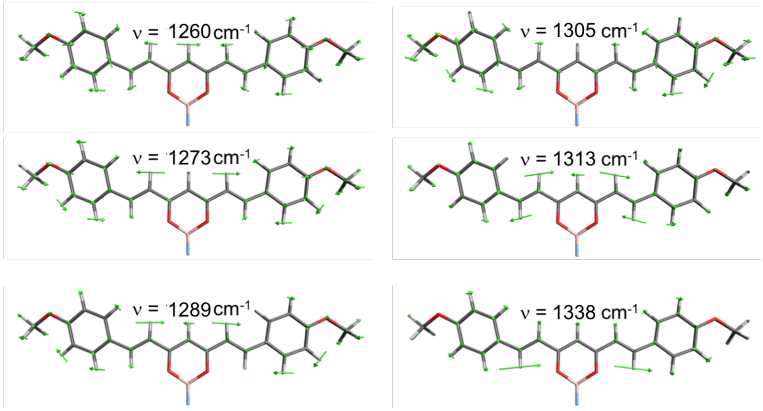

Figure A.7: Frequency modes of **1** computed at the ωB97X-D potentially involved in the vibronic profile of absorption spectra (experimental vibronic gap ∼1260 cm^{-1}).

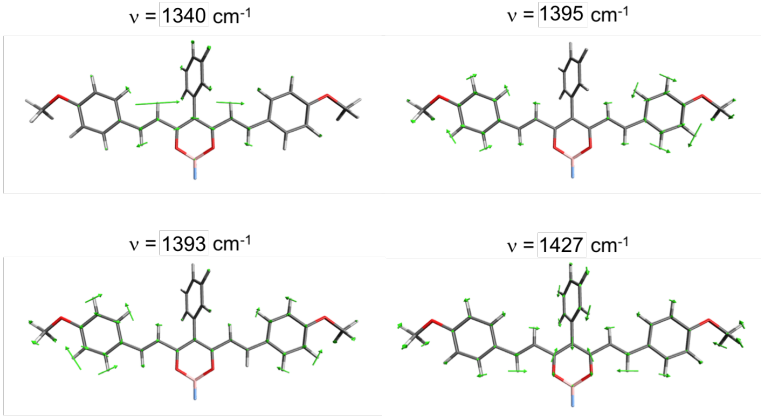

Figure A.8: Frequency modes of **3** computed at the ωB97X-D potentially involved in the vibronic profile of absorption spectra (experimental vibronic gap ∼1320 cm^{-1}).

A.6 Diabatization of low-lying states

A.6.1 Diabatization scheme: Edmiston-Ruedenberg localization

Diabatic electronic states $\{|\Xi_i\rangle\}$ are obtained through the mixing of N adiabatic states $\{|\phi_j\rangle\}$ via a rotation matrix $\mathbf{U}$ as:

$$|\Xi_i\rangle = \sum_{j=1}^{N} |\phi_j\rangle U_{ji};\ i = 1...N \tag{A.3}$$

There are several techniques for generating the rotation matrix $\mathbf{U}$ using a variety of different approaches. This rotation matrix is chosen by optimizing some diabatization function $f(\mathbf{U})$. In this case we use the Edmiston-Ruedenberg (ER) diabatization scheme, corresponding to the maximization of self-interaction energy:

$$f_{ER}(\mathbf{U}) = f_{ER}(\{|\Xi_i\rangle\}) = \sum_{j=1}^{N} \int d\mathbf{R}_1 \int d\mathbf{R}_2 \frac{\langle \Xi_i|\rho(\mathbf{R}_2)|\Xi_i\rangle \langle \Xi_i|\rho(\mathbf{R}_1)|\Xi_i\rangle}{|\mathbf{R}_1 - \mathbf{R}_2|} \tag{A.4}$$

where the density operator at position $\mathbf{R}$ is

$$\rho(\mathbf{R}) = \sum_j \delta(\mathbf{R} - \mathbf{r}^{(j)}) \tag{A.5}$$

and $\mathbf{r}^{(j)}$ represents the position of the j-th electron.

A.6.2 Decomposition in the diabatic basis: dimers

state	Z_{inter}	Z_{intra}
S_1	67	33
S_2	74	26
S_3	66	34
S_4	23	77
S_5	54	46
S_6	33	67
S_7	34	66
S_8	49	51

Table A.11: Contributions (in %) of the diabatic states (Z_{inter} and Z_{intra}) for the eight lowest adiabatic states (S_i, $i = 1, 8$) of dimer **1'**.

state	Z_{inter}	Z_{intra}	Z_{meso}
S_1	60	38	2
S_2	72	27	1
S_3	14	86	0
S_4	11	89	0
S_5	22	20	58
S_6	46	18	36
S_7	43	32	25
S_8	31	7	62
S_9	22	70	8
S_{10}	80	10	10

Table A.12: Contributions (in %) of the diabatic states for the ten lowest adiabatic states (S_i, $i = 1, 10$) of dimer **3'**. $Z_{\text{inter}} = Z_2 + Z_3 + Z_7 + Z_8$, $Z_{\text{intra}} = Z_1 + Z_4 + Z_9 + Z_{10}$ and $Z_{\text{meso}} = Z_5 + Z_6$.

A.6.3 Electronic Hamiltonians

By definition, the adiabatic states of a system $\{|\phi_j\rangle\}$ are those electronic states that diagonalize the electronic Hamiltonian, assuming that the nuclei are fixed. The spectrum ($\{E_j\}$) of these adiabatic states yields fixed-nuclei energies for the ground and excited electronic states of a system. The off-diagonal elements of the Hamiltonian ($H_{ij} = \langle Z_i|\hat{H}|Z_j\rangle$) are known as *electronic couplings*.

Electronic Hamiltonians of curcumin monomers

Diabatic Hamiltonian ($\mathbf{H}_{diab}$) and adiabatic energies ($\mathbf{E}_{ad}$) for curcumin derivative **1** computed at the B3LYP/6-31+G(d) level within TDA in vacuum (values in eV):

$$\mathbf{H}_{diab} = \begin{bmatrix} 3.22 & 0.22 \\ 0.22 & 3.22 \end{bmatrix}; \ \mathbf{E}_{ad} = \begin{bmatrix} 2.98 \\ 3.42 \end{bmatrix} \tag{A.6}$$

Diabatic Hamiltonian ($\mathbf{H}_{diab}$) and adiabatic energies ($\mathbf{E}_{ad}$) for curcumin derivative **2** computed at the B3LYP/6-31+G(d) level within TDA in vacuum (values in eV):

$$\mathbf{H}_{diab} = \begin{bmatrix} 2.94 & 0.02 \\ 0.02 & 3.30 \end{bmatrix}; \ \mathbf{E}_{ad} = \begin{bmatrix} 2.94 \\ 3.30 \end{bmatrix} \tag{A.7}$$

Diabatic Hamiltonian ($\mathbf{H}_{diab}$) and adiabatic energies ($\mathbf{E}_{ad}$) for curcumin derivative **3** ($\theta = 90°$) computed at the B3LYP/6-31+G(d) level within TDA in vacuum (values in eV):

$$\mathbf{H}_{diab} = \begin{bmatrix} 3.25 & 0.33 & -0.02 \\ 0.33 & 3.25 & 0.02 \\ -0.02 & 0.02 & 3.32 \end{bmatrix}; \ \mathbf{E}_{ad} = \begin{bmatrix} 2.92 \\ 3.32 \\ 3.59 \end{bmatrix} \tag{A.8}$$

Diabatic Hamiltonian ($\mathbf{H}_{diab}$) and adiabatic energies ($\mathbf{E}_{ad}$) for curcumin derivative **3** ($\theta = 62°$) computed at the B3LYP/6-31+G(d) level within TDA in vacuum (values in eV):

$$\mathbf{H}_{diab} = \begin{bmatrix} 3.11 & 0.33 & 0.04 \\ 0.33 & 3.11 & -0.04 \\ 0.04 & -0.04 & 2.72 \end{bmatrix}; \ \mathbf{E}_{ad} = \begin{bmatrix} 2.56 \\ 3.18 \\ 3.21 \end{bmatrix} \tag{A.9}$$

Electronic Hamiltonians of curcumin dimers

Diabatic Hamiltonian ($\mathbf{H}_{diab}$) and adiabatic energies ($\mathbf{E}_{ad}$) for curcumin derivative dimer **1'** computed at the B3LYP/6-31+G(d) level within TDA in vacuum (values in eV):

$$\mathbf{H}_{diab} = \begin{bmatrix} 3.15 & 0.20 & 0.02 & 0.00 & 0.03 & 0.13 & -0.18 & -0.07 \\ 0.20 & 3.15 & 0.00 & 0.11 & 0.01 & 0.03 & 0.04 & 0.15 \\ 0.02 & 0.00 & 3.15 & 0.20 & 0.11 & 0.14 & -0.15 & -0.03 \\ 0.00 & 0.11 & 0.20 & 3.15 & 0.11 & -0.08 & -0.03 & -0.02 \\ 0.03 & 0.01 & 0.11 & 0.11 & 3.20 & 0.11 & 0.14 & -0.05 \\ 0.13 & 0.03 & 0.14 & -0.08 & 0.11 & 3.20 & 0.11 & -0.16 \\ -0.18 & 0.04 & -0.15 & -0.03 & 0.14 & 0.11 & 3.29 & 0.09 \\ -0.07 & 0.15 & -0.03 & -0.02 & -0.05 & -0.16 & 0.09 & 3.29 \end{bmatrix} ; \mathbf{E}_{ad} = \begin{bmatrix} 2.48 \\ 2.90 \\ 3.03 \\ 3.10 \\ 3.28 \\ 3.33 \\ 3.39 \\ 3.41 \end{bmatrix} \quad \text{(A.10)}$$

Diabatic Hamiltonian ($\mathbf{H}_{diab}$) and adiabatic energies ($\mathbf{E}_{ad}$) for curcumin derivative dimer **2'** computed at the B3LYP/6-31+G(d) level within TDA in vacuum (values in eV):

$$\mathbf{H}_{diab} = \begin{bmatrix} 2.92 & 0.00 & 0.00 & 0.00 & 0.00 & 0.00 & 0.00 & 0.00 \\ 0.00 & 2.95 & 0.00 & 0.00 & 0.00 & 0.00 & 0.00 & 0.00 \\ 0.00 & 0.00 & 2.98 & 0.01 & 0.00 & 0.00 & 0.00 & 0.00 \\ 0.00 & 0.00 & 0.01 & 3.04 & 0.00 & 0.00 & 0.00 & 0.00 \\ 0.00 & 0.00 & 0.00 & 0.00 & 3.22 & 0.01 & 0.00 & 0.00 \\ 0.00 & 0.00 & 0.00 & 0.00 & 0.01 & 3.27 & 0.00 & 0.00 \\ 0.00 & 0.00 & 0.00 & 0.00 & 0.00 & 0.00 & 3.28 & 0.02 \\ 0.00 & 0.00 & 0.00 & 0.00 & 0.00 & 0.00 & 0.02 & 3.28 \end{bmatrix} ; \mathbf{E}_{ad} = \begin{bmatrix} 2.92 \\ 2.95 \\ 2.98 \\ 3.04 \\ 3.22 \\ 3.27 \\ 3.28 \\ 3.28 \end{bmatrix} \quad \text{(A.11)}$$

Diabatic Hamiltonian ($\mathbf{H}_{diab}$) and adiabatic energies ($\mathbf{E}_{ad}$) for curcumin derivative dimer **3'** computed at the B3LYP/6-31+G(d) level within TDA in vacuum (values in eV):

$$\mathbf{H}_{diab} = \begin{bmatrix} 2.50 & 0.00 & 0.00 & 0.12 & 0.00 & 0.00 & 0.00 & 0.00 & 0.00 & 0.00 \\ 0.00 & 2.60 & -0.19 & 0.00 & 0.00 & 0.00 & 0.00 & 0.00 & 0.00 & 0.00 \\ 0.00 & -0.19 & 2.62 & 0.00 & 0.00 & 0.00 & 0.00 & 0.00 & 0.00 & 0.00 \\ 0.12 & 0.00 & 0.00 & 2.66 & 0.00 & 0.00 & 0.00 & 0.00 & 0.00 & 0.00 \\ 0.00 & 0.00 & 0.00 & 0.00 & 2.72 & 0.16 & 0.00 & 0.00 & 0.00 & 0.00 \\ 0.00 & 0.00 & 0.00 & 0.00 & 0.16 & 2.73 & 0.00 & 0.00 & 0.00 & 0.00 \\ 0.00 & 0.00 & 0.00 & 0.00 & 0.00 & 0.00 & 2.77 & -0.09 & 0.07 & 0.07 \\ 0.00 & 0.00 & 0.00 & 0.00 & 0.00 & 0.00 & -0.09 & 2.77 & 0.07 & 0.07 \\ 0.00 & 0.00 & 0.00 & 0.00 & 0.00 & 0.00 & 0.07 & 0.07 & 2.78 & -0.08 \\ 0.00 & 0.00 & 0.00 & 0.00 & 0.00 & 0.00 & 0.07 & -0.08 & 0.07 & 2.79 \end{bmatrix}; \mathbf{E}_{ad} = \begin{bmatrix} 2.39 \\ 2.40 \\ 2.58 \\ 2.69 \\ 2.73 \\ 2.75 \\ 2.77 \\ 2.89 \\ 2.91 \\ 2.93 \end{bmatrix} \quad \text{(A.12)}$$

A.7 Fragment charge distribution

A.7.1 Curcumin derivatives: monomers

Comp.	State	Fragment			
		PMP_1	DOB	PMP_2	
1	Z_1	0.347	-0.322	-0.025	
	Z_2	-0.031	-0.326	0.357	
		TPA	DOB	PMP	
2	Z_1	0.450	-0.392	-0.057	
	Z_2	0.038	-0.374	0.343	
		PMP_1	DOB	PMP_2	mPh
3	Z_1	0.345	-0.325	-0.020	0.000
$\theta = 90°$	Z_2	-0.020	-0.325	0.345	0.000
	Z_3	0.042	-0.400	0.042	0.315
3	Z_1	0.346	-0.323	-0.020	-0.002
$\theta = 62°$	Z_2	-0.001	-0.324	0.347	-0.010
	Z_3	0.040	-0.394	0.050	0.302

Table A.13: Relative Mulliken fragment charges of **diabatic** states of curcumin monomers **1-3** with respect to the ground state charge distribution computed at the B3LYP/6-31+G(d) level.

Comp.	State	Fragment			
		PMP_1	DOB	PMP_2	
1	S_1	0.113	-0.234	0.120	-
	S_2	0.203	-0.415	0.212	-
		TPA	DOB	PMP	
2	S_1	0.449	-0.391	-0.057	-
	S_2	0.021	-0.362	0.341	-
		PMP_1	DOB	PMP_2	mPh
3	S_1	0.110	-0.235	0.120	0.005
$\theta = 90°$	S_2	0.042	-0.400	0.042	0.315
	S_3	0.205	-0.420	0.210	0.005
3	S_1	0.067	-0.330	0.066	0.190
$\theta = 62°$	S_2	0.142	-0.354	0.139	0.071
	S_3	0.157	-0.346	0.156	0.033

Table A.14: Relative Mulliken fragment charges of **adiabatic** states of curcumin monomers **1-3** with respect to the ground state charge distribution computed at the B3LYP/6-31+G(d) level.

A.7.2 Curcumin derivatives: dimers

	Fragment					
diabat	PMP_{1a}	DOB_1	PMP_{1b}	PMP_{2a}	DOB_2	PMP_{2b}
Z_1	0.000	-0.310	0.012	0.000	-0.037	0.335
Z_2	0.010	-0.310	0.000	0.340	-0.040	0.000
Z_3	0.000	-0.036	0.338	0.000	-0.310	0.008
Z_4	0.338	-0.026	0.000	0.001	-0.315	0.000
Z_5	0.000	-0.111	0.111	0.109	-0.109	0.000
Z_6	0.109	-0.110	0.000	0.000	-0.109	0.110
Z_7	0.000	-0.110	0.110	0.000	-0.111	0.111
Z_8	0.109	-0.109	0.000	0.110	-0.110	0.000

Table A.15: Relative Mulliken fragment charges of **diabatic** states of curcumin dimer **1'** (folded) with respect to the ground state charge distribution computed at the B3LYP/6-31+G(d) level. Nomenclature: PMP_{1a}-DOB_1-PMP_{1b}-$(CH_2)_8$-PMP_{2b}-DOB_2-PMP_{2a}.

	Fragments					
diabat	TPA_1	DOB_1	PMP_1	TPA_2	DOB_2	PMP_2
Z_1,Z_2	0.450	-0.400	-0.050	0.450	-0.450	-0.050
Z_3,Z_4	0.210	-0.260	0.085	-0.018	-0.155	-0.100
Z_5,Z_6	0.145	-0.190	0.0520	-0.005	-0.210	0.100
Z_7,Z_8	0.030	-0.370	0.335	0.030	-0.370	0.335

Table A.16: Relative Mulliken fragment charges of **diabatic** states of curcumin dimer **2'** (V-shape) with respect to the ground state charge distribution computed at the B3LYP/6-31+G(d) level. Nomenclature: TPA_1-DOB_1-PMP_1-$(CH_2)_8$-PMP_2-DOB_2-TPA_2.

	Fragment					
state	TPA_1	DOB_1	PMP_1	TPA_2	DOB_2	PMP_2
S_1	0.422	-0.394	-0.008	0.392	-0.476	0.065
S_2	0.398	-0.469	0.071	0.418	-0.408	-0.009
S_3	0.216	-0.256	0.012	0.038	-0.146	0.135
S_4	0.032	-0.143	0.133	0.219	-0.257	0.013
S_5	0.164	-0.168	0.078	0.007	-0.187	0.103
S_6	0.003	-0.186	0.100	0.170	-0.164	0.077
S_7	0.034	-0.360	0.335	0.014	-0.362	0.339
S_8	0.011	-0.361	0.338	0.039	-0.360	0.333

Table A.17: Mulliken analysis of the difference in charge in comparison to the ground state for the **adiabatic** states for the dimer **2'** (V-shape) computed at the B3LYP/6-31+G(d) level. Nomenclature: TPA_1-DOB_1-PMP_1-$(CH_2)_8$-PMP_2-DOB_2-TPA_2.

	Fragment							
diabat	$m\mathrm{Ph}_1$	PMP_{1a}	DOB_1	PMP_{1b}	PMP_{2a}	DOB_2	PMP_{2b}	$m\mathrm{Ph}_2$
Z_1	-0.006	0.199	-0.193	0.005	0.005	-0.194	0.211	-0.070
Z_2	0.001	0.152	-0.091	0.005	0.005	-0.163	0.089	0.001
Z_3	0.002	0.090	-0.162	0.005	0.004	-0.090	0.149	0.001
Z_4	0.001	0.078	-0.169	0.039	0.063	-0.111	0.096	0.002
Z_5	0.002	0.005	-0.002	0.002	0.041	-0.379	0.042	0.287
Z_6	0.291	0.041	-0.379	0.039	0.005	-0.004	0.003	0.002
Z_7	0.111	0.053	-0.211	0.048	0.044	-0.210	0.051	0.113
Z_8	0.109	0.049	-0.210	0.044	0.056	-0.207	0.050	0.111
Z_9	0.113	0.045	-0.211	0.051	0.052	-0.210	0.051	0.109
Z_{10}	0.107	0.052	-0.209	0.045	0.050	-0.210	0.053	0.112

Table A.18: Mulliken analysis of the difference in charge in comparison to the ground state for the diabatic states of dimer **3'** (folded form) computed at the B3LYP/6-31+G(d) level. Nomenclature: ($m\mathrm{Ph}_1$,PMP_{1a})-DOB_1-PMP_{1b}-$(CH_2)_8$-PMP_{2b}-DOB_2-(PMP_{2a},$m\mathrm{Ph}_2$).

A.8 Splitting of S_1 and S_2 in dimer 2'

The evaluation of the (classical) dipole-dipole interaction (equation A.13) corresponding to the interaction between monomeric excitations in dimer **2'** has been done by considering the following parameters from S_1 transition in monomer **1** and the optimized V-shape structure of dimer **2'** in DCM solution at the B3LYP/6-31+G(d) computational level.

$$\Delta E = \frac{1}{4\pi\varepsilon_0}\left[\frac{\mathbf{d}_1 \cdot \mathbf{d}_2}{|\mathbf{R}|^3} - 3\frac{(\mathbf{R}\cdot\mathbf{d}_1)(\mathbf{R}\cdot\mathbf{d}_2)}{|\mathbf{R}|^5}\right] \tag{A.13}$$

where $\mathbf{d}_i$ are the transition dipole moments for the two monomers, $\mathbf{R}$ is the distance between the two dipoles and ΔE is the energy shift of the excitation energies of the dimer with respect to the transition energy for the monomer. Data: $|\mathbf{d}_i| = 36.3865$ D; $|\mathbf{R}| = 18.52$ Å; $\theta_{12} = 65.36^{\text{o}}$; $\theta_{12} = 65.36^{\text{o}}$; $\theta_1 = 57.79^{\text{o}}$; $\theta_2 = 56.85^{\text{o}}$.

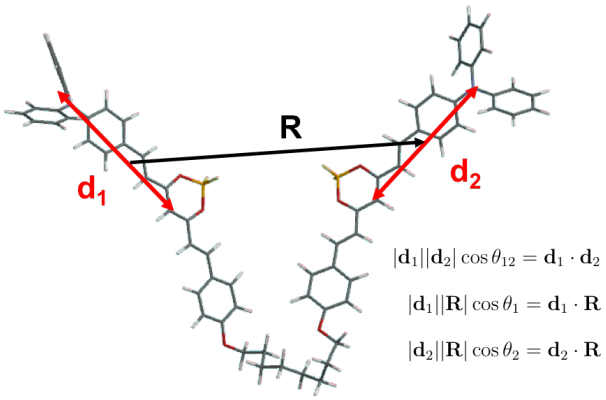

Figure A.9: Dipole-dipole interaction representation for dimer **2'**.

The gap between the two lowest singlet states of the dimer, i.e. Davydson splitting, is obtained as the sum of the energy shifts corresponding to in-phase and out-of-phase combinations of the $\mathbf{d}_1$ and $\mathbf{d}_2$ dipoles and corresponds to $\Delta E_{Dav} = 2\Delta E = 0.11$ eV.

A.9 Dimer 2': CAM-B3LYP calculations

Electronic structure of low-lying states of curcumin dimers **1'** and **3'** obtained with hybrid GGA (B3LYP) and long-range corrected (CAM-B3LYP) functionals provide qualitatively the same transitions with excitation energies systematically larger for CAM-B3LYP. On the other hand, the nature of electronic transitions (beyond S_2 state) in **2'** present larger discrepancies between B3LYP and CAM-B3LYP due to the large interchromophoric separation in **2'** and the strong stabilization of inter-CT transitions by non LRC functionals, such as B3LYP. In the following we present additional calculations on the singlet excited states of dimer **2'**.

dimer	state	ΔE	strength
	S_1	3.73	1.965
	S_2	3.73	1.906
	S_3	4.00	0.898
2'	S_4	4.00	0.867
(V-shape)	S_5	4.34	0.006
	S_6	4.35	0.005
	S_7	4.45	0.015
	S_8	4.46	0.172

Table A.19: Excitation energies (in eV) and oscillator strengths (in parenthesis) computed at the CAM-B3LYP/6-31+G(d) level within TDA in gas phase for the open form of **2'** dimer.

dimer	state	ΔE
	Z_1	3.73
	Z_2	3.73
	Z_3	3.99
2'	Z_4	4.00
(V-shape)	Z_5	4.32
	Z_6	4.34
	Z_7	4.45
	Z_8	4.45

Table A.20: Diabatic excitation energies (in eV) computed at the CAM-B3LYP/ 6-31+G* level (within TDA) in gas phase for the V-shaped form of **2'** dimer.

	Fragment					
diabat	TPA_1	DOB_1	PMP_1	TPA_2	DOB_2	PMP_2
Z_1,Z_2	0.430	-0.420	-0.010	0.430	-0.420	-0.010
Z_3,Z_4	0.030	-0.370	0.335	0.030	-0.370	0.335
Z_5	0.000	-0.080	0.210	0.000	-0.150	0.020
Z_6	0.000	-0.150	0.020	-0.005	-0.080	0.210
Z_7	0.150	-0.050	0.015	0.000	-0.120	0.005
Z_8	0.000	-0.120	0.005	0.150	-0.050	0.015

Table A.21: Mulliken analysis of the difference in charge in comparison to the ground state for the two diabatic states for the dimer **2'** (V-shape) computed at the CAM-B3LYP/6-31+G(d) level. Nomenclature: TPA_1-DOB_1-PMP_1-$(CH_2)_8$-PMP_2-DOB_2-TPA_2.

Appendix B

Flavylium fluorophores as near-infrared emitters

B.1 Atomic charges

Table B.1: Sum of the Mulliken charges for the atoms in the donor (D) and acceptor (A) groups for the S_0 and S_1 states of **F1-7**, **F7a** and **F7b** molecules in their respective energy minimum. Charge at D column corresponds to the average between D_1 and D_2 moieties.

	S_0		S_1	
molecule	D	A	D	A
F1	0.495	0.010	0.601	-0.202
F3	0.486	0.028	0.595	-0.189
F5	0.495	0.010	0.605	-0.210
F7	0.492	0.016	0.602	-0.204
F7a	0.479	0.041	0.596	-0.192
F7b	0.488	0.024	0.607	-0.213

B.2 Excitation energies

Table B.2: Functional dependence of calculated (full) TDDFT and TDA $S_0 \rightarrow S_1$ energies (E_{GS}^{vert}, in eV) for the **F3** molecule. Second-order perturbative corretion to the configuration interaction singles (CIS(D)) and its spin-opposite scaled version (SOSCIS(D)) have been performed with the resolution of the identity (RI) approximation. All calculations have been done with the 6-31+G(d,p) basis set. Oscillator strengths are given in parenthesis. CIS(D) and SOSCIS(D) oscillator strengths are obtained with the CIS transition dipole moment. Experimental absorption maximum is 1.66 eV.

functional	Full TDDFT	TDA
PBE	1.76 (2.145)	1.90 (2.996)
B3LYP	1.89 (2.783)	2.04 (3.076)
M06-2X	1.99 (2.037)	2.12 (3.012)
CAM-B3LYP	2.03 (2.049)	2.15 (2.876)
ωB97X-D	2.06 (2.138)	2.15 (3.045)
CIS		2.59 (2.220)
CIS(D)		1.63 (1.397)
SOSCIS(D)		1.28 (1.097)

Table B.3: Functional and basis set dependence of calculated (full) TDDFT and TDA $S_0 \rightarrow S_1$ energies (E_{GS}^{vert}, in eV) for the **F7a** molecule. Second-order perturbative corretion to the configuration interaction singles (CIS(D)) and its spin-opposite scaled version (SOSCIS(D)) have been performed with the resolution of the identity (RI) approximation. Oscillator strengths are given in parenthesis. CIS(D) and SOSCIS(D) oscillator strengths are obtained with the CIS transition dipole moment. Experimental absorption maximum is 1.21 eV.

functional	basis	Full TDDFT	TDA
B3LYP	6-311++G(d,p)	1.57 (2.763)	1.75 (4.157)
B3LYP	6-31+G(d,p)	1.57 (2.763)	1.75 (4.157)
PBE	6-31+G(d,p)	1.50 (2.379)	1.67 (3.518)
M06-2X	6-31+G(d,p)	1.56 (2.850)	1.69 (3.460)
CAM-B3LYP	6-31+G(d,p)	1.59 (2.942)	1.70 (3.091)
ωB97X-D	6-31+G(d)	1.55 (2.837)	1.67 (3.291)
CIS	6-31+G(d,p)		1.97 (2.790)
CIS(D)	6-31+G(d,p)		1.20 (1.695)
SOSCIS(D)	6-31+G(d,p)		0.74 (1.050)

Table B.4: Functional dependence of $S_1 \rightarrow S_0$ (E_{ES}^{vert}, in eV) calculated at the TDDFT level with and without TDA and the 6-31+G(d,p) basis for the **F7a** molecule . Oscillator strengths are given in parenthesis. Experimental emission maximum is 1.19 eV.

method	TDDFT	TDA
B3LYP	1.19 (2.801)	1.28 (3.598)
CAM-B3LYP	1.24 (2.885)	1.36 (3.265)

Table B.5: Norm of the transition dipole moment (in atomic units) for the $S_0 \rightarrow S_1$ (ground state geometry) and $S_1 \rightarrow S_0$ (excited state geometry) for **F1-7** molecules computed at the B3LYP/6-31+G(d,p) level in dichloromethane.

molecule	$S_0 \rightarrow S_1$	$S_1 \rightarrow S_0$
F1	3.054	4.010
F3	3.649	4.648
F5	3.754	4.898
F7	3.918	5.316

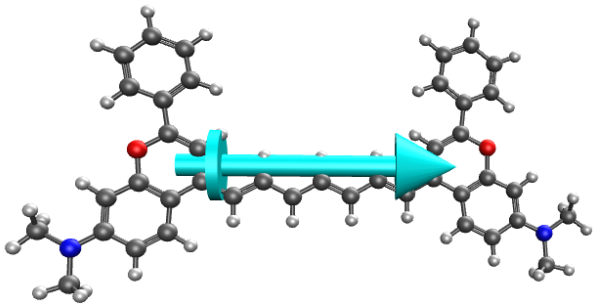

Figure B.1: Representation of the $S_0 \rightarrow S_1$ transition dipole moment vector of **F7** computed at the B3LYP/6-31+G(d,p) level in dichloromethane. Transition dipole moments in the rest of the **Fn** series show similar alignment on the long molecular axis.

B.3 Diabatic states

Table B.6: Sum of the change in Mulliken charges upon excitation to diabatic states CT_1 ($D_1 \rightarrow A$) and CT_2 ($D_2 \rightarrow A$) for **F1-7** molecules. D_1 and D_2 indicate donor groups, and A corresponds to the electron acceptor bridge.

molecule	diabat	D_1	A	D_2
F1	CT_1	0.318	-0.308	-0.010
	CT_2	-0.020	-0.306	0.326
F3	CT_1	0.321	-0.310	-0.011
	CT_2	-0.019	-0.309	0.328
F5	CT_1	0.322	-0.309	-0.013
	CT_2	-0.016	-0.309	0.325
F7	CT_1	0.320	-0.308	-0.012
	CT_2	-0.014	-0.310	0.324

Table B.7: Vertical excitation energies at the ground (E_{GS}^{vert}) and excited (E_{ES}^{vert}) state minima, zero-point vibrational energies (ZPVE), and adiabatic (E_{adia}) and 0-0 (E_{0-0}) energies of the series of derivatives calculated at the TDDFT/B3LYP/6-31+G(d,p) level in dichloromethane. All energy values are in eV.

molecule	E_{GS}^{ZPVE}	E_{ES}^{ZPVE}	E_{GS}^{vert}	E_{ES}^{vert}	E_{adia}	E_{0-0}
F1	9.17	9.14	2.09	1.83	1.89	1.86
F3	17.55	17.53	1.89	1.66	1.79	1.77
F5	18.43	18.35	1.73	1.44	1.62	1.54
F7	19.48	19.47	1.59	1.31	1.48	1.47
F7a	21.36	21.35	1.57	1.19	1.45	1.44
F7b	20.74	20.72	1.44	1.06	1.37	1.35

Table B.8: Vertical excitation energies at the ground (E_{GS}^{vert}) and excited (E_{ES}^{vert}) state minima of the series of derivatives calculated at the TDA/B3LYP/6-31+G(d,p) level in dichloromethane. Oscillator strengths are reported in parentheses. All energy values are in eV.

molecule	E_{GS}^{vert}	E_{ES}^{vert}
F1	2.20 (2.077)	1.98 (2.049)
F3	1.98 (2.988)	1.75 (2.312)
F5	1.80 (2.458)	1.53 (2.822)
F7	1.69 (2.612)	1.39 (3.235)
F7a	1.66 (2.963)	1.28 (3.598)
F7b	1.52 (2.956)	1.14 (3.552)

Appendix C

Photophysics of molecular aggregates from excited state diabatization

C.1 Diabatic Hamiltonian

Adiabatic energies in terms of diabatic state energies and couplings can be achieved through the diagonalization of the diabatic Hamiltonian. In the case of a symmetric dimer, this can be written as:

$$\mathbf{H}_{diab} = \begin{bmatrix} E_{LE} & V_{DC} & V_e & V_h \\ V_{DC} & E_{LE} & V_h & V_e \\ V_e & V_h & E_{CT} & V_{CT} \\ V_h & V_e & V_{CT} & E_{CT} \end{bmatrix} \tag{C.1}$$

Block diagonalization of equation C.1 results in:

$$\mathbf{H} = \begin{bmatrix} E_{FE}^{(+)} & 0 & V_e + V_h & 0 \\ 0 & E_{FE}^{(-)} & 0 & V_e - V_h \\ V_e + V_h & 0 & E_{CR}^{(+)} & 0 \\ 0 & V_e - V_h & 0 & E_{CR}^{(-)} \end{bmatrix} \tag{C.2}$$

where $E_{FE}^{(\pm)} = E_{LE} \pm V_{DC}$ and $E_{CR}^{(\pm)} = E_{CT} \pm V_{CT}$ correspond to the energies of the symmetric/antisymmetric Frenkel excitons (FE) and charge resonances (CR) respectively. Finally,

adiabatic energies are obtained as the full diagonlization of $\mathbf{H}_{diab}$.

$$\mathbf{H}_{adiab} = \begin{bmatrix} E_1^{(+)} & 0 & 0 & 0 \\ 0 & E_2^{(+)} & 0 & 0 \\ 0 & 0 & E_1^{(-)} & 0 \\ 0 & 0 & 0 & E_2^{(-)} \end{bmatrix} \tag{C.3}$$

$$E_1^{(\pm)} = \frac{1}{2}\left[E_{FE}^{(\pm)} + E_{CR}^{(\pm)} - \sqrt{(E_{FE}^{(\pm)} - E_{CR}^{(\pm)})^2 + 4(V_e \pm V_h)^2}\right] \tag{C.4}$$

$$E_2^{(\pm)} = \frac{1}{2}\left[E_{FE}^{(\pm)} + E_{CR}^{(\pm)} + \sqrt{(E_{FE}^{(\pm)} - E_{CR}^{(\pm)})^2 + 4(V_e \pm V_h)^2}\right] \tag{C.5}$$

with eigenvectors written in the ($\Phi_{FE}^{(\pm)}$, $\Phi_{CR}^{(\pm)}$) basis as:

$$\Psi_1^{(\pm)} = \frac{\Phi_{FE}^{(\pm)} + c_1^{(\pm)}\Phi_{CR}^{(\pm)}}{\sqrt{1 + c_1^{(\pm)2}}};\ \Psi_2^{(\pm)} = \frac{\Phi_{FE}^{(\pm)} + c_2^{(\pm)}\Phi_{CR}^{(\pm)}}{\sqrt{1 + c_2^{(\pm)2}}} \tag{C.6}$$

where

$$c_1^{(\pm)} = \frac{1}{2(V_e \pm V_h)}\left[E_{CR}^{(+)} - E_{FE}^{(+)} - \sqrt{(E_{FE}^{(\pm)} - E_{CR}^{(\pm)})^2 + 4(V_e \pm V_h)^2}\right] \tag{C.7}$$

$$c_2^{(\pm)} = \frac{1}{2(V_e \pm V_h)}\left[E_{CR}^{(+)} - E_{FE}^{(+)} + \sqrt{(E_{FE}^{(\pm)} - E_{CR}^{(\pm)})^2 + 4(V_e \pm V_h)^2}\right] \tag{C.8}$$

Notice that the charge resonance amplitudes $\lambda_i = |c_{CR}^{(i)}|$ are defined as:

$$\lambda_i = \frac{c_i^{(\pm)}}{\sqrt{1 + c_i^{(\pm)2}}} \tag{C.9}$$

C.2 Electronic couplings

Definition of signed electronic couplings $W_X^{(i)}$ as the product of normalized amplitude products and off-diagonal terms of the diabatic Hamiltonian:

$$W_{DC}^{(i)} = \text{sign}_{DC}^{(i)} \langle \Phi_{10} | \hat{H} | \Phi_{01} \rangle = \frac{c_{10}^{(i)} c_{01}^{(i)}}{|c_{10}^{(i)} c_{01}^{(i)}|} \langle \Phi_{10} | \hat{H} | \Phi_{01} \rangle \tag{C.10}$$

$$W_{h}^{(i)} = \text{sign}_{h}^{(i)} \langle \Phi_{10} | \hat{H} | \Phi_{AC} \rangle = \frac{c_{10}^{(i)} c_{AC}^{(i)}}{|c_{10}^{(i)} c_{AC}^{(i)}|} \langle \Phi_{10} | \hat{H} | \Phi_{AC} \rangle \tag{C.11}$$

$$W_{h'}^{(i)} = \text{sign}_{h'}^{(i)} \langle \Phi_{01} | \hat{H} | \Phi_{CA} \rangle = \frac{c_{01}^{(i)} c_{CA}^{(i)}}{|c_{01}^{(i)} c_{CA}^{(i)}|} \langle \Phi_{01} | \hat{H} | \Phi_{CA} \rangle \tag{C.12}$$

$$W_{e}^{(i)} = \text{sign}_{e}^{(i)} \langle \Phi_{10} | \hat{H} | \Phi_{CA} \rangle = \frac{c_{10}^{(i)} c_{CA}^{(i)}}{|c_{10}^{(i)} c_{CA}^{(i)}|} \langle \Phi_{10} | \hat{H} | \Phi_{CA} \rangle \tag{C.13}$$

$$W_{e'}^{(i)} = \text{sign}_{e'}^{(i)} \langle \Phi_{01} | \hat{H} | \Phi_{AC} \rangle = \frac{c_{01}^{(i)} c_{AC}^{(i)}}{|c_{01}^{(i)} c_{AC}^{(i)}|} \langle \Phi_{01} | \hat{H} | \Phi_{AC} \rangle \tag{C.14}$$

$$W_{CT}^{(i)} = \text{sign}_{CT}^{(i)} \langle \Phi_{AC} | \hat{H} | \Phi_{CA} \rangle = \frac{c_{CA}^{(i)} c_{AC}^{(i)}}{|c_{CA}^{(i)} c_{AC}^{(i)}|} \langle \Phi_{AC} | \hat{H} | \Phi_{CA} \rangle \tag{C.15}$$

where $c_X^{(i)}$ indicates the amplitude of the X-diabat in the i-adiabatic state. Notice that for a symmetric dimer $W_h^{(i)} = W_{h'}^{(i)}$ and $W_e^{(i)} = W_{e'}^{(i)}$.

C.3 Basis set effect

Contributions to the excitation energy of S_1 dark state of the eclipsed (D_{2h}) ethylene dimer for different molecular separations computed at the CIS/6-31G(d) level.

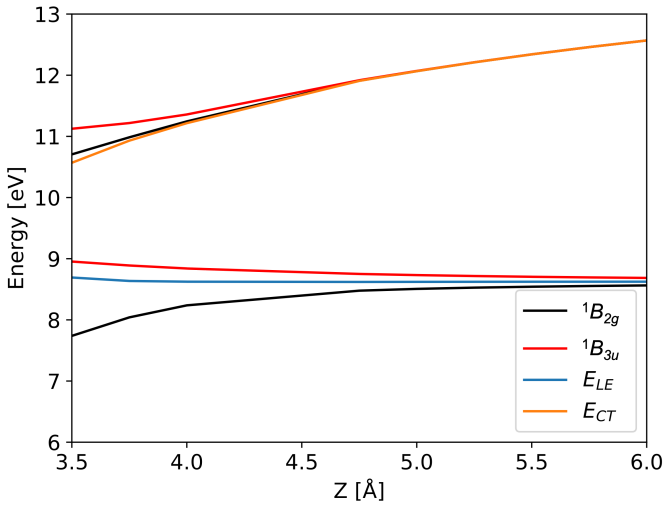

Figure C.1: Energy profiles (in eV) of the four lowest $\pi \rightarrow \pi^*$ excited singlet states and diabatic LE and CT energies for the eclipsed ethylene dimer at different intermolecular separations (z in Å) computed at the CIS/6-31G(d) level.

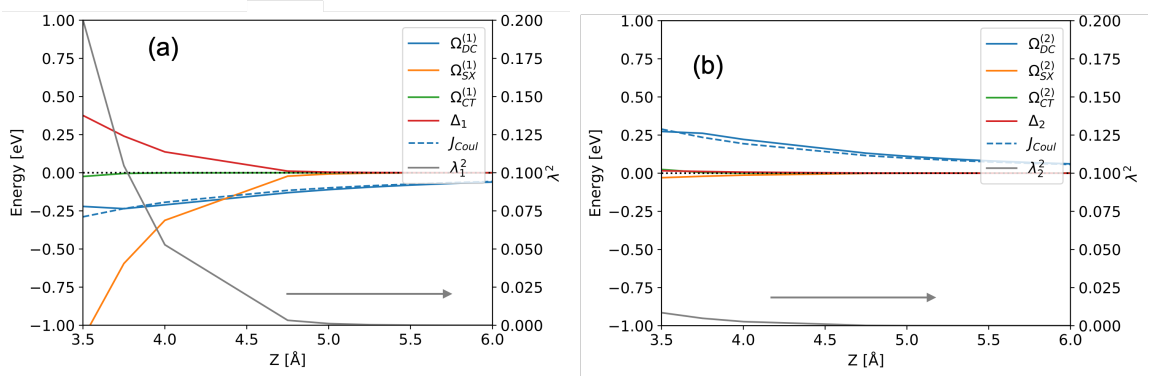

Figure C.2: Contributions to the (a) dark S_1 and (b) bright S_2 excitation energies (in eV) and λ_i^2 of both excited singlets for the eclipsed ethylene dimer at different intermolecular separations computed at the CIS/6-31G(d) level. J_{Coul} corresponds to the classical dipole-dipole Coulomb interaction.

C.4 Direct coupling in ethylene dimer

In order to analyze the in more detail the origin of the direct coupling energy contribution in the lowest excited state of the D_{2h} ethylene dimer, we decompose $W_{DC}^{(1)}$ in one electron ($\Omega_{DC,1}^{(1)}$), Coulomb ($\Omega_{DC,1}^{(1)}$) and exchange ($\Omega_{DC,K}^{(1)}$) contributions defined as:[**?**]

$$\Omega_{DC}^{(1)} = \Omega_{DC,1}^{(1)} + \Omega_{DC,J}^{(1)} + \Omega_{DC,K}^{(1)} \tag{C.16}$$

$$\Omega_{DC,1}^{(1)} = \text{sign}_{DC}^{(1)} \left(\sum_{iab} t_{Xi}^{a} t_{i}^{Yb} F_{ab} - \sum_{iab} t_{i}^{Xa} t_{j}^{Ya} F_{ij} \right) \tag{C.17}$$

$$\Omega_{DC,J}^{(1)} = \text{sign}_{DC}^{(1)} \left(\sum_{ijab} t_{i}^{Xa} t_{j}^{Yb} (ia|jb) \right) \tag{C.18}$$

$$\Omega_{DC,K}^{(1)} = -\text{sign}_{DC}^{(1)} \left(\sum_{ijab} t_{i}^{Xa} t_{j}^{Yb} (ij|ab) \right) \tag{C.19}$$

where indices i, j (a, b) correspond to occupied (virtual) orbitals, t_i^a are the CIS excitation amplitues, F_{ij} are Fock matrix elements, $(ij|ab)$ are two electron orbital integrals (equation 19), X and Y indicate 10 and 01 excitonic diabats, respectively.

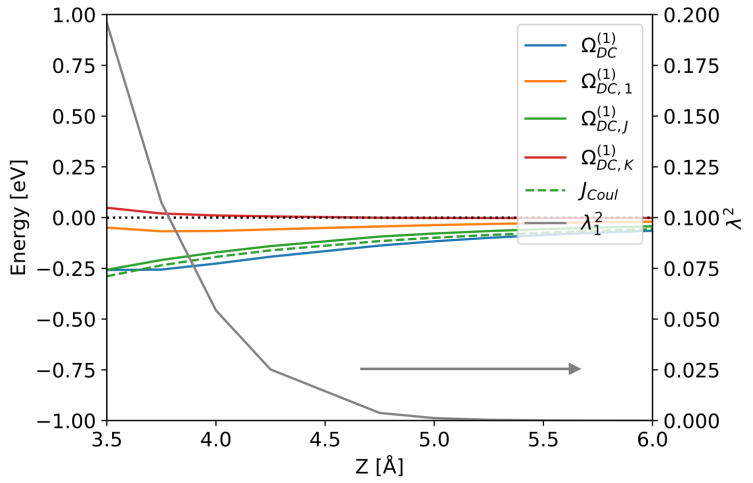

Figure C.3: Decomposition of the direct coupling $\Omega_{DC}^{(1)}$ for the dark S_1 state in terms of $\Omega_{DC,1}^{(1)}$, $\Omega_{DC,J}^{(1)}$, and $\Omega_{DC,K}^{(1)}$; and λ_1^2 for the eclipsed ethylene dimer at different intermolecular separations computed at the CIS/6-31G level. J_{Coul} corresponds to the classical dipole-dipole Coulomb interaction.

C.5 Slip-stacked ethylene dimer

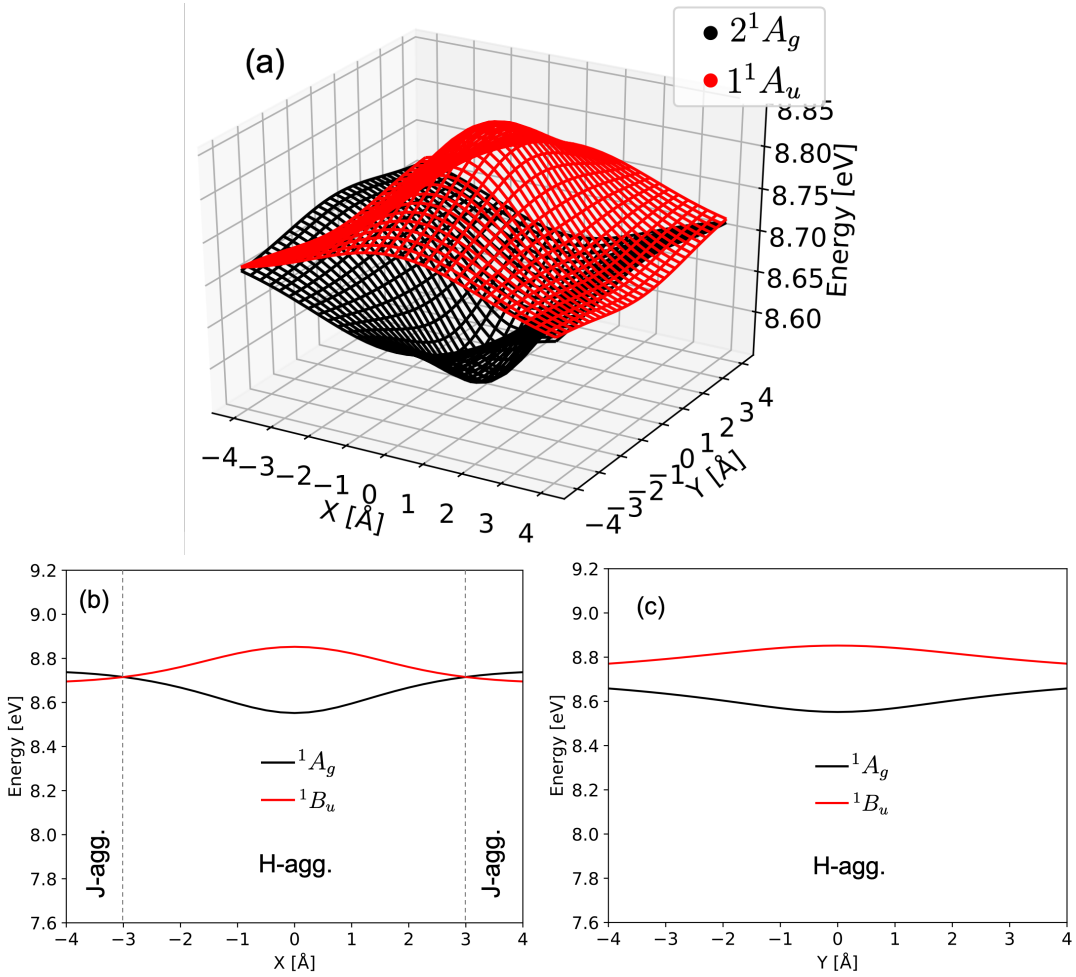

Figure C.4: Adiabatic energies (in eV) of the two lowest excited singlet states in the xy-plane (a), and corresponding energy profiles along the long (b) and short (c) axes for the coplanar ethylene dimer at $z = 4.7$ Å, computed at the CIS/6-31G level.

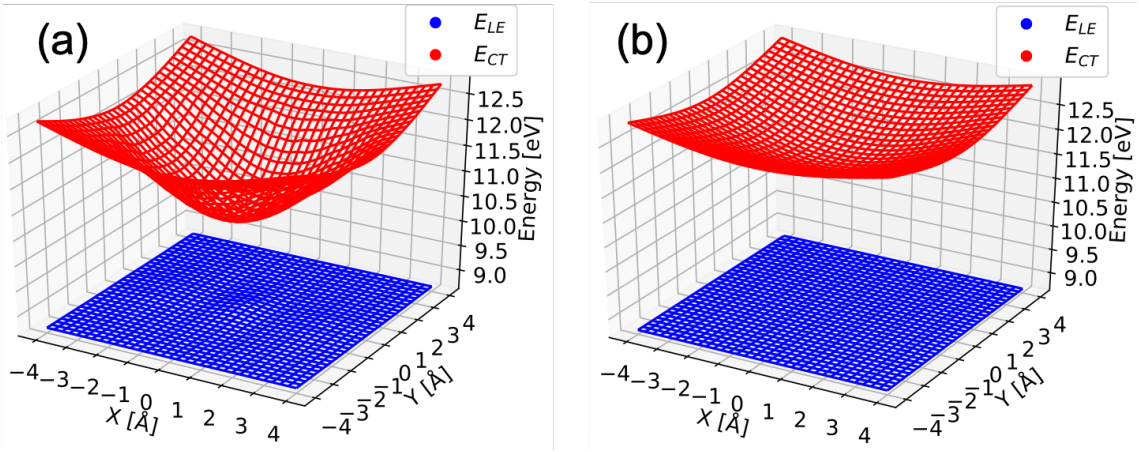

Figure C.5: Excitation energies (in eV) of the LE (blue) and CT (red) diabats in the xy-plane for the coplanar ethylene dimer at (a) $z = 3.5$ Å and (b) $z = 4.7$ Å, computed at the CIS/6-31G level.

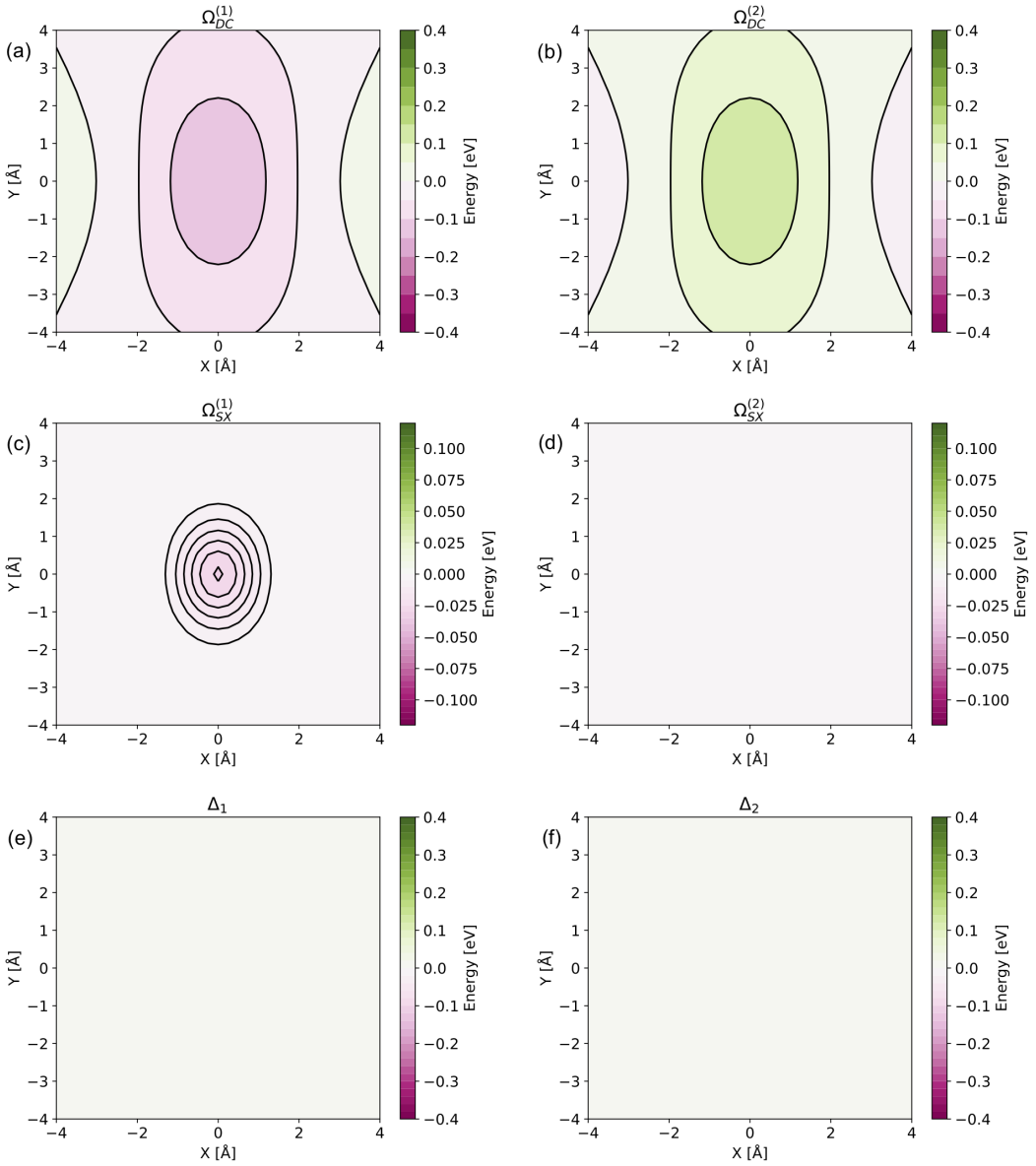

Figure C.6: Contributions (in eV) to the excitation energies for the two lowest excited singlets in the xy-plane at $z = 4.7$ Å computed at the CIS/6-31G level. (a,b) Direct couplings ($\Omega_{DC}^{(i)}$); (c,d) super-exchange ($\Omega_{SX}^{(i)}$); and (e,f) second order energy term Δ_i.

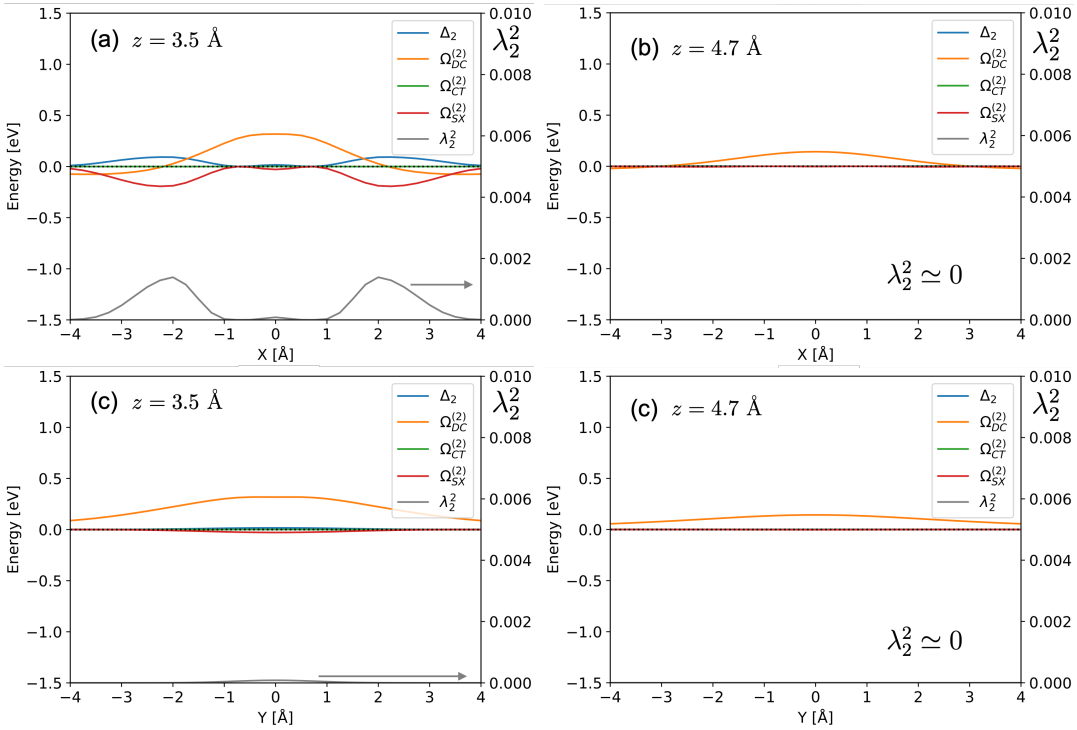

Figure C.7: Energy contributions (in eV) and LE/CT mixings (λ_2^2) to the excitation energies to the 1^1B_u state along the long molecular x-axis with $y = 0.0$ Å and at (a) $z = 3.5$ Å and (b) $z = 4.7$ Å, and along the short molecular y-axis with $x = 0.0$ Å and at (c) $z = 3.5$ Å and (d) $z = 4.7$ Å, computed at the CIS/6-31G level.

Bibliography

[1] L. Serrano-Andres and M. Merchan. Are the five natural DNA/RNA base monomers a good choice from natural selection?: A photochemical perspective. *J. Photochem. Photobiol. C - Photochem. Rev.*, 10:21, 2009.

[2] C. Middleton, K. de La Harpe, C. Su, Y. Law, C. Crespo-Hernandez, and B. Kohler. DNA excited-state dynamics: From single bases to the double helix. *Annu Rev. Phys. Chem.*, 60:217, 2009.

[3] M. Barbatti. The role of tautomers in the UV absorption of urocanic acid. *Phys. Chem. Chem. Phys.*, 13:4686, 2011.

[4] D. Polli, P. Altoe, O. Weigart, K.M. Spillane, C. Manzoni, D. Brida, G. Tomasello, G. Orlandi, P. Kukura, R. A. Mathies, M. Garavelli, and G. Cerullo. Conical intersection dynamics of the primary photoisomerization event in vision. *Nature*, 467:440, 2010.

[5] Y. Cheng and G. Fleming. Dynamics of light harvesting in photosynthesis. *Annu. Rev. Phys. Chem.*, 60:241, 2009.

[6] A. Drew, P. Harbach, J. Mewes, and M. Wormit. Quantum chemical excited state calculations on pigment-protein complexes require thorough geometry re-optimization of experimental crystal structures. *Theor. Chem. Acc.*, 125:419, 2010.

[7] C. Daniel, J. Full, L. González, C. Lupulescu, J. Manz, A. Merli, S. Vajda, and L. Woste. Deciphering the reaction dynamics underlying optimal control laser fields. *Science*, 299:536, 2003.

[8] W.R. Duncan, W.M. Stier, and O.V. Prezhdo. Ab initio nonadiabatic molecular dynamics of the ultrafast electron injection across the alizarin-TiO_2 interface. *J. Am. Chem. Soc.*, 127:7941, 2005.

[9] Y. Shang, Q. Li, L. Meng, D. Wang, and Z. Shuai. Computational characterization of organic photovoltaic devices. *Theor. Chem. Acc.*, 129:291, 2011.

[10] J.-L. Brédas, J. E. Norton, J. Cornil, and V. Coropceanu. Molecular understanding of organic solar cells: The challenges. *Acc.Chem.Res.*, 42:1691, 2009.

[11] A. M. Virshup, C. Punwong, T. V. Pogorelov, B. A. Lindquist, C. Ko, and T. J. Martinez. Photodynamics in complex environments: ab initio multiple spawning quantum mechanical/molecular mechanical dynamics. *Acc. Chem. Res.*, 113:3280, 2009.

[12] G. Groenhof, M. Bouxin-Cademartory, B. Hess, S. P. de Visser, H. J. C. Berendsen, M. Olivucci, and M. A. Robb. Photoactivation of the photoactive yellow protein: why photon absorption triggers a trans-to-cis isomerization of the chromophore in the protein. *J. Am. Chem. Soc.*, 126:4228, 2004.

[13] M. Bockmann, Doltsinis N. L., and D. Marx. Unraveling a chemically enhanced photoswitch: bridged azobenzene. *Angew. Chem.*, 122:3454, 2010.

[14] B. F. Habenicht and O. V. Prezhdo. Time-domain ab initio study of nonradiative decay in a narrow graphene ribbon. *J. Phys. Chem. C.*, 113:14067, 2009.

[15] T. Petrenko and F. Neese. Analysis and prediction of absorption band shapes, fluorescence band shapes, resonance raman intensities, and excitation profiles using the time-dependent theory of electronic spectroscopy. *J. Chem. Phys.*, 127:164319, 2007.

[16] M. Barbatti, A.J.A. Aquino, and H. Lischka. The uv absorption of nucleobases: semi-classical ab initio spectra simulations. *Phys. Chem. Chem. Phys.*, 12:4959, 2010.

[17] M. Stenrup and A. Larson. A computational study of radiationless deactivation mechanisms of furan. *Chem. Phys.*, 379:6, 2011.

[18] H. R. Hudock, B. G. Levine, A. L. Thompson, H. Satzger, D. Townsend, N. Gador, S. Ullrich, A. Stolow, and T. J. Martinez. Ab initio molecular dynamics and time-resolved photoelectron spectroscopy of electronically excited uracil and thymine. *J. Phys. Chem. A*, 11:8500, 2007.

[19] J. L. Banal, B. Zhang, D. J. Jones, K. P. Ghiggino, and W. W. H. Wong. Emissive molecular aggregates and energy migration in luminescent solar concentrators. *Acc. Chem. Res.*, 50(1):49–57, 2017.

[20] N. J. Hestand and F. C. Spano. Molecular aggregate photophysics beyond the kasha model: Novel design principles for organic materials. *Acc. Chem. Res.*, 50(2):341–350, 2017.

[21] G. J. Hedley, A. Ruseckas, and I. D. W. Samuel. Light harvesting for organic photovoltaics. *Chem. Rev.*, 117(2):796–837, 2017.

[22] K. H. Park, W. Kim, J. Yang, and D. Kim. Excited-state structural relaxation and exciton delocalization dynamics in linear and cyclic pi-conjugated oligothiophenes. *Chem. Soc. Rev.*, 47:4279–4294, 2018.

[23] H. Yamagata, J. Norton, E. Hontz, Y. Olivier, D. Beljonne, J. L. Brédas, R. J. Silbey, and F. C. Spano. The nature of singlet excitons in oligoacene molecular crystals. *J. Chem. Phys.*, 134(20):204703, 2011.

[24] J. Cornil, D. Beljonne, J.-P. Calbert, and J.-L. Brédas. Interchain interactions in organic pi-conjugated materials: Impact on electronic structure, optical response, and charge transport. *Adv. Mater.*, 13(14):1053–1067.

[25] G. M. Day. Current approaches to predicting molecular organic crystal structures. *Crystallogr. Rev.*, 17(1):3–52, 2011.

[26] D. E. LaLonde, J. D. Petke, and G.M. Maggiora. Evaluation of approximations in molecular exciton theory. 1. Applications to dimeric systems of interest in photosynthesis. *J. Phys. Chem.*, 92:4746–4752, 1988.

[27] D. Lee, L. Greenman, M. Sarovar, and K.B. Whaley. Ab initio calculation of molecular aggregation effects: A coumarin-343 case study. *J. Phys. Chem.*, 117:11072–11085, 2013.

[28] O. Uranga-Barandiaran, M. Catherin, E. Zaborova, A. D'Aléo, F. Fages, F. Castet, and D. Casanova. Optical properties of quadrupolar and bi-quadrupolar dyes: intra and inter chromophoric interactions. *Phys. Chem. Chem. Phys.*, 20(38):24623–24632, 2018.

[29] E. D. Cosco, J. R. Caram, O. T. Bruns, D. Franke, R. A. Day, E. P. Farr, M. G. Bawendi, and E. M. Sletten. Flavylium polymethine fluorophores for near- and shortwave infrared imaging. *Angew. Chem. Int. Ed.*, 56(42):13126–13129, 2017.

[30] Olatz Uranga-Barandiaran, David Casanova, and Frédéric Castet. Flavylium fluorophores as near-infrared emitters. *ChemPhysChem*, 21(20):2243–2248, 2020/10/19 2020.

[31] Abel Carreras, Olatz Uranga-Barandiaran, Frédéric Castet, and David Casanova. Photophysics of molecular aggregates from excited state diabatization. *J. Chem. Theory Comput.*, 15(4):2320–2330, 04 2019.

[32] M.A. Ratner and G.C. Schatz. *Introduction to Quantum Mechanics in Chemistry; Prentice Hall: Upper Saddle River, NJ*, 2001.

[33] M. Kasha. Characterization of electronic transitions in complex molecules. *Discuss. Faraday Soc.*, 9:14–19, 1950.

[34] M. Kasha, H. R. Rawls, and M. A. El-Bayoumi. The exciton model in molecular spectroscopy. *Pure Appl. Chem.*, 11:371–392, 1965.

[35] M. Kasha. Energy transfer mechanisms and the molecular exciton model for molecular aggregates. *Radiat. Res.*, 20(1):55–70, 1963.

[36] R. M. Hochstrasser and M. Kasha. Application of the exciton model to mono-molecular lamellar systems. *Photochem. Photobiol.*, 3(4):317–331, 2018/12/17 1964.

[37] R. D. Harcourt, K. P. Ghiggino, G. D. Scholes, and S. Speiser. On the origin of matrix elements for electronic excitation (energy) transfer. *J. Chem. Phys.*, 105(5):1897–1901, 1996.

[38] D.L. Dexter. A theory of sensitized luminescence in solids. *J. Chem. Phys.*, 21:836, 1953.

[39] L. D. Lavis and R. T. Raines. Bright ideas for chemical biology. *ACS Chem. Biol.*, 3(3):142–155, 2008.

[40] M. B. Smith and J. Michl. Singlet fission. *Chem. Rev.*, 110(11):6891–6936, 2010.

[41] M. B. Smith and J. Michl. Recent advances in singlet fission. *Annu. Rev. Phys. Chem.*, 64(1):361–386, 2013.

[42] D. Casanova. Theoretical modeling of singlet fission. *Chem. Rev.*, 118(15):7164–7207, 2018.

[43] N.J. Turro. *Modern Molecular Photochemistry.* University Science Books, 1991.

[44] Yuning Hong, Jacky W. Y. Lam, and Ben Zhong Tang. Aggregation-induced emission. *Chem. Soc. Rev.*, 40:5361–5388, 2011.

[45] C. C. Mead and D. G. Truhlar. Conditions for the definition of a strictly diabatic electronic basis for molecular systems. *J. Chem. Phys.*, 77(12):6090–6098, 1982.

[46] J. E. Subotnik, R. J. Cave, R. P. Steele, and N. Shenvi. The initial and final states of electron and energy transfer processes: Diabatization as motivated by system-solvent interactions. *J. Chem. Phys.*, 130(23):234102, 2009.

[47] C. Edmiston and K. Ruedenberg. Localized atomic and molecular orbitals. *Rev. Mod. Phys.*, 35:457, 1963.

[48] D.R. Hartree. The wave mechanics of an atom with non-coulombic central field: parts I, II, and III. *Proc. Cambridge Philos. Soc*, 24:89, 1928.

[49] D.L. Dexter. Naherungsmethode zur losung des quantenmechanischen mehrkorperproblems. *Eur. Phys. J.*, 61:126–148, 1930.

[50] A. Szabo and N.S. Ostlund. Modern quantum chemistry: Introduction to advanced electronic structure theory. *Dover Publications, INC. Mineola, New York*, 1996.

[51] A. Dreuw and M. Head-Gordon. Single-reference ab initio methods for the calculation of excited states of large molecules. *Chem. Rev.*, 105:4009–4037, 2005.

[52] M. Head-Gordon, R.J. Rico, M. Oumi, and T. Lee. A doubles correction to electronic excited states from configuration interaction in the space of single substitutions. *Chem. Phys. Lett.*, 219:21, 1994.

[53] M. Head-Gordon, D. Maurice, and M. Oumi. A perturbative correction to restricted open shell configuration interaction with single substitutions for excited states of radicals. *Chem. Phys. Lett.*, 246:114, 1995.

[54] H. Christof and W. Florian. CC2 excitation energy calculations on large molecules using the resolution of the identity approximation. *J. Chem. Phys.*, 113:5154, 2000.

[55] C. Hattig and K. Hald. Implementation of RI-CC2 triplet excitation energies with an application to trans-azobenzene. *Phys. Chem. Chem. Phys.*, 4:2111, 2002.

[56] Y.M. Rhee and M. Head-Gordon. Scaled second-order perturbation corrections to configuration interaction singles: Efficient and reliable excitation energy methods. *J. Phys. Chem. A*, 111:5314, 2007.

[57] Jiří Čížek. On the correlation problem in atomic and molecular systems. calculation of wavefunction components in ursell-type expansion using quantum-field theoretical methods. *The Journal of Chemical Physics*, 45(11):4256–4266, 1966.

[58] O. Sinanoglu, O. Sinanoğlu, and K.A. Brueckner. *Three Approaches to Electron Correlation in Atoms.* A chemistry-physics interface. Yale University Press, 1970.

[59] P. Hohenberg and W. Kohn. Inhomogeneous electron gas. *Phys. Rev.*, 136, 1964.

[60] J.C. Slater. *Quantum Theory of Molecules and Solids. Vol.4. The Self-Consistent Field for Molecules and Solids; McGraw-Hill*, 1974.

[61] Mel Levy. Universal variational functionals of electron densities, first-order density matrices, and natural spin-orbitals and solution of the v-representability problem. *Proceedings of the National Academy of Sciences*, 76(12):6062–6065, 1979.

[62] W. Kohn and L.J Sham. Self-consistent equations including exchange and correlation effects. *Annu. Rev. Phys. Chem.*, 140:A1133, 1965.

[63] E.K.U. Gross and W. Kohn. Arbitrary-order density functional response theory from automatic differentiation. *Ad. Quant. Chem.*, 21:255, 1990.

[64] M.E. Casida. *Recent Advances in Computational Chemistry Vol 1, Recent Advances in Density Functional Methods, Part 1, World Scientific: Singapore*, 1995.

[65] M.A.L. Marques, C.A. Ullrich, F. Nogueira, A. Rubio, K. Burke, and E.K.U. Gross. *Time-Dependent Density Functional Theory.* Lecture Notes in Physics. Springer Berlin Heidelberg, 2006.

[66] N.T. Maitra. Perspective: Fundamental aspects of time-dependent density functional theory. *J. Chem. Phys.*, 144:220901, 2016.

[67] E. Runge and E.K.U. Gross. Density-functional theory for time-dependent systems. *Phys. Rev. Lett.*, 52:997, 1984.

[68] S. Hirata and M. Head-Gordon. Time-dependent density functional theory within the tamm-dancoff approximation. *Chem. Phys. Lett.*, 314:291, 1999.

[69] M.E. Casida and M. Huix-Rotland. Progress in time-dependent density-functional theory. *Annu. Rev. Phys.Chem.*, 63:287, 2012.

[70] A. Drew, G.R. Fleming, and M. Head-Gordon. Charge-transfer state as a possible signature of a zeaxanthin–chlorophyll dimer in the non-photochemical quenching process in green plants. *Phys. Chem.*, 107:6500, 2003.

[71] A. Drew, J.L. Weisman, and M. Head-Gordon. Long-range charge-transfer excited states in time-dependent density functional theory require non-local exchange. *J. Chem. Phys.*, 119:2943, 2003.

[72] A Drew, G.R. Fleming, and M. Head-Gordon. Chlorophyll fluorescence quenching by xanthophylls. *Phys. Chem. Chem. Phys.*, 5:3247, 2003.

[73] D.J. Tozer, R.D. Amos, N.C. Handy, B.J. Roos, and L. Serrano-Andres. Does density functional theory contribute to the understanding of excited states of unsaturated organic compounds? *J. Mol. Phys.*, 97:859, 1999.

[74] A.L. Sobolewski and W. Domcke. Ab initio study of the excited-state coupled electron–proton-transfer process in the 2-aminopyridine dimer. *Chem. Phys.*, 73:294, 2003.

[75] A. Drew and M. Head-Gordon. Failure of time-dependent density functional theory for long-range charge-transfer excited states: The zincbacteriochlorin-bacteriochlorin and bacteriochlorophyll-spheroidene complexes. *J. Am. Chem. Soc.*, 126:4007, 2004.

[76] D.J. Tozer. Relationship between long range charge-transfer excitation energy error and integer discontinuity in Kohn-Sham theory. *Chem. Phys.*, 119:12697, 2005.

[77] A. Drew, J.L. Weisman, and M. Head-Gordon. Long-range charge-transfer excited states in time-dependent density functional theory require non-local exchange. *J. Chem. Phys.*, 119:2943, 2003.

[78] J.P. Perdew and A. Zunger. Self-interaction correction to density-functional approximations for many-electron systems. *Phys. Rev. B*, 23:5048, 1981.

[79] A. Dreuw and M. Head-Gordon. Failure of time-dependent density functional theory for long-range charge-transfer excited states: The zincbacteriochlorin bacteriochlorin and bacteriochlorophyll spheroidene complexes. *J. Am. Chem. Soc.*, 126(12):4007–4016, 2004.

[80] H. Iikura, T. Tsuneda, Yanai T., and Hirao K. A long-range correction scheme for generalized-gradient-approximation exchange functionals. *J. Chem. Phys.*, 115:3540, 2001.

[81] T.M. Henderson, B.G. Janesko, and G.E. Scuseria. Generalized gradient approximation model exchange holes for range-separated hybrids. *J. Chem. Phys.*, 128:194105, 2008.

[82] D. Casanova. The role of the π-linker in donor-π-acceptor organic dyes for high-performance sensitized solar cells. *Chem. Phys. Chem.*, 12:2979, 2011.

[83] D. Casanova, F.P. Rotzinger, and M. Gratzel. Computational study of promising organic dyes for high-performance sensitized solar cells. *J. Chem. Theory Comput.*, 6:1219, 2010.

[84] J.-D. Chai and M. Head-Gordon. Systematic optimization of long-range corrected hybrid density functionals. *J. Chem. Phys.*, 128:084106, 2008.

[85] F. Jensen. Atomic orbital basis sets. *Comput. Mol. Sci.*, 3:273–295, 2013.

[86] B. Liu and A.D. McLean. Accurate calculation of the attractive interaction of two ground state helium atoms. *J.Chem. Phys.*, 59(8):4557–4558, 1973.

[87] N.R. Kestner. He-He interaction in the SCF-MO approximation. *J.Chem.Phys.*, 48(1):252–257, 1968.

[88] S. F. Boys and F. Bernardi. The calculation of small molecular interactions by the differences of separate total energies. some procedures with reduced errors. *Mol.Phys.*, 19:553–566, 1970.

[89] J. Tomasi, B Mennucci, and R Cammi. Quantum mechanical continuum solvation models. *Chem. Rev.*, 105:2999, 2005.

[90] B. Mennucci. Polarizable continuum model. *Wiley Interdicip. Rev.: Comput. Mol. Sci.*, 2:386, 2012.

[91] J.M. Herbert and A.W. Lange. In many-body effects and electrostatics in multi-scale computations of biomolecules. *Pan Stanford*, 2015.

[92] S. Miertus, E. Scrocco, and J. Tomasi. Electrostatic interaction of a solute with a continuum. a direct utilization of ab initio molecular potentials for the prevision of solvent effects. *Chem. Phys.*, 55(1):117–129, 1981.

[93] S. Miertus and J. Tomasi. Approximate evaluations of the electrostatic free energy and internal energy changes in solution processes. *Chem. Phys.*, 65(2):239–245, 1982.

[94] Roberto Cammi and Benedetta Mennucci. Linear response theory for the polarizable continuum model. *J. Chem. Phys.*, 110(20):9877–9886, 1999.

[95] R. Cammi and J. Tomasi. Nonequilibrium solvation theory for the polarizable continuum model: A new formulation at the scf level with application to the case of the frequency-dependent linear electric response function. *Int. J. Quantum Chem.*, 56(S29):465–474, 1995.

[96] M. Klessinger and J. Michl. *Excited States and Photo-Chemistry of Organic Molecules*. Wiley, 1996.

[97] R. Mulliken. Electronic population analysis on LCAO–MO molecular wave functions. II. overlap populations, bond orders, and covalent bond energies. *J. Chem. Phys.*, 23:1841, 1955.

[98] R. Mulliken. Criteria for the construction of good self-consistent-field molecular orbital wave functions, and the significance of lcao-mo population analysis. *J. Chem. Phys.*, 36:3428, 1962.

[99] A.E. Reed. Natural population analysis. *J. Chem. Phys.*, 83:735, 1985.

[100] A.E. Reed. Intermolecular interactions from a natural bond orbital, donor-acceptor viewpoint. *Chem.Rev.*, 88:899–926, 1988.

[101] K.B. Wiberg and P.R. Rablen. Comparison of atomic charges derived via different procedures. *J. Comput. Chem.*, 14:1504–1518, 1993.

[102] A. Felouat, A. D'Aléo, and F. Fages. Synthesis and photophysical properties of difluoroboron complexes of curcuminoid derivatives bearing different terminal aromatic units and a meso-aryl ring. *J. Org. Chem.*, 78(9):4446–4455, 2013.

[103] G. Bai, C. Yu, C. Cheng, E. Hao, Y. Wei, X. Mu, and L. Jiao. Syntheses and photophysical properties of bf2 complexes of curcumin analogues. *Org. Biomol. Chem.*, 12:1618–1626, 2014.

[104] Y. Li, J. Yang, H. Liu, J. Yang, L. Du, H. Feng, Y. Tian, J. Cao, and C. Ran. Tuning the stereo-hindrance of a curcumin scaffold for the selective imaging of the soluble forms of amyloid beta species. *Chem. Sci.*, 8:7710–7717, 2017.

[105] A. Polishchuk, M. Stanko, A. Kulinich, and M. Shandura. D-pi-a-pi-d dyes with a 1,3,2-dioxaborine cycle in the polymethine chain: Efficient long-wavelength fluorophores. *Eur. J. Org. Chem.*, 2018(2):240–246, 2018.

[106] K. Kamada, T. Namikawa, S. Senatore, C. Matthews, P. Lenne, O. Maury, C. Andraud, M. Ponce-Vargas, B. Le Guennic, D. Jacquemin, P. Agbo, D. D. An, S. S. Gauny, X. Liu, R. J. Abergel, F. Fages, and A. D'Aléo. Boron difluoride curcuminoid fluorophores with enhanced two-photon excited fluorescence emission and versatile living-cell imaging properties. *Chem. Eur. J.*, 22(15):5219–5232, 2016.

[107] A. D'Aléo, A. Felouat, V. Heresanu, A. Ranguis, D. Chaudanson, A. Karapetyan, M. Giorgi, and F. Fages. Two-photon excited fluorescence of bf2 complexes of curcumin analogues: toward nir-to-nir fluorescent organic nanoparticles. *J. Mater. Chem. C*, 2:5208–5215, 2014.

[108] F. Archet, D. Yao, S. Chambon, M. Abbas, A. D'Aléo, G. Canard, M. Ponce-Vargas, E. Zaborova, B. Le Guennic, G. Wantz, and F. Fages. Synthesis of bioinspired curcuminoid small molecules for solution-processed organic solar cells with high open-circuit voltage. *ACS Energy Letters*, 2(6):1303–1307, 2017.

[109] D.-H. Kim, A. D'Aléo, X.-K. Chen, A. D. S. Sandanayaka, D. Yao, L. Zhao, T. Komino, E. Zaborova, G. Canard, Y. Tsuchiya, E. Choi, J. W. Wu, F. Fages, J.-L. Brédas, J.-C. Ribierre, and C. Adachi. High-efficiency electroluminescence and amplified spontaneous emission from a thermally activated delayed fluorescent near-infrared emitter. *Nat. Photonics*, 12(2):98–104, February 2018.

[110] F. C. De Schryver, P. Collart, J. Vandendriessche, R. Goedeweeck, A. M. Swinnen, and M. Van der Auweraer. Intramolecular excimer formation in bichromophoric molecules linked by a short flexible chain. *Acc. Chem. Res.*, 20(5):159–166, 1987.

[111] Kangning Liang, Mohammad S. Farahat, Jerry Perlstein, Kock-Yee Law, and David G. Whitten. Exciton interactions in nonconjugated squaraine dimers. mechanisms for cou-

pling and consequences for photophysics and photochemistry. *J. Am. Chem. Soc.*, 119(4):830–831, 1997.

[112] A. Zitzler-Kunkel, E. Kirchner, D. Bialas, C. Simon, and F. Würthner. Spacer-modulated differentiation between self-assembly and folding pathways for bichromophoric merocyanine dyes. *Chem. Eur. J.*, 21(42):14851–14861, 2015.

[113] J.-P. Desvergne, Henri B.-L., and R. Sarrebeyroux. Study of nonconjugated bichromophores linked by a polyether chain. 1. photochemical synthesis of crown-ethers from bis-(9-anthryloxy) polyoxaalkanes. *Isr. J. Chem.*, 18(3-4):220–226.

[114] P. Klán and P. J. Wagner. Intramolecular triplet energy transfer in bichromophores with long flexible tethers. *J. Am. Chem. Soc.*, 120(9):2198–2199, 1998.

[115] S.-L. Zhang, M. J. Lang, S. Goodman, C. Durnell, V. Fidlar, G. R. Fleming, and N.-C. C. Yang. Donor-acceptor interaction and photochemistry of polymethylene-linked bichromophores in solution. *J. Am. Chem. Soc.*, 118(38):9042–9051, 1996.

[116] L. Lu, R. J. Lachicotte, T. L. Penner, J. Perlstein, and D. G. Whitten. Exciton and charge-transfer interactions in nonconjugated merocyanine dye dimers: Novel solvatochromic behavior for tethered bichromophores and excimers. *J. Am. Chem. Soc.*, 121(36):8146–8156, 1999.

[117] F. Würthner. Dipole–dipole interaction driven self-assembly of merocyanine dyes: From dimers to nanoscale objects and supramolecular materials. *Acc. Chem. Res.*, 49(5):868–876, 2016.

[118] J.-D. Chai and M. Head-Gordon. Long-range corrected hybrid density functionals with damped atom-atom dispersion corrections. *Phys. Chem. Chem. Phys.*, 10:6615–6620, 2008.

[119] H.B. Jansen and P. Ros. Non-empirical molecular orbital calculations on the protonation of carbon monoxide. *Chem. Phys. Lett.*, 3(3):140 – 143, 1969.

[120] B. Liu and A. D. McLean. Accurate calculation of the attractive interaction of two ground state helium atoms. *J. Chem. Phys.*, 59(8):4557–4558, 1973.

[121] S.F. Boys and F. Bernardi. The calculation of small molecular interactions by the differences of separate total energies. some procedures with reduced errors. *Mol. Phys.*, 19(4):553–566, 1970.

[122] NIST computational chemistry comparison and benchmark database. NIST standard reference database number 101. Editor: Russell D. Johnson III. http://cccbdb.nist.gov/. Release 19, April 2018.

[123] S. Hirata and M. Head-Gordon. Time-dependent density functional theory within the Tamm–Dancoff approximation. *Chem. Phys. Lett.*, 314(3):291 – 299, 1999.

[124] T. Yanai, D. P. Tew, and N. C. Handy. A new hybrid exchange–correlation functional using the coulomb-attenuating method (CAM-B3LYP). *Chem. Phys. Lett.*, 393(1):51 – 57, 2004.

[125] T. N. Truong and E. V. Stefanovich. A new method for incorporating solvent effect into the classical, ab initio molecular orbital and density functional theory frameworks for arbitrary shape cavity. *Chem. Phys. Lett.*, 240(4):253 – 260, 1995.

[126] V. Barone and M. Cossi. Quantum calculation of molecular energies and energy gradients in solution by a conductor solvent model. *J. Phys. Chem. A*, 102(11):1995–2001, 1998.

[127] M. Cossi, N. Rega, G. Scalmani, and V. Barone. Energies, structures, and electronic properties of molecules in solution with the C-PCM solvation model. *J. Comput. Chem.*, 24(6):669–681, 2003.

[128] R. Cammi and B. Mennucci. Linear response theory for the polarizable continuum model. *J. Chem. Phys.*, 110(20):9877–9886, 1999.

[129] M. Cossi and V. Barone. Time-dependent density functional theory for molecules in liquid solutions. *J. Chem. Phys.*, 115(10):4708–4717, 2001.

[130] J. E. Subotnik, R. J. Cave, R. P. Steele, and N. Shenvi. The initial and final states of electron and energy transfer processes: Diabatization as motivated by system-solvent interactions. *J. Chem. Phys.*, 130(23):234102, 2009.

[131] M. J. Frisch, G. W. Trucks, H. B. Schlegel, G. E. Scuseria, M. A. Robb, J. R. Cheeseman, G. Scalmani, V. Barone, B. Mennucci, G. A. Petersson, H. Nakatsuji, M. Caricato, X. Li, H. P. Hratchian, A. F. Izmaylov, J. Bloino, G. Zheng, J. L. Sonnenberg, M. Hada, M. Ehara, K. Toyota, R. Fukuda, J. Hasegawa, M. Ishida, T. Nakajima, Y. Honda, O. Kitao, H. Nakai, T. Vreven, J. A. Montgomery, Jr., J. E. Peralta, F. Ogliaro, M. Bearpark, J. J. Heyd, E. Brothers, K. N. Kudin, V. N. Staroverov, R. Kobayashi, J. Normand, K. Raghavachari, A. Rendell, J. C. Burant, S. S. Iyengar, J. Tomasi, M. Cossi, N. Rega, J. M. Millam, M. Klene, J. E. Knox, J. B. Cross, V. Bakken, C. Adamo, J. Jaramillo, R. Gomperts, R. E. Stratmann, O. Yazyev, A. J. Austin, R. Cammi, C. Pomelli, J. W. Ochterski, R. L. Martin, K. Morokuma, V. G. Zakrzewski, G. A. Voth, P. Salvador, J. J. Dannenberg, S. Dapprich, A. D. Daniels, Farkas, J. B. Foresman, J. V. Ortiz, J. Cioslowski, and D. J. Fox. Gaussian 09 revision d01. Gaussian Inc. Wallingford CT 2009.

[132] Y. Shao, Z. Gan, E. Epifanovsky, A. T. B. Gilbert, M. Wormit, J. Kussmann, A. W. Lange, A. Behn, J. Deng, X. Feng, D. Ghosh, M. Goldey, P. R. Horn, L. D. Jacobson, I. Kaliman, R. Z. Khaliullin, T. Kús, A. Landau, J. Liu, E. I. Proynov, Y. M. Rhee, R. M. Richard, M. A. Rohrdanz, R. P. Steele, E. J. Sundstrom, H. L. Woodcock III, P. M. Zimmerman, D. Zuev, B. Albrecht, E. Alguire, B. Austin, G. J. O. Beran, Y. A. Bernard, E. Berquist, K. Brandhorst, K. B. Bravaya, S. T. Brown, D. Casanova, C.-M. Chang, Y. Chen, S. H. Chien, K. D. Closser, D. L. Crittenden, M. Diedenhofen, R. A. DiStasio Jr., H. Dop, A. D. Dutoi, R. G. Edgar, S. Fatehi, L. Fusti-Molnar, A. Ghysels, A. Golubeva-Zadorozhnaya, J. Gomes, M. W. D. Hanson-Heine, P. H. P. Harbach, A. W. Hauser, E. G. Hohenstein, Z. C. Holden, T.-C. Jagau, H. Ji, B. Kaduk, K. Khistyaev, J. Kim, J. Kim, R. A. King, P. Klunzinger, D. Kosenkov, T. Kowalczyk, C. M. Krauter, K. U. Lao, A. Laurent, K. V. Lawler, S. V. Levchenko, C. Y. Lin, F. Liu, E. Livshits, R. C. Lochan, A. Luenser, P. Manohar, S. F. Manzer, S.-P. Mao, N. Mardirossian, A. V.

Marenich, S. A. Maurer, N. J. Mayhall, C. M. Oana, R. Olivares-Amaya, D. P. O'Neill, J. A. Parkhill, T. M. Perrine, R. Peverati, P. A. Pieniazek, A. Prociuk, D. R. Rehn, E. Rosta, N. J. Russ, N. Sergueev, S. M. Sharada, S. Sharmaa, D. W. Small, A. Sodt, T. Stein, D. Stück, Y.-C. Su, A. J. W. Thom, T. Tsuchimochi, L. Vogt, O. Vydrov, T. Wang, M. A. Watson, J. Wenzel, A. White, C. F. Williams, V. Vanovschi, S. Yeganeh, S. R. Yost, Z.-Q. You, I. Y. Zhang, X. Zhang, Y. Zhou, B. R. Brooks, G. K. L. Chan, D. M. Chipman, C. J. Cramer, W. A. Goddard III, M. S. Gordon, W. J. Hehre, A. Klamt, H. F. Schaefer III, M. W. Schmidt, C. D. Sherrill, D. G. Truhlar, A. Warshel, X. Xua, A. Aspuru-Guzik, R. Baer, A. T. Bell, N. A. Besley, J.-D. Chai, A. Dreuw, B. D. Dunietz, T. R. Furlani, S. R. Gwaltney, C.-P. Hsu, Y. Jung, J. Kong, D. S. Lambrecht, W. Liang, C. Ochsenfeld, V. A. Rassolov, L. V. Slipchenko, J. E. Subotnik, T. Van Voorhis, J. M. Herbert, A. I. Krylov, P. M. W. Gill, and M. Head-Gordon. Advances in molecular quantum chemistry contained in the q-chem 4 program package. *Mol. Phys.*, 113:184–215, 2015.

[133] M. Rivoal, E. Zaborova, G. Canard, A. D'Aléo, and F. Fages. Synthesis, electrochemical and photophysical studies of the borondifluoride complex of a meta-linked biscurcuminoid. *New J. Chem.*, 40:1297–1305, 2016.

[134] G. Canard, M. Ponce-Vargas, D. Jacquemin, B. Le Guennic, A. Felouat, M. Rivoal, E. Zaborova, A. D'Aléo, and F. Fages. Influence of the electron donor groups on the optical and electrochemical properties of borondifluoride complexes of curcuminoid derivatives: a joint theoretical and experimental study. *RSC Adv.*, 7:10132–10142, 2017.

[135] K. Narasimha and M. Jayakannan. Pi-conjugated polymer anisotropic organogel nanofibrous assemblies for thermoresponsive photonic switches. *ACS Appl. Mater. Interfaces*, 6(21):19385–19396, 2014.

[136] S. Sanyal, A. Painelli, S. K. Pati, F. Terenziani, and C. Sissa. Aggregates of quadrupolar dyes for two-photon absorption: the role of intermolecular interactions. *Phys. Chem. Chem. Phys.*, 18:28198–28208, 2016.

[137] C. R. Martinez and B. L. Iverson. Rethinking the term "π-stacking". *Chem. Sci.*, 3:2191–2201, 2012.

[138] C. Janiak. A critical account on π-π stacking in metal complexes with aromatic nitrogen-containing ligands. *J. Chem. Soc., Dalton Trans.*, pages 3885–3896, 2000.

[139] S. Alvarez. A cartography of the van der Waals territories. *Dalton Trans.*, 42:8617–8636, 2013.

[140] F. C. Spano. The spectral signatures of Frenkel polarons in H- and J-aggregates. *Acc. Chem. Res.*, 43(3):429–439, 2010.

[141] V. May and O. Kühn. *Charge and Energy Transfer Dynamics in Molecular Systems.* Wiley-VCH, 2004.

[142] A. Dreuw and M. Head-Gordon. Failure of time-dependent density functional theory for long-range charge-transfer excited states: The zincbacteriochlorin bacteriochlorin and bacteriochlorophyll spheroidene complexes. *J. Am. Chem. Soc.*, 126(12):4007–4016, 2004.

[143] Kenry, Y. Duan, and B. Liu. Recent advances of optical imaging in the second near-infrared window. *Adv. Mat.*, 30(47):1802394, 2018.

[144] G. Hong, A. L. Antaris, and H. Dai. Near-infrared fluorophores for biomedical imaging. *Nat. Biomed. Eng.*, 1(1):0010, 2017.

[145] J. Zhao, D. Zhong, and S. Zhou. NIR-I-to-NIR-II fluorescent nanomaterials for biomedical imaging and cancer therapy. *J. Mater. Chem. B*, 6(3):349–365, 2018.

[146] Z. Tao, G. Hong, C. Shinji, C. Chen, S. Diao, A. L. Antaris, B. Zhang, Y. Zou, and H. Dai. Biological imaging using nanoparticles of small organic molecules with fluorescence emission at wavelengths longer than 1000 nm. *Angew. Chem. Int. Ed.*, 52(49):13002–13006, 2013.

[147] A. L. Antaris, H. Chen, K. Cheng, Y. Sun, G. Hong, C. Qu, S. Diao, Z. Deng, X. Hu, B. Zhang, X. Zhang, O. K. Yaghi, Z. R. Alamparambil, X. Hong, Z. Cheng, and H. Dai. A small-molecule dye for NIR-II imaging. *Nat. Mater.*, 15(2):235–242, 2016.

[148] A. L. Antaris, H. Chen, S. Diao, Z. Ma, Z. Zhang, S. Zhu, J. Wang, A. X. Lozano, Q. Fan, L. Chew, M. Zhu, K. Cheng, X. Hong, H. Dai, and Z. Cheng. A high quantum yield molecule-protein complex fluorophore for near-infrared II imaging. *Nat. Comm.*, 8(1):15269, 2017.

[149] X.-D. Zhang, H. Wang, A. L. Antaris, L. Li, S. Diao, R. Ma, A. Nguyen, G. Hong, Z. Ma, J. Wang, S. Zhu, J. M. Castellano, T. Wyss-Coray, Y. Liang, J. Luo, and H. Dai. Traumatic brain injury imaging in the second near-infrared window with a molecular fluorophore. *Adv. Mat.*, 28(32):6872–6879, 2016.

[150] S. Zhu, Q. Yang, A. L. Antaris, J. Yue, Z. Ma, H. Wang, W. Huang, H. Wan, J. Wang, S. Diao, B. Zhang, X. Li, Y. Zhong, K. Yu, G. Hong, J. Luo, Y. Liang, and H. Dai. Molecular imaging of biological systems with a clickable dye in the broad 800- to 1,700-nm near-infrared window. *Proc. Nat. Acad. Sci.*, 114(5):962, 2017.

[151] Q. Yang, Z. Ma, H. Wang, B. Zhou, S. Zhu, Y. Zhong, J. Wang, H. Wan, A. Antaris, R. Ma, X. Zhang, J. Yang, X. Zhang, H. Sun, W. Liu, Y. Liang, and H. Dai. Rational design of molecular fluorophores for biological imaging in the NIR-II window. *Adv. Mat.*, 29(12):1605497, 2017.

[152] Q. Yang, Z. Hu, S. Zhu, R. Ma, H. Ma, Z. Ma, H. Wan, T. Zhu, Z. Jiang, W. Liu, L. Jiao, H. Sun, Y. Liang, and H. Dai. Donor engineering for nir-ii molecular fluorophores with enhanced fluorescent performance. *J. Am. Chem. Soc.*, 140(5):1715–1724, 2018.

[153] A. Dreuw and M. Head-Gordon. Failure of time-dependent density functional theory for long-range charge-transfer excited states: The zincbacteriochlorin bacteriochlorin and bacteriochlorophyll spheroidene complexes. *J. Am. Chem. Soc.*, 126(12):4007–4016, 2004.

[154] T. N. Truong and E. V. Stefanovich. A new method for incorporating solvent effect into the classical, ab initio molecular orbital and density functional theory frameworks for arbitrary shape cavity. *Chem. Phys. Lett.*, 240(4):253–260, 1995.

[155] V. Barone and M. Cossi. Quantum calculation of molecular energies and energy gradients in solution by a conductor solvent model. *J. Phys. Chem. A*, 102(11):1995–2001, 1998.

[156] M. Cossi, N. Rega, G. Scalmani, and V. Barone. Energies, structures, and electronic properties of molecules in solution with the c-pcm solvation model. *J. Comput. Chem.*, 24(6):669–681, 2003.

[157] R. Cammi and B. Mennucci. Linear response theory for the polarizable continuum model. *J. Chem. Phys.*, 110(20):9877–9886, 1999.

[158] M. Cossi and V. Barone. Time-dependent density functional theory for molecules in liquid solutions. *J. Chem. Phys.*, 115(10):4708–4717, 2001.

[159] G. Canard, M. Ponce-Vargas, D. Jacquemin, B. Le Guennic, A. Felouat, M. Rivoal, E. Zaborova, A. D'Aléo, and F. Fages. Influence of the electron donor groups on the optical and electrochemical properties of borondifluoride complexes of curcuminoid derivatives: a joint theoretical and experimental study. *RSC Adv.*, 7(17):10132–10142, 2017.

[160] C.-P. Hsu, S. Hirata, and M. Head-Gordon. Excitation energies from time-dependent density functional theory for linear polyene oligomers: Butadiene to decapentaene. *J. Phys. Chem. A*, 105(2):451–458, 2001.

[161] F. Terenziani, A. Painelli, C. Katan, M. Charlot, and M. Blanchard-Desce. Charge instability in quadrupolar chromophores: Symmetry breaking and solvatochromism. *J. Am. Chem. Soc.*, 128(49):15742–15755, 2006.

[162] E. E. Jelley. Spectral absorption and fluorescence of dyes in the molecular state. *Nature*, 138:1009, 1936.

[163] G. Scheibe. Reversible polymerisation als ursache neuartiger absorptionsbanden von farbstoffen. *Kolloid-Z.*, 82(1):1–14, 1938.

[164] E. G. McRae and M. Kasha. Enhancement of phosphorescence ability upon aggregation of dye molecules. *J. Chem. Phys.*, 28(4):721–722, 1958.

[165] S. Baluschev, T. Miteva, V. Yakutkin, G. Nelles, A. Yasuda, and G. Wegner. Up-conversion fluorescence: Noncoherent excitation by sunlight. *Phys. Rev. Lett.*, 97:143903, 2006.

[166] T. N. Singh-Rachford and F. N. Castellano. Photon upconversion based on sensitized triplet–triplet annihilation. *Coord. Chem. Rev.*, 254(21):2560 – 2573, 2010.

[167] J. Zhao, S. Ji, and H. Guo. Triplet–triplet annihilation based upconversion: from triplet sensitizers and triplet acceptors to upconversion quantum yields. *RSC Adv.*, 1(6):937–950, 2011.

[168] T. F. Schulze and T. W. Schmidt. Photochemical upconversion: present status and prospects for its application to solar energy conversion. *Energy Environ. Sci.*, 8:103–125, 2015.

[169] J. Mei, N. L. C. Leung, R. T. K. Kwok, J. W. Y. Lam, and B. Z. Tang. Aggregation-induced emission: Together we shine, united we soar! *Chem. Rev.*, 115(21):11718–11940, 2015.

[170] C. J. Bardeen. The structure and dynamics of molecular excitons. *Annu. Rev. Phys. Chem.*, 65(1):127–148, 2014.

[171] C. D. Cruz, P. R. Christensen, E. L. Chronister, D. Casanova, M. O. Wolf, and C. J. Bardeen. Sulfur-bridged terthiophene dimers: How sulfur oxidation state controls inter-chromophore electronic coupling. *J. Am. Chem. Soc.*, 137(39):12552–12564, 2015.

[172] C. Climent, M. Barbatti, M. O. Wolf, C. J. Bardeen, and D. Casanova. The photophysics of naphthalene dimers controlled by sulfur bridge oxidation. *Chem. Sci.*, 8:4941–4950, 2017.

[173] F. T. Smith. Diabatic and adiabatic representations for atomic collision problems. *Phys. Rev.*, 179:111–123, 1969.

[174] M. Baer. Adiabatic and diabatic representations for atom-molecule collisions: Treatment of the collinear arrangement. *Chem. Phys. Lett.*, 35(1):112 – 118, 1975.

[175] T. H. Top and M. Baer. Incorporation of electronically nonadiabatic effects into bimolecular reactive systems. I. theory. *J. Chem. Phys.*, 66(3):1363–1371, 1977.

[176] T. Pacher, L. S. Cederbaum, and H. Köppel. Approximately diabatic states from block diagonalization of the electronic hamiltonian. *J. Chem. Phys.*, 89(12):7367–7381, 1988.

[177] R. J. Cave and M. D. Newton. Calculation of electronic coupling matrix elements for ground and excited state electron transfer reactions: Comparison of the generalized mulliken–hush and block diagonalization methods. *J. Chem. Phys.*, 106(22):9213–9226, 1997.

[178] V. May, O. Kühn, O. Kuhn, K. & John Wiley Schulten, and Sons Inc. *Charge and Energy Transfer Dynamics in Molecular Systems*. Wiley-VCH, 2004.

[179] Th. Förster. Zwischenmolekulare energiewanderung und fluoreszenz. *Ann. Phys.*, 437(1-2):55–75, 1948.

[180] H. Yamagata, C. M. Pochas, and F. C. Spano. Designing J- and H-aggregates through wave function overlap engineering: Applications to poly(3-hexylthiophene). *J. Phys. Chem. B*, 116(49):14494–14503, 2012.